2021

Alternative splicing of ANXA7 dictates receptor tyrosine kinase fates in glioblastoma

Sindhu Nair
University of Alabama at Birmingham

ALTERNATIVE SPLICING OF ANXA7 DICTATES RECEPTOR TYROSINE KINASE FATES IN GLIOBLASTOMA

by

SINDHU NAIR

MARKUS BREDEL, CHAIR
SUSAN BELLIS
CHENBEI CHANG
JAMES COLLAWN
STUART J. FRANK

A DISSERTATION

Submitted to the graduate faculty of The University of Alabama at Birmingham,
in partial fulfillment of the requirements for the degree of
Doctor of Philosophy

BIRMINGHAM, ALABAMA

2021

ALTERNATIVE SPLICING OF ANXA7 DICTATES RECEPTOR TYROSINE KINASE FATES IN GLIOBLASTOMA

SINDHU NAIR

GRADUATE BIOMEDICAL SCIENCES: CANCER BIOLOGY

ABSTRACT

Alternative splicing (AS) is a tightly regulated process essential for lineage specification in complex tissues like the brain. Dysregulated splicing in glioblastoma (GBM) is a mechanism exploited by tumor cells to retain or splice out exons consequently rewiring isoform-specific protein interactions to sustain tumor phenotypes. Receptor tyrosine kinases (RTK) amplifications are frequent events in GBM driving tumor growth and progression and are key targets for chemotherapy. However, RTK targeting in GBM has achieved limited success predominantly due to adaptive mechanisms of resistance in a constantly evolving tumor microenvironment. Clonal populations and crosstalk between RTKs sustain heterogeneity within a tumor leading to the failure of targeted RTK therapies. We previously found that monosomy of chromosome 10 caused haploinsufficiency of tumor suppressor *ANXA7* with a concurrent amplification of *EGFR* indicating an inhibitory effect of ANXA7 on EGFR signaling in GBM. ANXA7, a member of the annexin family, binds membranes in a calcium dependent manner and regulates endo- and exocytosis. *ANXA7* is alternatively spliced by PTBP1 into either isoform 1 (I1), containing a cassette exon, or isoform 2 (I2) lacking the cassette exon. In GBM, high levels of PTBP1 ensure splicing of *ANXA7* in favor of I2 with a subsequent elevation of EGFR signaling. Reintroducing I1 into GBM cells lead to a decrease in tumor growth and angiogenesis along with an inhibition of EGFR signaling.

How I1 mediates EGFR downregulation is not clear. In this dissertation we dissect the mechanism by which ANXA7 isoforms have divergent impacts on RTK signaling in GBM. I1 mediates the sorting of multiple RTKs such as EGFR, MET, PDGFRα and EGFRvIII for lysosomal degradation thereby abrogating signaling while RTKs are recycled in I2 expressing cells. Using predictive structural modeling, we show that the cassette exon region in I1 encloses a domain that potentially interacts with RTKs as well as components of the endocytic machinery conferring it with the unique ability to target RTKs for lysosomal degradation. The overarching goal of this study is to better understand the functional impact of AS in GBM and how targeting AS to retain tumor suppressive isoforms could offer an alternative approach to target GBM.

Keywords: Glioblastoma, alternative slicing, ANXA7, RTK signaling, endocytosis

DEDICATION

This dissertation is dedicated to my parents Vamanan and Shobha Nair, who have unconditionally supported every single decision I have made in my life right from a late career change to moving halfway across the world to pursue a PhD. Everything I am today is because of their constant encouragement to pursue excellence. Thank you for everything, I am extremely lucky to have you both in my life.

ACKNOWLEDGMENTS

I would like to first thank my mentor, Dr. Markus Bredel, for his support and guidance over the past five years, and for helping me grow as a scientist. Thank you for allowing me to pursue different ideas, for being patient and understanding, and for motivating me to do better. I am extremely grateful for your mentorship.

I am grateful to my committee members Dr. Susan Bellis, Dr. Chenbei Chang, Dr. James Collawn, and Dr. Stuart Frank for their valuable critiques and input that helped hone my scientific thought process. I would like to thank my collaborators and UAB core facility members who took time out to train me and give me scientific advice.

Rajani Rajbhandari, lab manager extraordinaire, who taught me lab skills, who I vented to, shared my joys and sadness with, and who has made me a more organized person. Thank you for being there for me through this journey, always ready with extra food and laughs when I needed it. I thank past members of the Bredel lab and colleagues in the Department of Radiation Oncology.

I have been fortunate to have amazing friends here at UAB who have kept me sane and made life outside the lab fun. You have all enriched my grad school experience and I cannot thank you all enough.

Lastly, none of this would have been possible without my parents and sister who put up with different versions of me that directly correlated with experimental results. They have motivated me, comforted me, and celebrated with me during every step of grad school for which I am extremely grateful.

TABLE OF CONTENTS

Page

LIST OF TABLES

LIST OF FIGURES

Figure *Page*

CHAPTER 1: INTRODUCTION

CHAPTER 2: ALTERNATIVE SPLICING OF ANXA7 DICTATES RECEPTOR TYROSINE KINASE FATES IN GLIOBLASTOMA

CHAPTER 3: NOVEL *EGFR* ECTODOMAIN MUTATIONS ASSOCIATED WITH LIGAND- INDEPENDENT ACTIVATION AND CETUXIMAB RESISTANCE IN HEAD AND NECK CANCER

LIST OF ABBREVIATIONS

ANXA7	Annexin A7
AS	Alternative splicing
ASO	Antisense Oligonucleotides
CDKN2A	Cyclin Dependent Kinase Inhibitor 2A
CHI3L1	Chitinase 3 Like 1
CIE	Clathrin-Independent Endocytosis
CME	Clathrin-Mediated Endocytosis
CNS	Central Nervous System
EE	Early Endosome
EGFR	Epidermal Growth Factor Receptor
GABRA1	Gamma-Aminobutyric Acid Type A Receptor Subunit Alpha1
GBM	Glioblastoma
GTPases	Guanosine triphosphatases
IDH	Isocitrate Dehydrogenase
JAK	Janus kinase
MAP	Mitogen-Activated Kinase
mTOR	Mammalian Target of Rapamycin
NEFL	Neurofilament Light Chain
NF1	Neurofibromatosis 1

NKX2-2	NK2 Homeobox 2 *(NKX2-2)*
OLIG2	Oligodendrocyte transcription factor
PDGFRA	Platelet Derived Growth Factor Receptor alpha
PIK3CA	Phosphatidylinositol-4,5-Bisphosphate 3-Kinase Catalytic Subunit Alpha
PPI	Protein-Protein Interactions
PTB	Phosphotyrosine-Binding
PTBP1	Polypyrimidine Tract Binding Protein 1
PTBP1	Polypyrimidine Tract–Binding Protein 1
PTEN	Phosphatase and Tensin Homolog
RAB	Ras Analog In Brain
RB	Retinoblastoma
RBM22	RNA Binding Motif Protein 22
RBM3	RNA Binding Motif Protein 3
RTK	Receptor Tyrosine Kinase
SH2	Src Homology-2
SLC12A5	K-Cl Cotransporter A5
SRSF3	Serine And Arginine Rich Splicing Factor 3
SYT1	Synaptotagmin 1
TCGA	The Cancer Genome Atlas
TERT	Telomerase Reverse Transcriptase
TKI	Tyrosine Kinase Inhibitors
TMZ	Temozolomide
TP53	Tumor Protein P53

CHAPTER 1: INTRODUCTION

BRAIN TUMORS

Brain tumors are a heterogenous group of neoplasms, encompassing both benign and malignant tumors, arising within the central nervous system (CNS). Amongst the deadliest of cancers, malignant brain tumors are challenging to treat owing to their location as well as their tendency to invade locally leading to neurological symptoms like headaches, seizures, cognitive dysfunction, and focal deficits (1, 2). Malignant brain tumors can be primary, those that arise in the brain, or secondary, cancers that arise elsewhere in the body and metastasize to the brain (3, 4). Prior classification of brain tumors was based on histopathology, differentiation, cell of origin, and immunohistochemical expression of lineage-associated proteins. In 2016, the WHO reclassified brain tumors by integrating both histology and molecular parameters such as genetic and epigenetic modifications that confer distinct characteristics to different tumors (5). Broadly, primary brain tumors are classified as gliomas – those that arise from glial cells or glial precursor cells such as astrocytes, oligodendrocytes, and ependymal cells; non-glioma tumors – those that rise from cells in the brain that are not glial (5).

Gliomas

Gliomas are a diverse group of malignant brain tumors that based on their putative cell of origin are sub-classified as astrocytomas, oligodendrogliomas, ependymomas, or mixed gliomas (6-8). Additionally, gliomas can be characterized as "diffuse" or "non-diffuse" based on their ability to migrate and invade over large distances within the brain (8). With the advent of next-generation sequencing, comprehensive molecular analyses have helped in subtyping tumors based on specific molecular markers that modulate tumor behavior and treatment response. Diffuse gliomas are now broadly sub-classified based on the following mutations – isocitrate dehydrogenase 1 and 2 (IDH) status, loss of heterozygosity for 1p/19q (co-deletions with IDH have also been reported), mutations in telomerase reverse transcriptase gene (*TERT)* promoter region, alpha-thalassemia/mental retardation syndrome X-linked gene (ATRX), O[6]-methylguanine-DNA methyltransferase (MGMT) promoter methylation and tumor protein p53 gene (TP53) mutations. Based on histological tumor grades, gliomas are classified as diffuse astrocytomas (grade II), anaplastic astrocytoma, IDH-mutant (grade III) and glioblastoma, IDH wild-type/mutant (grade IV) (5, 7-9).

Glioblastoma

Glioblastoma (GBM), a WHO grade IV astrocytoma, is the most malignant and commonly occurring tumor accounting for 80% of all malignant brain tumors (2, 6, 10). GBMs are sub-classified as primary, those arising de novo, or secondary, those that arise from pre-existing low grade astrocytomas (11). The global incidence of GBM is roughly

10 per 100,000 persons, while in the United States it accounts for about 3.21 per 100,000 persons (7, 12). The median age of diagnosis is 65 years with a peak observed at 75-85 years; a higher incidence is observed in males as compared to females with GBM occurring 1.58 times more common in males (7, 12, 13). Clinically, patients may present with generalized or focal signs and symptoms depending on the duration of the disease. Symptoms also depend upon the area infiltrated and destroyed by the tumor via necrosis, intracranial pressure, and tumor location. Common symptoms include headaches, seizures, sensory and motor disturbances (6, 14, 15). Histologically, GBMs exhibit abundant atypia including cellular and nuclear polymorphism, hypercellularity, increased vascularization and necrotic foci, a seminal feature of GBMs. Necrotic foci are formed due to hypoxic areas within the central regions as the tumors expand in size peripherally (16, 17). Additionally, GBMs are highly invasive locally and extensively infiltrate the surrounding brain parenchyma. Tumor cells typically migrate along pre-existing vasculature, white matter tracts, subpial and subarachnoid spaces (18, 19). However, GBMs rarely metastasize and remain confined to the brain (16, 20).

Despite advances in research and clinical regimens, GBMs remain one of the most devastating tumors with a dismal prognosis. Surgical resection alone is insufficient to eliminate the tumor due to the microscopic invasion of tumor cells into surrounding parenchyma. Currently, the standard-of-care remains maximal surgical resection, followed by radiotherapy and concomitant chemotherapy with Temozolomide (TMZ), an alkylating agent (21, 22). However, prognosis is poor in afflicted patients with a median survival of approximately 14 to 15 months post-diagnosis (22, 23) and a 5-year survival that has remained relatively consistent at about 5.8%, amongst the lowest of all cancers

(12, 24). In addition, high rates of recurrence are observed in a vast majority of patients (25, 26). A combination of physiologic, pathologic, and molecular factors contributes towards treatment failure and recurrence in GBMs.

Heterogeneity in Glioblastomas

A characteristic feature of GBMs is the presence of extensive cellular and genetic heterogeneity between patients (intertumoral) or within a single tumor itself (intratumoral). Heterogeneity can pertain to factors such as tumor location, phenotype, metabolic signatures, signaling pathways and tumor microenvironment (27, 28). Tumor cells may arise from one or more clones leading to the formation of clusters adding to the genetic complexity of the tumor. With the subsequent accumulation of multiple mutations over time, the cells in these clusters may transform so much so that they lose any resemblance to their cell of origin (29). In addition, studies have shown that a high level of plasticity exists in GBMs where in expression patterns in individual tumor regions may change due to selective pressure during glioma development, factors such as mutational burden, treatment-induced plasticity and temporal heterogeneity (leading edge vs. tumor core) (30-32).

Consequently, most GBMs are therapeutically resistant as standardized treatment modalities fail necessitating the need for personalized therapies that target specific markers or relevant characteristics of each tumor. Recently, extensive transcriptomic analyses of a panel of patient-derived GBM samples by the cancer genome atlas (TCGA)

have identified specific molecular signatures enabling the classification of GBMs into clinically relevant subtypes with distinct behaviors.

Molecular Subtyping of Glioblastoma

Initial genome-wide profiling of 206 GBM samples carried out by the TCGA in 2008 revealed that frequent genetic alterations were observed with respect to three critical signaling pathways – receptor tyrosine kinase (RTK) signaling, p53 and retinoblastoma (RB) pathway (33). Concurrent mutations were also observed with respect to genes of the Phosphatidylinositol-4,5-Bisphosphate 3-Kinase Catalytic Subunit Alpha (PIK3CA), Cyclin Dependent Kinase Inhibitor 2A (CDKN2A) and Phosphatase and Tensin Homolog (PTEN) deletions. It was concluded that mutations in RTK, p53 and RB genes were obligatory driver events in most GBMs but with varying patterns and concomitant mutations in other key pathways described above (33).

Subsequently, Verhaak et al. studied gene expression profiles using bulk-sequencing in a panel of patient samples and independent datasets from the public domain and found distinct molecular signatures with respect to commonly mutated genes in GBM such as epidermal growth factor receptor (*EGFR*), Neurofibromatosis 1 (*NF1*), Platelet derived growth factor receptor alpha (*PDGFRA*), *IDH1*, *TP53* and *CDKN2A* (34). Subtypes were accordingly named: Classical, Neural, Proneural and Mesenchymal. Each subtype was associated with a distinct clinical behavior, inherent signatures of a putative cell of origin and therapeutic response.

Classical GBM is characterized by the amplification of chromosome 7 paired with a loss of chromosome 10 and a resultant amplification of *EGFR*, an RTK, in approximately 97% of cases. Concurrent loss of *TP53* and/or *CDKN2A* was also observed. The classical subtype retained a distinct signature associated with murine astrocytes and responded well to concurrent chemo- and radiotherapy with significantly reduced mortality.

Proneural GBM is associated with alterations in *PDGFRA* and point mutations in *IDH1*. Focal amplification of *PDGFRA* with a resultant high level of gene expression was observed exclusively in this subtype. Gene signatures associated with oligodendrocytic development genes such as *PDGFRA*, NK2 Homeobox 2 *(NKX2-2)* and Oligodendrocyte transcription factor *(OLIG2)* was observed; astrocytic signatures were absent. Clinically, the proneural subtype was found to be associated with an overall younger age group and showed a trend towards longer survival.

The neural subtype of GBM exhibits high expression of neuronal markers such as Neurofilament Light Chain (*NEFL),* Gamma-Aminobutyric Acid Type A Receptor Subunit Alpha1 (*GABRA1),* Synaptotagmin 1 (*SYT1)* and K-Cl cotransporter A5 (*SLC12A5).* However, subsequent analyses on the neural subtype have revealed a lack of characteristic gene abnormalities indicating it to be non-tumor specific and to be more likely detected in normal brain tissue alluding to contamination in previous analyses. At present, the neural subtype is either not included in GBM gene-expression profiling and if included, is merged with the proneural subtype (33, 35).

The mesenchymal subtype of GBM is associated predominantly with focal hemizygous deletions in NF1 with co-mutations in PTEN. Additionally, expression of

mesenchymal markers such as Chitinase 3 Like 1 (*CHI3L1)* and *MET* proto-oncogene was observed. Genes in the tumor necrosis factor super family pathway and NF-κB pathway were highly expressed possibly associated with higher overall necrosis and inflammation in this subtype. Strong cultured astroglial signatures with a high activity of markers linked with dedifferentiated tumors were observed. Mesenchymal GBMs responded well to aggressive treatment; a significant decrease in mortality was observed in patients treated with concurrent chemo- and radiotherapy (33).

Whole exome sequencing by Brennan et al. in a larger dataset found significant amplification events in RTKs such as *EGFR, MET, PDGFRA,* and *FGFR*. At least one RTK was altered in 67.3% of GBMs - *EGFR* (57.4%), *PDGFRA* (13.1%), *MET* (1.6%), and *FGFR2/3* (3.2%). 11% of GBMs highly expressed *EGFRvIII*, a truncated version of *EGFR*, and directly associated with a more aggressive phenotype. Additionally, mutations in *EGFR* were accompanied by concomitant mutations in *MET* or *PDGFRA* demonstrating a pattern of intratumoral heterogeneity (36).

The evolution in sequencing technologies was allowed researchers to investigate heterogeneity at a single cell level. Patel et al., using single-cell RNA-sequencing, found that cell-to-cell variability in gene expression existed within a single tumor especially with respect to RTK signaling pathways such as *EGFR, FGFR1, PDGFRA* and *FGF1* underscoring the importance of RTK signaling in GBM (37). More recently, Wang et al. matched profiles of primary and recurrent gliomas and found that phenotypic plasticity existed in GBMs in response to treatment including subtype switching. The tumor microenvironment played an important role in promoting transcriptomic adaptability and

transition between subtypes in order to escape therapeutic vulnerabilities (35). Intratumoral heterogeneity in GBM is highlighted in Figure 1.

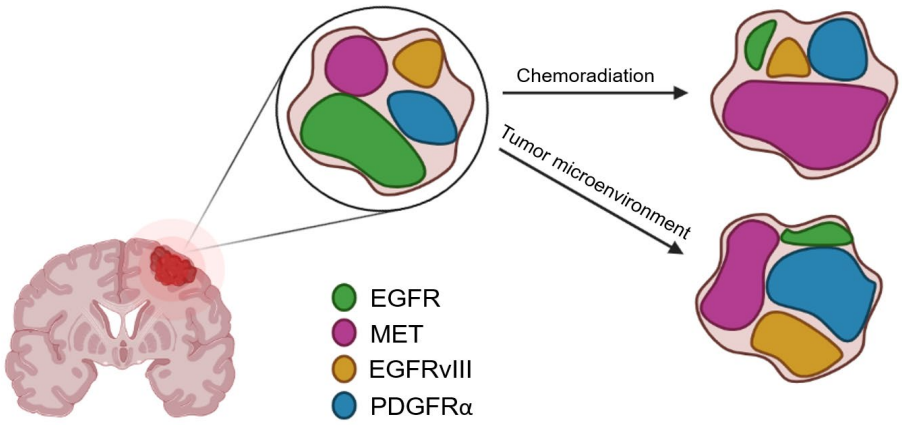

Figure 1. Intratumoral heterogeneity in glioblastoma. Colored areas represent different regions within a tumor overexpressing a specific RTK and the evolution of RTK signatures in response to stimuli such as chemoradiation to evade targeted therapy and/or in response to microenvironmental factors.

RECEPTOR TYROSINE KINASES

RTKs are cell-surface receptors and regulators of critical cellular processes such as growth and differentiation, metabolism, motility, and the cell cycle. RTKs share a common structural basis - an extracellular ligand binding domain, a transmembrane region and an intracellular tyrosine kinase domain that activates key downstream pathways (38, 39). Physiologically, RTKs are activated by the binding of receptor-specific ligands in the extracellular region. This leads to receptor homo- or hetero-dimerization enabling trans-autophosphorylation while simultaneously releasing an auto-inhibitory tether. This dynamic conformational change recruits downstream signaling

molecules containing Src homology-2 (SH2) or phosphotyrosine-binding (PTB) domains which then recruit proteins such as phosphatidylinositol 3-kinase (PI3K), SRC, adaptor proteins such as SHC, GRB2, transcriptional factors like signal transducer and activator of transcription (STAT), ubiquitin ligases and phospholipases (PLC-γ). These molecules phosphorylate specific residues on the tyrosine kinase domain and finally activate downstream signal cascades, such as the RAS/RAF/mitogen-activated kinase (MAP), PI3K/AKT/mammalian target of rapamycin (mTOR), PLC-γ/protein kinase C and Janus kinase (JAK)/STAT pathway necessary for vital biological processes (39-42). Once activated, downregulation of RTK signaling occurs either due to the unavailability of ligand or via endocytosis-mediated lysosomal degradation, a major deactivation pathway.

Receptor Endocytosis

Endocytosis is a mechanism involving the plasma membrane and a host of cargo proteins necessary for nutrient uptake, regulation of RTK signaling, maintenance of plasma membrane lipid, and protein homeostasis (43). The endocytic pathway is a stepwise mechanism that utilizes vesicles budding off the plasma membrane and then undergoing fusion and fission with various compartments of the pathway, a process regulated by several hundred proteins.

Several endocytic pathways can mediate the internalization and sorting of receptors. Two of the most studied pathways include – clathrin-mediated endocytosis (CME) defined by the presence of clathrin coats on the vesicles; clathrin-independent endocytosis (CIE) which encompasses multiple pathways dependent on the presence of cholesterol-rich membrane rafts for internalization (41, 44). Post-activation, residues in

the tyrosine kinase domain serve as interaction sites for ubiquitination, a posttranslational modification necessary to target RTKs for degradation (45, 46). c-Cbl, an E3 ubiquitin ligase, binds to a specific phosphorylated residue of the RTK and then recruits E2 enzyme that tags the RTK with ubiquitin. Ubiquitinated RTKs then interact with specific residues for CME (clathrin adaptor AP-2) or CIE (epsin and Epsin15) and are subsequently internalized into vesicles and trafficked to the early endosome (EE) (44, 46). The early endosome serves as a focal point where the fate of an RTK is decided-cessation of signaling by sorting to the lysosomes or recycling of the receptor back to the plasma membrane.

Endocytic sorting is regulated by a family of proteins called Ras analog in brain (Rab) which are small guanosine triphosphatases (GTPases) that belong to the Ras-like GTPase superfamily and can regulate vesicle trafficking (47, 48). The Rab family binds to different effectors of the endocytic pathway by regulating vesicular transport, including budding, transport, tethering, docking, and fusion stages. 66 Rab proteins are encoded in the human genome with most Rabs having overlapping yet distinct functions. Some of the well-studied Rabs in receptor endocytosis include Rab4 (fast recycling endosomes), Rab5 (early endosome), Rab 7 (late endosome), Rab11 (slow recycling endosome) and Rab25 (recycling endosomes) (48, 49).

RTK Signaling Networks and Therapeutic Resistance

Given the extent of heterogeneity and the co-existence of multiple RTK mutations in GBM, it is now evident that a complex RTK signaling network exists driving GBM progression. Studies have shown that the tumor microenvironment plays an important

role in the co-activation of RTKs as an adaptive response to stimuli such as - hypoxic conditions, motility, and migration in response to targeted therapy using tyrosine kinase inhibitors (TKI) (50-52). Snuderl et al. observed the coexistence of intermingled functional and actively dividing *EGFR*, *MET*, and *PDGFRA*-amplified subclones in varying ratios in 15 GBM samples and reasoned that there existed a selection pressure for the growth of each subclone (53). Similarly, two other studies found the existence of distinct subpopulations with multiple RTK amplifications in variable proportions (54, 55). More importantly, rewiring of signaling networks was observed within days of targeted therapy (56) indicating that mosaic amplification and/or concurrent activation of other RTKs leads to therapeutic resistance in GBM. This underscores the need to better understand conserved biological mechanisms that downregulate RTK signaling in GBM.

ALTERNATIVE SPLICING

Alternative splicing (AS) is a regulatory mechanism by which exons of gene transcripts can be spliced in different arrangements to generate multiple protein variants. AS contributes to proteome complexity and diversifies gene functions with as many as 90-95% of the human genes undergoing AS (57-59). AS is regulated by a complex machine called the spliceosome consisting of small nuclear RNAs and other splicing factors that assemble on the pre-mRNA (60). The main types of AS patterns have been described in Figure 2. Cassette exon skipping is the most prevalent pattern in vertebrates followed by alternative selection of 5' and 3' sites (61, 62).

Large-scale proteomics analyses have revealed that AS patterns strongly correlate with tissue types and that this tissue-specific AS is conserved across vast evolutionary distances. More importantly, tissue-specific isoforms were abundantly present in the nervous and cardiac tissues indicating that AS is vital during the development of the heart and brain (63-65). In the brain, AS regulates the development and maintenance of cell and tissue types and the establishment of neuronal networks. Splicing regulatory networks during neural development ensures that exon networks are

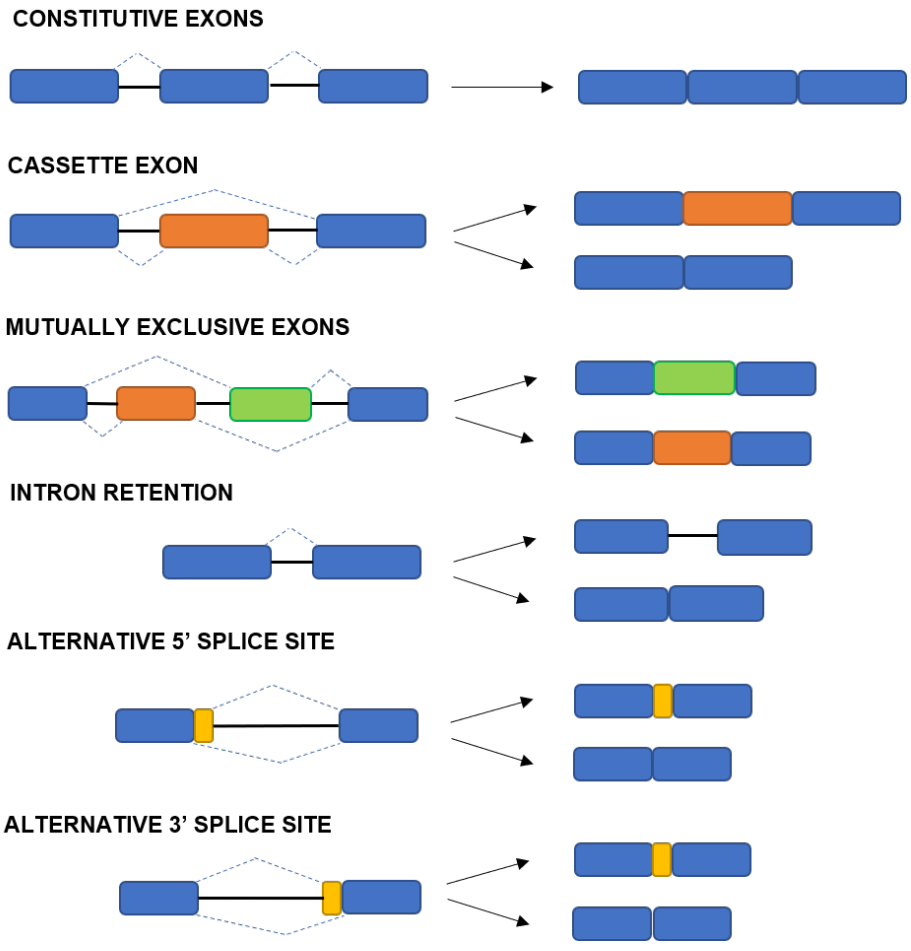

Figure 2. Commonly observed alternative splicing patterns

tightly regulated temporally during the transition from a neural precursor to a neuronal subtype. Consequently, the inclusion or exclusion of exons modulates protein-protein interactions (PPI) during neurogenesis via the presence/absence of domains encoded by these exons (60, 63, 66, 67). Splicing aberrations in any of the genes regulating neural development or within the spliceosome itself can contribute to gliomagenesis and GBM progression.

Alternative Splicing in Glioblastoma

Recent studies have implicated dysregulated AS as a potential biomarker for GBM. Reprogramming of AS networks in GBM cells were observed to not only play a role in cancer progression but also modulated treatment response and patient prognosis (68, 69). In two separate studies, exon skipping or cassette exon splicing was found to be the most frequent AS event in a cohort of GBM samples. Additionally, prognostic modeling for survival prediction showed a positive correlation between higher AS signatures and lower survival (68, 70). Comparison in AS events between primary and recurrent GBM showed that splicing patterns of a gene evolved and in some cases were reversed in recurrent GBM indicating that tumor cells manipulated AS to better adapt to the microenvironment and to enhance invasiveness and motility (71). Mutations in spliceosomal components such as SRSF3, RBM22, PTBP1 and RBM3 have been specifically observed in GBMs as compared to healthy brain tissue (69). More importantly, splicing aberrations have been reported in genes that regulate important cellular processes in GBM like apoptosis, cell growth, metabolism, invasion, and membrane trafficking which are important for GBMs growth and progression (72). For

example, lysosomal degradation via endocytosis is the predominant mechanism by which RTK signaling is downregulated (46). This mechanism is tightly regulated spatiotemporally and splicing aberrations in genes involved in vesicular trafficking and can tilt the balance from degradation to recycling with respect to RTK fates potentiating GBM growth. Studies have shown that splicing defects in endocytic regulatory genes that traffic EGFR like CD44 and annexin A7 (ANXA7 amplified EGFR signaling in GBM by impairing degradation (72).

ANNEXINS

Annexins are an evolutionarily conserved multigene family with membrane and phospholipid binding properties. Annexins typically form networks or scaffolds in a calcium-dependent manner and act as membrane recruitment platforms in order to regulate multiple cellular functions such as membrane structure, vesicular transport, endo- or exocytosis and calcium homeostasis (73-75).

The vertebrate annexin superfamily consists of 12 subfamilies identified as A1-A11, A13. Structurally, each annexin is composed of two domains - a conserved C-terminal protein core composed of annexin repeats, each approximately 70 amino acids long, and a divergent N-terminal domain that is unique to and confers functional specificity to each annexin (Figure 3). While the C-terminal repeats of annexins bind to negatively charged membranes in a calcium-dependent manner, the N-terminal domain has been shown to act as substrates for kinases or binding sites for interaction partners necessary for a broad range of cellular processes (76, 77).

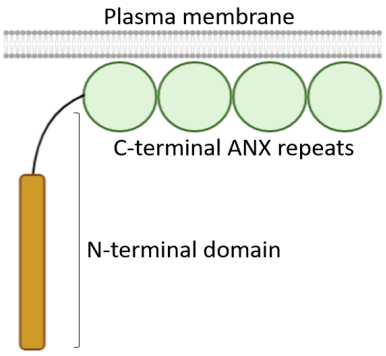

Figure 3. Annexin structure. Annexin repeats (green) are conserved in all annexins and bind to phospholipid membranes; the N-terminal domain (yellow) is variable in length and confers each annexin its unique function.

Annexins also undergo post-translational modifications such as myristoylation and phosphorylation leading to surface remodeling of individual annexins accounting for much of the subfamily specificity in annexin interactions (73). Annexins are predominantly cytosolic with some annexins (A11, A12) translocating to the nucleus during specific processes. In the cytosol, they may be reversibly associated with the plasma membrane, cytoskeletal proteins, and extracellular matrix proteins depending on their function and necessity for a specific biological process (73, 74). It has recently become evident that dysregulation of annexin expression is directly correlated with a host of diseases such as cancers, autoimmune disorders, neurological, blood, and metabolic diseases (77). Annexins have been implicated in multiple cancers with each annexin having divergent expression profiles and impact based on the cancer type (Table 1).

Table 1. Expression of Annexins in various cancers

ANNEXIN	Upregulated	Downregulated	References
ANXA1	Liver, lung, colorectal, pancreatic, skin, GBM	Prostate, cervix, larynx, lymphoma, oral	(78), (79), (80),(81), (82)
ANXA2	Liver, breast, cervical, gastric, GBM, hematological (ALL, APL, MM)	Colorectal, prostate, esophageal	(78), (83), (84), (85), (86), (87)
ANXA3	Liver, breast, lung, colorectal, ovarian	Thyroid	(78) , (88), (89, 90), (91), (92)
ANXA4	Liver, breast, gastric, ovarian, colorectal, pancreatic	Prostate	(78), (93), (94), (95)
ANXA5	Liver, pancreatic, sarcoma, breast, GBM	Gastric, ovarian	(78), (96), (92), (97), (98)
ANXA6	Breast, ovarian	Ovarian, epidermoid, liver	(92), (99), (100), (101), (102)
ANXA7	Liver, colorectal, breast, multiple myeloma	GBM, ovarian, prostate, melanoma	(78, 92), (103), (104, 105)
ANXA8	Ovarian, gastric, pancreatic	Cholangiocarcinoma	(92), (106), (107), (108)
ANXA9	Colorectal	Head and neck squamous cell carcinoma	(109), (110)
ANXA10	Head and neck, thyroid	Liver, bladder, gastric	(78), (110), (111), (112), (113)
ANXA11	Ovarian, glioma, liver, gastric		(92), (114), (115), (116)
ANXA13	Cholangiocarcinoma, colorectal	Ovarian	(117), (118), (92)

ANNEXIN A7

ANXA7, previously known as synexin, was the first annexin to be discovered. Structurally, ANXA7 contains the longest N-terminal domain of all the annexins, about 200 amino acids long, and is known to bind membranes in a calcium-dependent manner. Like other annexins, ANXA7 is involved in exo- and endocytosis, calcium channel homeostasis, and has additional unique functions like chromaffin granule aggregation and platelet aggregation (104).

ANXA7 is located on chromosome 10q21 and spans a total of 14 exons. *ANXA7* is alternatively spliced by a pre-mRNA processing molecule, polypyrimidine tract–binding protein 1 (PTBP1), into two isoforms - a longer isoform containing cassette exon 6 (I1) and/or a shorter isoform lacking the cassette exon (I2) with molecular masses of 51 and 47 KDa respectively. ANXA7 is predominantly found in the cytosol and is associated with membranous and vesicular structures. ANXA7 expression is tissue-specific – while I2 alone is found ubiquitously, both I2 and I1 together are found in the brain and heart, and I1 exclusively in the mature skeletal muscle (119). In the human brain, ANXA7 is found exclusively in astroglial cells and modulates calcium-dependent signaling processes and astrocyte proliferation (119).

AS of *ANXA7* is lineage specific – I1 expression is predominantly observed in normal brain tissue while I2 expression is observed in astrocytes, neural and glial precursor cells suggesting that this patterned expression of splice variants could be restricted to lineages that could potentially give rise to GBM (120). Interestingly, monosomy of chromosome 10, where *ANXA7* is located, is a frequent event in GBM with the resultant haploinsufficiency of *ANXA7* inadequate to sustain its tumor suppressive

effect. Concurrently, an increase in EGFR protein levels and signaling was observed indicating that a tumorigenic synergism existed between *ANXA7* loss and *EGFR* amplification that potentiated GBM tumorigenicity (121). Ferrarese et al. found that GBMs expressed high levels of PTBP1 that mediated *ANXA7* exon skipping in favor of I2 with a subsequent increase in EGFR signaling due to failure in lysosomal sorting for degradation. Re-introducing I1 into GBM cells leads to EGFR signaling attenuation and a consequent decrease in tumor size and angiogenesis indicative of the tumor suppressive effect of I1. They concluded that the AS of *ANXA7* in GBM is lineage specific, where splicing traits are inherited from GBM precursor cells and exploited to promote tumor progression via EGFR signaling (120).

RATIONALE FOR RESEARCH

The research presented in this dissertation dissects the mechanism by which I1 acts as a tumor suppressor by regulating RTK signaling in GBM. Previous work from our group has established that *ANXA7* isoforms differentially regulate EGFR fates in GBM and that dysregulated splicing in favor of I2 is a mechanism selected for by GBM cells. How and why *ANXA7* isoforms regulate divergent EGFR fates in GBM remains unclear. Based on our previous findings, we hypothesize that ANXA7-I1, by virtue of the 22 amino acids encoded by cassette exon 6, binds to multiple RTKs and targets them for endosomal degradation suppressing GBM tumorigenicity.

Herein, we reintroduced I1 into GBM cells and observed how *ANXA7* isoforms dictated the fates of multiple RTKs such as EGFR, MET, PDGFRα, and EGFRvIII. Our

findings provide evidence that GBM cells manipulate AS of *ANXA7* that can rewire protein interaction networks altering the fates of these receptors such that they permit GBM progression.

CHAPTER 2

ALTERNATIVE SPLICING OF ANXA7 DICTATES RECEPTOR TYROSINE KINASE FATES IN GLIOBLASTOMA

by

SINDHU NAIR, VINESH PULIYAPPADAMBA, CENTDRIKA HURT, SUSAN E. NOZELL, RAJANI RAJBHANDARI, CHAMPION DEIVANAYAGAM, NORBERT SCHORMANN, JAMES A. BONNER, MARKUS BREDEL

Submitted to *Nature Neuroscience*

Format adapted for dissertation

ABSTRACT

Tissue regulated splicing is a tightly regulated process in the brain to maintain tissue identity and generate cell-specific isoforms of key proteins that regulate various cellular processes. Aberrant alternative splicing (AS), a frequent occurrence in glioblastoma (GBM), manipulates splicing in favor of isoforms that sustain tumor phenotypes by rewiring protein interactions. Annexin A7 (ANXA7) is a hydrophilic protein that binds membranes in a calcium-dependent manner, and it is important for membrane scaffolding and vesicle trafficking. *ANXA7* is spliced by PTBP1 in a lineage-specific manner into two isoforms - isoform 1 (I1), containing a cassette exon, or isoform 2 (I2) lacking the cassette exon. In GBM, *ANXA7* isoforms have contrasting impacts on EGFR signaling - I1 is tumor suppressive by inhibiting EGFR signaling while I2 augments EGFR signaling. Unfortunately, in GBM, high levels of PTBP1 ensure splicing of *ANXA7* in favor of I2 leading to perpetual signaling. By reintroducing I1 into GBM cells, we show, both structurally and functionally, how I1 acts as a master regulator of RTK signaling by mediating the sorting of multiple RTKs such as EGFR, MET, PDGFRα, and EGFRvIII for lysosomal degradation thereby abrogating signaling. In contrast, we find that RTKs are recycled in cells expressing I2. We show that knocking down I1 causes GBM cells to revert to an I2 phenotype by promoting recycling sustaining RTK signaling. Finally, we show that the cassette exon region in I1 encloses a domain that potentially interacts with RTKs and components of the endocytic machinery conferring it with the ability to target RTKs for lysosomal degradation. Collectively, we provide critical insight into how GBM cells exploit AS in favor of isoforms that perpetuate tumor growth and how targeting AS to retain tumor suppressive isoforms is a rational basis for therapeutic investigation.

INTRODUCTION

Alternative splicing (AS) is a post-transcriptional mechanism by which a single gene can generate multiple mRNAs isoforms and resultant protein products (1-3). An estimated 90-95% of human genes undergo AS, underscoring its role in the expansion of the proteome (4, 5). A tightly regulated process, AS impacts protein-protein interactions wherein transcripts can act as functional isoforms mediating similar functions, as functional alloforms mediating divergent functions, or where interaction partners of one isoform can interact with the other isoform (6, 7). Mutations or splicing defects in any component of the spliceosome machinery can disrupt AS leading to aberrant protein products or interactions, a mechanism that has been implicated in human tumorigenesis (2, 8, 9).

AS occurs at a significantly higher rate in complex tissues like the brain, testes and skeletal muscle (4, 8). In the brain, AS events are highly conserved and essential for neuronal differentiation and plasticity (10, 11). Genome-wide studies comparing splicing events in the normal brain and gliomas have shown aberrant AS to act as oncogenic drivers in glioma pathogenesis and progression (12-14). We previously reported that monosomy of chromosome 10 in GBM causes haploinsufficiency of the tumor suppressor gene Annexin A7 (*ANXA7*) with resultant augmentation of epidermal growth factor receptor (EGFR) signaling, a paradigmatic receptor tyrosine kinase (RTK) (15). ANXA7, a member of the annexin family, is a hydrophilic protein that binds membranes in a calcium-dependent manner and plays a role in membrane scaffolding and vesicle trafficking (16, 17). *ANXA7* is alternatively spliced into two isoforms by pre-mRNA binding protein polypyrimidine tract-binding protein 1 (PTBP1): a longer isoform

containing a cassette exon 6 (I1) or a shorter isoform lacking the cassette exon (I2). We have shown that elevated expression of PTBP1 in GBM was associated with preferential splicing of ANXA7 into I2 consequently enhancing EGFR signaling and tumor growth (18, 19). This splicing event occurs in a lineage-specific fashion in GBM cells and GBM-initiating precursor cells but not in mature neurons (18). Restitution of I1 in GBM cells leads to abrogation of EGFR signaling and a decrease in tumor growth and angiogenesis suggesting that I1 has tumor-suppressive capabilities in GBM (18). How and why ANXA7 isoforms regulate divergent EGFR fates in GBM remains unclear. Herein, we demonstrate how ANXA7 isoforms dictate the fates of multiple tumorigenic RTKs in glioma cells such as EGFR, Mesenchymal epithelial receptor (MET), platelet-derived growth factor receptor alpha (PDGFRα), and EGFR variant III (EGFRvIII). Our findings provide evidence that GBM cells manipulate lineage-specific AS of ANXA7 into isoforms that rewire receptor-endocytosis interaction networks leading to divergent fates of these receptors driving GBM progression.

RESULTS

I1 downregulates RTK signaling via lysosomal degradation.

We previously showed that ANXA7-I1 represses EGFR signaling in GBM cells by targeting it for lysosomal degradation (18). This observation prompted us to further investigate if ANXA7-I1 similarly regulates other tumorigenic RTKs in GBM cells, including MET, PDGFRα, and EGFRvIII. We transfected multiple GBM cells lines expressing endogenous I2 with empty vector (EV), ANXA7-I2 (I2), or ANXA7-I1 (I1)

(Supplemental Fig 1). Additionally, we created a Tet-inducible system to overexpress the ligand-independent, mutant EGFRvIII in GBM cells; tetracycline binds with the Tet repressor leading to the activity of the promoter and expression of EGFRvIII. Since EGFRvIII exhibits a deletion of exons 2-7 of the *EGFR* gene, it renders the mutant receptor incapable of binding ligand and therefore Tet activation was used as a signal activation timepoint.

To observe if I1 impacted RTK levels in GBM cells, we stimulated EV and I1 cells with the respective ligands for EGFR (EGF), MET (HGF), and PDGFRα (PDGFA) and tetracycline for EGFRvIII cells. We observed a sustained reduction in both activated and total RTK levels in a time-dependent manner in I1 cells compared to the EV cells indicative of signaling attenuation due to receptor degradation (Fig 1 A-B). The impact of I1-mediated downregulation of RTKs was confirmed independently in multiple GBM cell lines modified to express I1 (Supplemental Fig 2). To confirm if the receptors were indeed being sorted for lysosomal degradation, we assessed the colocalization of RTKs with LAMP1, a lysosomal marker, and used appropriate degradation timepoints for each RTK. We observed colocalization of RTKs with LAMP1 exclusively in I1 cells confirming sorting for degradation; this was absent in EV cells (Fig 1C). We speculated that I1 regulates RTK sorting by potentially binding to the lysosomes. To test this, we used a proximity ligation assay (PLA) that detects protein-protein binding. We found positive ANXA7-LAMP1 interactions specifically in the I1 cells; a complete absence of interaction was observed in the EV cells indicating that I1 plays a direct role in sorting RTKs to the lysosomes for degradation (Fig 1D). Collectively, these data show that re-

introducing I1 in GBM cells leads to the downregulation of multiple RTKs via I1-mediated sorting to the lysosomes.

I1 binds to and maintains sustained interactions with multiple RTKs.

To define the binding interactions between RTKs and I1 or I2, we used PLA and co-immunoprecipitation (co-IP) assays. We first assessed ANXA7-RTK binding in I1, and EV cells using PLA and found that post-ligand stimulation, positive interactions were seen with respect to all RTKs indicating that both isoforms are bound to RTKs post-activation (Fig 2A). Next, we used co-IP to investigate ANXA7-RTK interactions before and after ligand stimulation. We found that isoform-RTK binding dynamics varied from receptor to receptor. Post-activation, all RTKs strongly interacted with I1; however, in EV cells only PDGFRα and EGFRvIII showed an increase in binding with I2 post-activation, while a decrease in interaction was observed with respect to MET and EGFR (Fig 2B). In the absence of ligand stimulation, positive interactions were evident only in EGFR, EGFRvIII, and MET in I1 cells; in the EV cells, only EGFR and EGFRvIII interacted with I2 pre-activation. The interactions between ANXA7 isoforms and RTKs thus vary depending on receptor activation status and are RTK-specific.

Since ANXA7 is known to bind phospholipids and mediate membrane vesicle aggregation and since RTKs are internalized into vesicles post-activation, we sought to determine if ANXA7-RTK interactions occurred early in this internalization process. We found that RTKs and ANXA7 co-localized with each other in clustered endocytic pits at the plasma membrane in both EV and I1 cells as early as 5 minutes post-ligand

stimulation indicating that ANXA7 isoforms interact with proteins regulating the internalization process (Fig 2C). These results indicate that while both isoforms of ANXA7 bind RTKs, this interaction is strengthened in I1 cells post-receptor activation with subsequent clustering of the ANXA7-RTK complexes in vesicles indicating a potential role of ANXA7 isoforms in the internalization of RTKs.

RTKs are recycled via fast and slow recycling pathways in cells expressing I2.

Post activation, RTKs are internalized and sorted to the early endosome (EE), where they can undergo two fates: they can be trafficked to the lysosomes for degradation or recycled back to the surface for subsequent activation (20, 21). Since we found that RTKs were not sorted for degradation in the I2 cells, we hypothesized that sustained signaling observed in these cells could be due to receptor recycling. Receptor recycling is facilitated by small GTPases Rab11 and Rab4 that regulate slow and fast recycling pathways, respectively (22, 23). We assessed the colocalization of RTKs with Rab11- and Rab4-tagged recycling endosomes in cells expressing either EV or I1 post-ligand stimulation (Fig 3A-B). The staining patterns for slow and recycling endosomes differ in that Rab4-lined vesicles tend to aggregate at the cell surface while Rab11-lined slow recycling endosomes localize in the peri-nuclear region. Upon ligand stimulation, we found that RTKs colocalized with recycling endosomes, both slow and fast, exclusively in the EV cells expressing I2. This phenomenon was time-dependent and varied from RTK to RTK: colocalization with Rab11 peaked at 60 minutes with respect to EGFR, MET, and EGFRvIII, while PDGFRα sorted as early as 30 minutes. With regards to Rab4, colocalization was evident between 5 and 10 minutes for EGFR, PDGFRα, and

EGFRvIII, and between 15 and 20 minutes for MET. Collectively, while recycling was observed with all RTKs in EV cells, the temporal pattern differed between RTKs.

To delineate the mechanism behind RTK recycling in I2 cells, we chose to initially focus on the trafficking of EGFR as a paradigmatic RTK. We inhibited recycling using monensin, which prevents the sorting from the early endosomes to the recycling endosomes (24, 25). We pre-treated EV cells with monensin followed by EGF stimulation and then assessed activated and total EGFR levels. In the monensin-treated cells, we observed a 60% increase in EGFR levels at 120 minutes as compared to cells treated with vehicle control (Fig 3C-D). In addition, activated EGFR levels were significantly higher in monensin-treated cells at this timepoint. We confirmed the impact of monensin on the recycling of PDGFRα, MET, and EGFRvIII and found a similar increase in total levels of each RTK specifically in monensin-treated EV cells (Supplemental Fig 3). Intriguingly, we also found an increase in EGFRvIII in monensin-treated I1 cells. Studies have shown that EGFRvIII is almost always recycled due to low levels of E3 ubiquitin-protein ligase Cbl along with a hypophosphorylation at residue Y1045 leading to impaired lysosomal sorting and constitutive signaling (26-28). While overexpression of I1 in EGFRvIII cells downregulated signaling to an extent, some recycling was still evident in these cells explaining the monensin-induced increase of EGFRvIII in I1 cells.

Next, we hypothesized that EGFR levels might increase in monensin-treated cells due to its prolonged retention in the early endosomes within which it can continue signaling. We co-immunostained EGFR with Rab4 and Rab11 in EV cells with or without monensin treatment followed by EGF stimulation. EGFR failed to colocalize

with the recycling markers in monensin-treated cells indicative of failed sorting to the recycling endosomes. At the same timepoint (60 minutes), we found positive colocalization between EGFR and EEA1 (and early endosomal marker) suggesting that EGFR was instead being retained in the early endosome (Fig 3E). Collectively, these data establish that RTKs are sorted from the early endosomes to the fast and slow recycling endosomes exclusively in cells expressing I2 and inhibition of recycling causes RTKs to be retained in the early endosomes with failure of sorting to the slow and fast recycling endosomes. Therefore, ANXA7 isoforms act as functional alloforms by having divergent impacts on RTK fates in GBM cells: recycling in I2 cells contrasted with degradation in I1 cells.

Loss of I1 impairs EGFR sorting to the lysosomes and promotes recycling.

Having established that I1 and I2 have distinct effects on RTK signaling and sorting dynamics, we again chose to focus upon EGFR signaling and use it as a model to better understand how ANXA7 isoforms regulate receptor fates.

We first assessed the impact of ANXA7 depletion on EGFR degradation and trafficking by using a siRNA that knocks down both isoforms of ANXA7. We observed about a 40% increase in total EGFR levels in the I1/siANXA7 cells at the end of 60 minutes post-EGF stimulation suggesting failure of EGFR degradation in the absence of I1; EGFR levels remained unaffected in I2/siANXA7 cells (Fig 4 A-B). Additionally, we confirmed the impact of I1 knockdown on RTK degradation with respect to MET, PDGFRα, and EGFRvIII and observed a similar stabilization of RTK levels in

I1/siANXA7 cells, albeit to a lesser extent in EGFRvIII cells, indicating that downregulation of RTKs is regulated by I1 (S.Fig 4).

We next sought to confirm the impact of ANXA7 knockdown on EGFR trafficking by tracking its sorting to the early endosome, which is a common sorting station for both I2 and I1 post-internalization. While ANXA7 knockdown did not seem to impact the sorting of EGFR to the early endosome in the EV cells, it significantly impaired sorting in the I1/siANXA7 cells as compared to the control cells (Fig 4C). Quantification of colocalization revealed an about 40% decrease in EGFR-early endosome overlap in I1/siANXA7 cells (Fig 4D). Consequently, we tracked sorting to the lysosomes using the appropriate degradation timepoints for EV and I1 cells. EGFR also failed to colocalize with lysosomal marker LAMP1 in the I1/siANXA7 cells while sorting remained unaffected in the I2/siANXA7 cells (Fig 4E). These results suggest that I1 plays a role early in the endocytic process and is necessary for trafficking EGFR to the early endosome and subsequently to the lysosome. Since EGFR failed to sort to the lysosomes in the absence of I1, we questioned if EGFR was instead being recycled in these cells. Using similar timepoints, co-immunostaining of EGFR with Rab11 confirmed that EGFR indeed colocalized with recycling endosomes in I1/siANXA7 cells compared to control cells where colocalization was completely absent (Fig 4F). Together, these results show that I1 regulates the sorting of EGFR to the early endosome and lysosomes for degradation. While ANXA7 depletion does not appear to impact trafficking in cells expressing I2, deeming I2 inconsequential for sorting, EGFR is instead rerouted to the recycling pathway in I1 expressing cells augmenting signaling and thereby escaping the tumor suppressive effect of I1.

I1-mediated degradation of EGFR is clathrin-dependent.

Since the loss of ANXA7 impacted EGFR sorting to the early endosome in the I1 cells, we sought to determine if I1 was necessary for the internalization of EGFR at the cell surface post-activation. Endocytic internalization can be broadly classified as clathrin-mediated endocytosis (CME) or non clathrin endocytosis (NCE) (29-31). CME entails the internalization of RTKs into clathrin-coated pits, while NCE uses lipid raft-dependent mechanisms (32, 33). A large body of evidence points to CME acting as the major pathway for RTK internalization (29, 34, 35). However, clathrin depletion studies have shown that RTKs can also be internalized via NCE (34, 36). To delineate if ANXA7-mediated EGFR internalization relies on CME or NCE, we studied the colocalization of RTKs with clathrin (CME) or caveolin-1 (NCE) post-ligand stimulation in a time-dependent manner. Positive colocalization with clathrin was observed with respect to all RTKs in both I1 and EV cells (Fig 5A). However, colocalization with caveolin was absent for all RTKs except PDGFRα, which exhibited some colocalization (Supplemental Fig 5). Thus, CME appears to be the predominant pathway for ANXA7-mediated internalization of RTKs in GBM cells.

Next, we sought to assess if ANXA7 isoforms temporally regulate RTK internalization via CME. We again chose to focus on EGFR signaling. We observed a rapid and significantly higher rate of EGFR colocalization with clathrin as early as 5 minutes in I1 cells, while colocalization began at 10 minutes and peaked at 20 min in I2 cells (Fig 5B-C). Consequently, we found an increase in clathrin levels in I1 cells post-EGF stimulation suggesting a strong interaction between I1 and clathrin while internalizing EGFR (Fig 5D). We used a PLA to ascertain the ANXA7-clathrin

interaction and found significantly higher interaction in I1 cells at 10 minutes compared to EV cells indicating that I1 enhances the trafficking of EGFR to clathrin pits post-receptor activation (Fig 5E-F).

To confirm that CME was essential for I1-mediated sorting of EGFR to the early endosome, we used Pitstop2, a clathrin inhibitor (35). We observed significantly higher EGFR levels at 60 minutes post-ligand activation in Pitstop2-treated I1 cells indicating a possible failure of internalization and retention at the surface; EGFR levels remained unaffected in EV cells (Fig 5G). Finally, we investigated if ANXA7 depletion hampered the internalization of EGFR into clathrin pits. We treated EV and I1 cells with control or siANXA7 and monitored colocalization of EGFR with clathrin post-EGF stimulation (Fig 5H). EGFR failed to colocalize with clathrin specifically in I1/siANXA7 cells indicating that I1 is vital for EGFR internalization into clathrin pits. However, colocalization was evident in EV/siANXA7 cells indicating that I2 is not necessary for EGFR to associate with clathrin. Collectively, these results demonstrate that I1-mediated EGFR sorting and degradation is clathrin-dependent and loss of I1 causes failure of EGFR endocytosis, prolonging signaling at the cell surface.

Truncated I1 fails to sort EGFR for lysosomal degradation and instead sorts to the recycling endosomes.

Structurally, the inclusion of cassette exon 6 (encoding amino acids 145-167) is the only difference between I1 and I2 (Fig 6A). Since we observed RTK degradation only in cells expressing I1, we hypothesized that the amino acids encoded by exon 6 are

critical for I1-mediated sorting of RTKs for lysosomal degradation. To dissect the structural requirements essential for this mechanism, we again chose to focus on EGFR signaling and used Hek293T cells, which do not express EGFR but express endogenous I2. We created two truncated I1 mutants with deletions in the exon 6-encoded region, lacking amino acids 145-156 (I1-Δ1) or amino acids 157-167 (I1-Δ2) (Fig 6A). Hek293T cells were first transfected to express EGFR and then co-transfected with either an EV, full length I1 (I1-FL), I1-Δ1, or I1-Δ2 (Supplemental Fig 6A-B). We first compared EGFR levels between EV and I1-FL cells and found that introducing I1 into Hek293T cells leads to a sustained reduction in both activated and total EGFR levels, recapitulating our GBM model (Supplemental Fig 6D-E).

Next, we compared EGFR levels in our full length and truncated I1 models post EGF stimulation in a time-dependent manner. Compared to I1-FL or I1-Δ2 cells, we observed significantly high levels of activated and total EGFR in I1-Δ1 cells (Fig 6B-C). While degradation of EGFR was almost complete in I1-FL and I1-Δ2 cells at 120 minutes, EGFR levels remained consistently high in I1-Δ1 cells indicating a possible failure of degradation. We thus speculated that the motif necessary for I1-mediated degradation of EGFR localizes to the region of exon 6 encoding amino acids 145-156.

To monitor EGFR trafficking dynamics in EV, I1-FL, I1-Δ1, and I1-Δ2 cells, we co-stained EGFR with EEA1 or LAMP1 (Fig 6D). EGFR colocalized with EEA1 in EV, I1-FL, and I1-Δ2 cells indicating efficient sorting to the early endosome; in I1-Δ1 cells, EGFR remained localized at the cell surface indicating a delay in internalization (Fig 6D, top panel). At 30 minutes, colocalization with lysosomes was only observed in I1-FL and I1-Δ2 cells indicating the commencement of degradation (Fig 6D, bottom panel). In the

I1-Δ1 cells, EGFR exhibited continued surface retention at 30 minutes suggesting a delay or failure to be internalized and sorted for degradation. Due to the absence of lysosomal sorting in EV and I1-Δ1 cells, we investigated if EGFR was being recycled in these cells reminiscent of I2-expressing GBM cells. We stimulated EV, I1-FL and I1-Δ1 cells and co-stained EGFR with Rab4 or Rab11 (Fig 6E top; bottom). I1-Δ2 cells were not included as sorting and degradation of EGFR remained unaffected even in the absence of AA 157-167. We observed that EGFR co-localized with both Rab4- and Rab11-lined vesicles exclusively in EV and I1-Δ1 cells indicative of recycling akin to the I2-expressing cells. These results recapitulate what we observed in the GBM cells and indicate that the region within exon 6 that encodes amino acids 146-156 contains a motif that regulates EGFR sorting to the lysosomes. In the absence of this motif, EGFR is internalized at a slow rate and rerouted to the recycling pathway leading to unabated signaling.

ANXA7-I1 encodes a secondary structure amenable to form isoform-specific protein interactions.

Since we found that ANXA7 isoforms exhibited differential protein-protein interactions (PPI) leading to divergent RTK fates, we compared the protein structures of the isoforms to model whether the region encoded by the cassette exon allowed for isoform-specific PPI. As the ANXA7 protein has not been crystallized, we employed a hierarchical approach to protein structure prediction of the two isoforms using I-TASSER and the SWISS-MODEL server (37). The latter contained well-characterized models for the C-terminal domain spanning residues which are common to all members of the

Annexin family. We compared our C-terminal domain modeling on I-TASSER with the established models on the SWISS-MODEL server and found consistent secondary and tertiary structural architecture.

I2 contained two distinct domains, the N-terminal domain spanning residues 1-145, and the C-terminal domain containing the repeats spanning residues 167-488 (Fig 7A). The N-terminal domain of I2 contained a mixture of α-helices and β-sheets that appeared to form a stable fold. The N- and C-terminal domains were connected by a loop region resulting in multiple areas of contact and rendering an overall compact structure.

While the N-terminal (1-145) and C-terminal (167-488) domains adopted similar conformations in I1, the region encoded by cassette exon 6 (146-167) formed a helical segment, indicating the inherent propensity to form a secondary structure (Fig 7B). Intriguingly, this resulted in the N-terminal domain moving away from the C-terminal repeats thereby opening up a domain for potential interactions with other proteins. These structural models indicate that the secondary structure present in I1 and absent in I2 exposes short linear motifs within this region that can mediate interactions with peptides or domains of other proteins. Presumably, AAs 145-156 (Fig 6) in this secondary structure is necessary for PPI with RTKs and/or partners of the endocytic pathway during the process of I1-mediated RTK degradation. Collectively, these results indicate that the inclusion or exclusion of the cassette exon 6 during the lineage-specific AS of ANXA7 affects domain structure, rewires PPI networks, and dictates the fate of RTKs in GBM.

DISCUSSION

In this study, we elucidate, structurally and functionally, how lineage-specific alternative splicing of ANXA7 differentially impacts RTK trafficking and how GBMs benefit from aberrant AS in favor of I2, thereby subverting the inhibitory effect of I1 and promoting pro-tumorigenic signaling (Fig 8). Restitution of I1 in GBM cells is sufficient for tumor suppression by targeting multiple RTKs for endosomal degradation.

Approximately 60% of GBMs exhibit amplifications in oncogenic RTKs such as EGFR, MET, PDGFRα, and FGFR suggesting that their dysregulation is a major driver of gliomagenesis and progression (38-40). Additionally, EGFRvIII, a truncated mutant of EGFR, is a commonly occurring mutation in GBM (41-43). This constitutively active receptor enhances the tumorigenic potential of gliomas by virtue of its impaired internalization and degradation (26, 27). More importantly, genetic heterogeneity, where different RTKs are amplified in adjacent cell subpopulations within the same tumor, confers insensitivity to targeted therapies inhibiting a specific RTK (40). RTK coactivation or oncogenic switching are mechanisms by which glioma cells limit the efficacy of targeted inhibition by employing alternative or concurrent RTKs for pro-survival signaling (44-47). This clinical conundrum necessitates the need to understand tissue-specific conserved regulatory mechanisms that inhibit RTK signaling in order to develop therapeutic strategies that broadly target RTKs.

Comprehensive analyses have shown a significantly higher number of AS events occurring in cancers as compared to normal tissues underscoring their role in tumorigenesis and progression (48, 49). AS of RTK genes with their resulting impact on tumor growth and acquisition of drug resistance have been widely reported (13, 50-53).

However, AS events in genes that regulate RTKs post-activation remain understudied. Our study establishes AS of membrane-binding protein ANXA7 as a tissue-specific determinant of endocytic sorting of multiple RTKs in GBM. We define a novel mechanism by which two alloforms of a common endocytic regulator exert diverging functions on RTK fates in these challenging neoplasms. We demonstrate how a tissue-regulated splicing mechanism that is present in the tissue of GBM origin, when subverted, provides a selective advantage to GBM cells and, if reversed, may offer an avenue that could be potentially exploited therapeutically.

Interestingly, we see that phosphorylated RTK levels, in addition to total RTK levels, are also significantly lower during ANXA7 I1-mediated sorting. This could be possibly due to rapid sorting of the receptor to the early endosome or abrogation of RTK phosphorylation by I1 upon binding, which we intend to further investigate. Additionally, while both isoforms bind and internalize RTKs, only I1 has the ability to traffic RTKs to the lysosomes by forming an RTK-I1-lysosome complex. We presume I1 facilitates the interaction between the receptor and lysosome by acting as a scaffolding protein. This phenomenon has been previously observed for ANXA5 and ANXA6 which act as scaffolds for protein kinase C (PKC) translocation and signaling (54-56). Conversely, RTKs were recycled in cells expressing I2 indicating that the absence of the cassette exon deviates RTKs to the recycling pathway in order to sustain RTK signaling. Importantly, inhibiting recycling in these cells did not re-route EGFR to the lysosomal pathway confirming that the sequence necessary for lysosomal sorting is contained in the region encoded by the cassette exon present in I1 and spliced out in I2. Interestingly, Tanowitz et al reported divergent post-endocytic sorting fates for alternatively spliced G-protein

coupled receptor Mu-type opioid receptor (MOR1) that failed to recycle when exon 4 was spliced out. They concluded that the recycling sequence was localized to the exon 4 region of the MOR1 gene and was necessary for recycling to occur (57).

Loss of ANXA7 impacted internalization and degradation exclusively in I1 cells emphasizing the necessity of the sequence encoded by the cassette exon region for lysosomal sorting. Interestingly, EGFR was rerouted to the recycling pathway in the absence of I1 indicating that recycling could be an ANXA7-independent process that we found was unhindered in I2 cells even with ANXA7 depletion. This further suggests that I2 is largely non-functional in the sorting process of RTKs and is, therefore, the preferred isoform that GBM cells select for to drive transforming pathway signaling.

Multiple studies have shown that the decision regarding RTK fate, recycling or degradation, is made early in the endocytic process during CME and involves the recognition of endocytic sorting signals or tags by clathrin that are specific for recycling or degradation (58-60). Annexin family members have well-documented roles in the endocytic process with ANXA2 and ANXA6 shown to not only interact but deemed necessary for clathrin budding and assembly (61-64). Our observations add to this consensus by showing that an EGFR-I1-clathrin complex is formed immediately post-receptor activation. We propose that I1-mediated clathrin endocytosis is a two-fold mechanism: first, since I1 has a stronger interaction with clathrin early in the CME process, it accelerates the internalization of EGFR; second, depleting ANXA7 in I1 cells caused a failure of EGFR sorting to the early endosome and subsequently to the lysosomes. This mechanism would rely on a specific degradation motif being localized to the cassette exon 6-encoded region and is supported by our truncated I1 models where an

N-terminal truncation of 11 amino acids in the exon 6-encoded region of I1 caused the failure of EGFR degradation. Strikingly, this deletion was also sufficient to reroute EGFR to the recycling pathway and to augment signaling. Our isoform-based structural modeling further supports the notion of an endocytosis-determining binding motif within the cassette exon-encoded region. An increasing body of evidence shows how isoforms have different protein interaction profiles due to the inclusion or exclusion of cassette exons (65, 66). Tissue-specific exon splicing can give rise to isoforms that contain protein segments with conserved binding motifs or "interaction-promoting" regions which in turn rewire protein networks (6, 67). We speculate that the secondary structure formed in the cassette exon region in I1, and absent in I2, encodes a binding motif that interacts with a conserved RTK and/or endocytic motif to mediate degradation.

Several studies have identified a conserved mechanism for RTK endocytosis involving the activation of RTK microdomains and multiple downstream adaptor proteins including the Cbl and ubiquitin families (29, 68-72). The involvement of I1 in multiple steps of the endocytic process consolidates its role as a scaffold protein that steers the interaction of RTKs with various elements of the endocytic pathway necessary for lysosomal targeting. Further studies will be necessary to investigate how I1 interacts with other components of the endocytic machinery. Finally, elucidating potentially conserved motifs within EGFR, PDGFRα, MET, and EGFRvIII, which we presume could be putative binding sites for I1, will help to fully define the I1-RTK crosstalk.

In summary, our findings describe how tissue-dysregulated splicing of a tumor suppressor gene can generate protein variants with altered or divergent functions in endocytic sorting and thus drive RTK fate to establish a favorable environment for

tumorigenesis. Our work adds to the growing body of evidence that implies that subversion of tissue-specific AS mechanisms can act as complementary oncogenic drivers.

MATERIALS & METHODS

Cell lines & treatments

U251-MG, SNB19-MG, LN229, U87, and Hek293T were purchased from ATCC and maintained in 1X DMEM (Gibco) supplemented with 10% FBS (Sigma) and 5% Penstrep (Fisher). U251/EGFRvIII cells were maintained in Zeocin (Invitrogen) supplemented media (1 ug/ml). Cells were cultured in serum-free conditions for at least 16 hours before stimulation with ligands (20 ng/ml) for western blotting, immunofluorescence, and proximity ligation assays. For treatments with chemical compounds – cells were pretreated with recycling inhibitor Monensin (100μM) for 20 minutes, clathrin inhibitor Pitstop2 (20μM) for 15 minutes. Knockdown of ANXA7 was achieved using a scramble or siRNA (Dharmacon, M-010760-01) for 48 hours in Lipofectamine before ligand stimulation and knockdown was verified using western blotting.

Transfection and Viral Infection

Glioma cells overexpressing I1 or I2 - ANXA7-I1, ANXA7-I2, and/or an empty vector were overexpressed using a lentiviral vector (pCHMWS) with an EGFP tag. Lentiviral particles were prepared in Hek293T cells using packaging plasmids (pMD2.G and psPAX2) and were collected and filtered. GBM cells were infected using lentiviral

particles supplemented with polybrene (8 μg/ml, Sigma). GFP-positive cells were sorted using a flow cytometer (BD FACS Aria II) and expanded to create a stable cell line.

U251/EGFRvIII expressing cells - U251-MG cells were transfected with a regulatory plasmid (pcDNA6/TR), which encodes the tetracycline repressor. Next, cells were co-transfected with pcDNA4/TO/EGFRvIII followed by Zeocin selection. For initiation of EGFRvIII signaling 1 ug/ml of fresh Tetracycline was added to the media and inducibility was confirmed using western blotting.

ANXA7-I1 mutant models – Hek293T cells were transfected with EGFR-GFP (kindly provided by Alexander Sorkin, Addgene #32751) and GFP positive cells were sorted using flow cytometry. Subsequently, EGFR expressing cells were co- transfected with either an empty retroviral vector (pBabe kindly provided by Hartmut Land, Jay Morgenstern & Bob Weinberg, Addgene #1764), full-length I1 (pBbae-I1), or modified using Q5 site-directed mutagenesis kit (New England Biolabs) to express mutant I1. Primers for the deletion models are as follows – I1-Δ1 - AA 145-156 (F – TTCTCTCCTGTTTCTTTG, R – CTGACTAGGGTAAGTAGG); I1-Δ2 – AA 157-167 (F – CCTGCCACAGTGACTCAG, R - AACAGGATAGGAAGAAAAAGAATCTG). Positive clones were selected by Puromycin treatment (0.5 μg/ml) and verified by western blotting for ANXA7 expression. Lipofectamine was used for all transfections.

RTK Stimulation, Immunoblotting, and co-immunoprecipitation

GBM cells were grown to 70% confluency and serum starved for at least 16 hours followed by ligand stimulation with EGF, HGF, PDGFA (Biolegend, 20 ng/ml) or Tet (1 μg/ml). Whole cell lysate was collected in RIPA buffer supplemented with protease

inhibitor cocktail (100nM PMSF, 100mM sodium orthovanadate, 2.5 mg/ml aprotinin, 2.5 mg/ml leupeptin, 5nM Sodium Fluoride). Protein was resolved through SDS-PAGE under denaturing conditions, transferred to polyvinylidene difluoride (PVDF) membranes, and blocked in 5% non-fat milk in TBS-T. The following antibodies were used in immunoblotting analyses: ANXA7 (Santa Cruz, 17815), EGFR (Cell Signaling,4267) pEGFR (Y1068, Cell Signaling, 3777), PDGFRα (Cell Signaling, 3174), pPDGFRα (Cell Signaling, 2992), MET (Cell Signaling, 8198) pMET (Cell Signaling, 3133/3135), EGFRvIII (Novus Biologicals, 50599), β-actin (Cell Signaling, 3700) and α-tubulin (Cell Signaling, 3873). Incubation with HRP-conjugated secondary was performed and protein was detected using ECL chemiluminescence methods (Pierce ThermoScientific). Band densities were quantified using ImageJ software.

For co-IP, cells were washed and lysed in IP lysis buffer (0.1M HEPES, 5M NaCl, 0.5M EDTA, 1% NP-40) containing protease inhibitors. Lysates were disrupted using a 22-gauge needle and centrifuged at 10,000 rpm for 15 minutes at 4°C. Precleared lysates baited with mouse ANXA7 (Santa Cruz, 17815) and incubated with protein G plus agarose beads (Santa Cruz, 2002) overnight at 4°C with gentle rocking. The precipitates were washed the next day thrice with 1 ml lysis buffer, boiled in loading buffer for 8 minutes and subjected to SDS-PAGE and western blot analysis.

Immunofluorescence & confocal microscopy analysis

Cells were grown on autoclaved glass coverslips, serum starved, and treated with the appropriate ligand for each RTK. Cells were washed with cold PBS, fixed in 4% paraformaldehyde (PFA) for 10minutes, and washed again. Cells were then

permeabilized in 0.1% Tween in PBS (PBS-T) for 10 minutes, followed by blocking in 5% bovine serum albumin in PBS-T at room temperature. The following primary antibodies were used for endocytosis assays – EEA1 (Cell Signaling, 3288, 1:100), LAMP1 (Cell Signaling, 9091, 1:200), Rab4 (Novus Biologicals, 74519, 1:100), Rab11 (Cell Signaling, 5589, 1:100), Clathrin (Cell Signaling, 4796, 1:50) and Caveolin (Cell Signaling, 3267, 1:100) at 4°C overnight in blocking solution. The following day, cells were washed three times in PBS-T and incubated in either anti-mouse secondary antibody (Invitrogen, Alexa Flour 594) or anti-rabbit secondary antibody (Invitrogen, Alexa Flour 647) at 1:300 dilution for 1 hour at room temperature. Cells were then washed three times in PBS-T and mounted in Prolong anti-fade diamond mountant with DAPI (ThermoFisher, P36962) and imaged using a Nikon Structured Illumination super-resolution Microscope (SIM). Pearson's coefficient of colocalization was calculated using the NIS-Elements 5.0 imaging software on non-saturated pictures. At least 10-20 cells per field were quantified for each condition.

Proximity ligation assay (PLA)

The cells were grown on glass coverslips, washed, fixed and permeabilized as described above and PLA was performed using the Duolink PLA Fluorescence kit (Sigma, DUO92101). The cells were then blocked in Duolink blocking solution for 60 minutes at 37 °C in a humidified chamber. Primary antibodies used for immunofluorescence were diluted in Duolink antibody diluent at 1:100 along with Phalloidin (Thermofisher, A12381, 1:1000) to cross-stain actin filaments and incubated overnight at 4°C The next day, cells were washed in Duolink buffer A and incubated with mouse plus and rabbit

minus PLA probes for 60 min at 37 °C. After washing in buffer A, the cells were incubated for 30 min at 37 °C in Duolink Ligation buffer diluted in autoclaved water containing ligase. Following ligation, the cells were washed in buffer A, and then incubated for 100 min at 37 °C with the Duolink Amplification buffer containing polymerase. The cells were then washed three times in buffer B and mounted in Prolong anti-fade diamond mountant with DAPI (ThermoFisher, P36962) and imaged using a Nikon-SIM microscope. Quantitative analysis was performed using NIS-Elements 5.0 imaging software; at least 10 cells were assessed for each condition.

ANXA7 Isoform structural analyses

Isoform 1 (P20073: residues 1-487) and isoform 2 (P20073_2: residues 1-465) of human Annexin A7 (ANXA7) differ by an insert of 22 residues (Exon 6). A model for the C-terminal domain (Isoform 1: residue range 169-487; Isoform 2: residue range 147-465) of Annexin A7 is available from the SWISS-MODEL Repository (https://swissmodel.expasy.org/repository) (73) by searching for either 'ANXA7' or 'P20073'. This model is based on sequence homology (45% sequence identity) to human Annexin III (PDB code: 1aii). To model the N-terminal domain and identify the secondary structure of the 22-residue insert we submitted sequences of just the N-terminal domain(s) and also the entire protein for both isoforms to the I-TASSER (Iterative Threading ASSEmbly Refinement) web server (https://zhanglab.dcmb.med.umich.edu/I-TASSER/) (74-75). The models for the N-terminal domains of isoform 1 and isoform 2 were combined with the model for the C-terminal domain and subsequently analyzed.

Statistics

Relative fluorescence intensities, Pearson's colocalization coefficient, and western blotting experiments were compared with controls using the GraphPad Prism software (v.9). Data shown are representative of at least two independent experiments. Error bars represent the standard error of mean. Depending on the number of variables, results were analyzed for statistical significance by paired *t*-test, unpaired *t*-test, or two-way ANOVA. $p \leq 0.05$ was considered significant, with actual values represented by - *p < 0.05, **p <0.01, ***p < 0.001, ****p < 0.0001.

REFERENCES

1. Baralle FE, Giudice J. Alternative splicing as a regulator of development and tissue identity. Nat Rev Mol Cell Biol. 2017;18(7):437-51.
2. Bonnal SC, Lopez-Oreja I, Valcarcel J. Roles and mechanisms of alternative splicing in cancer - implications for care. Nat Rev Clin Oncol. 2020;17(8):457-74.
3. Lee Y, Rio DC. Mechanisms and Regulation of Alternative Pre-mRNA Splicing. Annu Rev Biochem. 2015;84:291-323.
4. Wang ET, Sandberg R, Luo S, Khrebtukova I, Zhang L, Mayr C, et al. Alternative isoform regulation in human tissue transcriptomes. Nature. 2008;456(7221):470-6.
5. Blencowe BJ. Alternative splicing: new insights from global analyses. Cell. 2006;126(1):37-47.
6. Yang X, Coulombe-Huntington J, Kang S, Sheynkman GM, Hao T, Richardson A, et al. Widespread Expansion of Protein Interaction Capabilities by Alternative Splicing. Cell. 2016;164(4):805-17.
7. Tsai CJ, Ma B, Nussinov R. Protein-protein interaction networks: how can a hub protein bind so many different partners? Trends Biochem Sci. 2009;34(12):594-600.
8. Roy B, Haupt LM, Griffiths LR. Review: Alternative Splicing (AS) of Genes As An Approach for Generating Protein Complexity. Curr Genomics. 2013;14(3):182-94.
9. Park E, Pan Z, Zhang Z, Lin L, Xing Y. The Expanding Landscape of Alternative Splicing Variation in Human Populations. Am J Hum Genet. 2018;102(1):11-26.

10. Lopez Soto EJ, Gandal MJ, Gonatopoulos-Pournatzis T, Heller EA, Luo D, Zheng S. Mechanisms of Neuronal Alternative Splicing and Strategies for Therapeutic Interventions. J Neurosci. 2019;39(42):8193-9.

11. Weyn-Vanhentenryck SM, Feng H, Ustianenko D, Duffie R, Yan Q, Jacko M, et al. Precise temporal regulation of alternative splicing during neural development. Nat Commun. 2018;9(1):2189.

12. Chen X, Zhao C, Guo B, Zhao Z, Wang H, Fang Z. Systematic Profiling of Alternative mRNA Splicing Signature for Predicting Glioblastoma Prognosis. Front Oncol. 2019;9:928.

13. Li Y, Ren Z, Peng Y, Li K, Wang X, Huang G, et al. Classification of glioma based on prognostic alternative splicing. BMC Med Genomics. 2019;12(1):165.

14. Xie ZC, Wu HY, Dang YW, Chen G. Role of alternative splicing signatures in the prognosis of glioblastoma. Cancer Med. 2019;8(18):7623-36.

15. Yadav AK, Renfrow JJ, Scholtens DM, Xie H, Duran GE, Bredel C, et al. Monosomy of chromosome 10 associated with dysregulation of epidermal growth factor signaling in glioblastomas. JAMA. 2009;302(3):276-89.

16. Gerke V, Creutz CE, Moss SE. Annexins: linking Ca2+ signalling to membrane dynamics. Nat Rev Mol Cell Biol. 2005;6(6):449-61.

17. Gerke V, Moss SE. Annexins: from structure to function. Physiol Rev. 2002;82(2):331-71.

18. Ferrarese R, Harsh GRt, Yadav AK, Bug E, Maticzka D, Reichardt W, et al. Lineage-specific splicing of a brain-enriched alternative exon promotes glioblastoma progression. J Clin Invest. 2014;124(7):2861-76.

19. Bredel M, Scholtens DM, Harsh GR, Bredel C, Chandler JP, Renfrow JJ, et al. A network model of a cooperative genetic landscape in brain tumors. JAMA. 2009;302(3):261-75.

20. Mellman I, Yarden Y. Endocytosis and cancer. Cold Spring Harb Perspect Biol. 2013;5(12):a016949.

21. Schmid SL. Reciprocal regulation of signaling and endocytosis: Implications for the evolving cancer cell. J Cell Biol. 2017;216(9):2623-32.

22. Grant BD, Donaldson JG. Pathways and mechanisms of endocytic recycling. Nat Rev Mol Cell Biol. 2009;10(9):597-608.

23. Somsel Rodman J, Wandinger-Ness A. Rab GTPases coordinate endocytosis. J Cell Sci. 2000;113 Pt 2:183-92.

24. Nishimura Y, Takiguchi S, Ito S, Itoh K. EGFstimulated AKT activation is mediated by EGFR recycling via an early endocytic pathway in a gefitinibresistant human lung cancer cell line. Int J Oncol. 2015;46(4):1721-9.

25. Wang Y, Pennock S, Chen X, Wang Z. Endosomal signaling of epidermal growth factor receptor stimulates signal transduction pathways leading to cell survival. Mol Cell Biol. 2002;22(20):7279-90.

26. Gan HK, Kaye AH, Luwor RB. The EGFRvIII variant in glioblastoma multiforme. J Clin Neurosci. 2009;16(6):748-54.

27. Grandal MV, Zandi R, Pedersen MW, Willumsen BM, van Deurs B, Poulsen HS. EGFRvIII escapes down-regulation due to impaired internalization and sorting to lysosomes. Carcinogenesis. 2007;28(7):1408-17.

28. Roepstorff K, Grovdal L, Grandal M, Lerdrup M, van Deurs B. Endocytic downregulation of ErbB receptors: mechanisms and relevance in cancer. Histochem Cell Biol. 2008;129(5):563-78.

29. Goh LK, Sorkin A. Endocytosis of receptor tyrosine kinases. Cold Spring Harb Perspect Biol. 2013;5(5):a017459.

30. Johannes L, Parton RG, Bassereau P, Mayor S. Building endocytic pits without clathrin. Nat Rev Mol Cell Biol. 2015;16(5):311-21.

31. Le Roy C, Wrana JL. Clathrin- and non-clathrin-mediated endocytic regulation of cell signalling. Nat Rev Mol Cell Biol. 2005;6(2):112-26.

32. Disanza A, Frittoli E, Palamidessi A, Scita G. Endocytosis and spatial restriction of cell signaling. Mol Oncol. 2009;3(4):280-96.

33. Kumari S, Mg S, Mayor S. Endocytosis unplugged: multiple ways to enter the cell. Cell Res. 2010;20(3):256-75.

34. Sigismund S, Argenzio E, Tosoni D, Cavallaro E, Polo S, Di Fiore PP. Clathrin-mediated internalization is essential for sustained EGFR signaling but dispensable for degradation. Dev Cell. 2008;15(2):209-19.

35. von Kleist L, Stahlschmidt W, Bulut H, Gromova K, Puchkov D, Robertson MJ, et al. Role of the clathrin terminal domain in regulating coated pit dynamics revealed by small molecule inhibition. Cell. 2011;146(3):471-84.

36. Hansen CG, Nichols BJ. Molecular mechanisms of clathrin-independent endocytosis. J Cell Sci. 2009;122(Pt 11):1713-21.

37. The Biozentrum UoB. [Available from: https://swissmodel.expasy.org/.

38. Brennan CW, Verhaak RG, McKenna A, Campos B, Noushmehr H, Salama SR, et al. The somatic genomic landscape of glioblastoma. Cell. 2013;155(2):462-77.

39. Cancer Genome Atlas Research N. Comprehensive genomic characterization defines human glioblastoma genes and core pathways. Nature. 2008;455(7216):1061-8.

40. Snuderl M, Fazlollahi L, Le LP, Nitta M, Zhelyazkova BH, Davidson CJ, et al. Mosaic amplification of multiple receptor tyrosine kinase genes in glioblastoma. Cancer Cell. 2011;20(6):810-7.

41. Zadeh G, Bhat KP, Aldape K. EGFR and EGFRvIII in glioblastoma: partners in crime. Cancer Cell. 2013;24(4):403-4.

42. Yang J, Yan J, Liu B. Targeting EGFRvIII for glioblastoma multiforme. Cancer Lett. 2017;403:224-30.

43. An Z, Aksoy O, Zheng T, Fan QW, Weiss WA. Epidermal growth factor receptor and EGFRvIII in glioblastoma: signaling pathways and targeted therapies. Oncogene. 2018;37(12):1561-75.

44. Stommel JM, Kimmelman AC, Ying H, Nabioullin R, Ponugoti AH, Wiedemeyer R, et al. Coactivation of receptor tyrosine kinases affects the response of tumor cells to targeted therapies. Science. 2007;318(5848):287-90.

45. Tan AC, Vyse S, Huang PH. Exploiting receptor tyrosine kinase co-activation for cancer therapy. Drug Discov Today. 2017;22(1):72-84.

46. Xu AM, Huang PH. Receptor tyrosine kinase coactivation networks in cancer. Cancer Res. 2010;70(10):3857-60.

47. Azuaje F, Tiemann K, Niclou SP. Therapeutic control and resistance of the EGFR-driven signaling network in glioblastoma. Cell Commun Signal. 2015;13:23.

48. Kahles A, Lehmann KV, Toussaint NC, Huser M, Stark SG, Sachsenberg T, et al. Comprehensive Analysis of Alternative Splicing Across Tumors from 8,705 Patients. Cancer Cell. 2018;34(2):211-24 e6.

49. Climente-Gonzalez H, Porta-Pardo E, Godzik A, Eyras E. The Functional Impact of Alternative Splicing in Cancer. Cell Rep. 2017;20(9):2215-26.

50. Babic I, Anderson ES, Tanaka K, Guo D, Masui K, Li B, et al. EGFR mutation-induced alternative splicing of Max contributes to growth of glycolytic tumors in brain cancer. Cell Metab. 2013;17(6):1000-8.

51. Weinholdt C, Wichmann H, Kotrba J, Ardell DH, Kappler M, Eckert AW, et al. Prediction of regulatory targets of alternative isoforms of the epidermal growth factor receptor in a glioblastoma cell line. BMC Bioinformatics. 2019;20(1):434.

52. Frampton GM, Ali SM, Rosenzweig M, Chmielecki J, Lu X, Bauer TM, et al. Activation of MET via diverse exon 14 splicing alterations occurs in multiple tumor types and confers clinical sensitivity to MET inhibitors. Cancer Discov. 2015;5(8):850-9.

53. Paik PK, Drilon A, Fan PD, Yu H, Rekhtman N, Ginsberg MS, et al. Response to MET inhibitors in patients with stage IV lung adenocarcinomas harboring MET mutations causing exon 14 skipping. Cancer Discov. 2015;5(8):842-9.

54. Hoque M, Rentero C, Cairns R, Tebar F, Enrich C, Grewal T. Annexins - scaffolds modulating PKC localization and signaling. Cell Signal. 2014;26(6):1213-25.

55. Dubois T, Oudinet JP, Mira JP, Russo-Marie F. Annexins and protein kinases C. Biochim Biophys Acta. 1996;1313(3):290-4.

56. Koese M, Rentero C, Kota BP, Hoque M, Cairns R, Wood P, et al. Annexin A6 is a scaffold for PKCalpha to promote EGFR inactivation. Oncogene. 2013;32(23):2858-72.

57. Tanowitz M, Hislop JN, von Zastrow M. Alternative splicing determines the post-endocytic sorting fate of G-protein-coupled receptors. J Biol Chem. 2008;283(51):35614-21.

58. Traub LM, Bonifacino JS. Cargo recognition in clathrin-mediated endocytosis. Cold Spring Harb Perspect Biol. 2013;5(11):a016790.

59. Traub LM. Tickets to ride: selecting cargo for clathrin-regulated internalization. Nat Rev Mol Cell Biol. 2009;10(9):583-96.

60. Heilker R, Spiess M, Crottet P. Recognition of sorting signals by clathrin adaptors. Bioessays. 1999;21(7):558-67.

61. Futter CE, White IJ. Annexins and endocytosis. Traffic. 2007;8(8):951-8.

62. Bandorowicz-Pikula J, Pikula S. Annexins and ATP in membrane traffic: a comparison with membrane fusion machinery. Acta Biochim Pol. 1998;45(3):721-33.

63. Creutz CE, Snyder SL. Interactions of annexins with the mu subunits of the clathrin assembly proteins. Biochemistry. 2005;44(42):13795-806.

64. Lin HC, Sudhof TC, Anderson RG. Annexin VI is required for budding of clathrin-coated pits. Cell. 1992;70(2):283-91.

65. Ghadie MA, Lambourne L, Vidal M, Xia Y. Domain-based prediction of the human isoform interactome provides insights into the functional impact of alternative splicing. PLoS Comput Biol. 2017;13(8):e1005717.

66. D'Antonio M, Masseroli M. Extraction, integration and analysis of alternative splicing and protein structure distributed information. BMC Bioinformatics. 2009;10 Suppl 12:S15.

67. Buljan M, Chalancon G, Eustermann S, Wagner GP, Fuxreiter M, Bateman A, et al. Tissue-specific splicing of disordered segments that embed binding motifs rewires protein interaction networks. Mol Cell. 2012;46(6):871-83.

68. Peschard P, Park M. Escape from Cbl-mediated downregulation: a recurrent theme for oncogenic deregulation of receptor tyrosine kinases. Cancer Cell. 2003;3(6):519-23.

69. Marmor MD, Yarden Y. Role of protein ubiquitylation in regulating endocytosis of receptor tyrosine kinases. Oncogene. 2004;23(11):2057-70.

70. Tsacoumangos A, Kil SJ, Ma L, Sonnichsen FD, Carlin C. A novel dileucine lysosomal-sorting-signal mediates intracellular EGF-receptor retention independently of protein ubiquitylation. J Cell Sci. 2005;118(Pt 17):3959-71.

71. Rogers MA, Fantauzzo KA. The emerging complexity of PDGFRs: activation, internalization and signal attenuation. Biochem Soc Trans. 2020;48(3):1167-76.

72. Cho KW, Park JH, Park CW, Lee D, Lee E, Kim DJ, et al. Identification of a pivotal endocytosis motif in c-Met and selective modulation of HGF-dependent

aggressiveness of cancer using the 16-mer endocytic peptide. Oncogene. 2013;32(8):1018-29.

73. Bienert S, Waterhouse A, de Beer TA, Tauriello G, Studer G, Bordoli L, et al. The SWISS-MODEL Repository-new features and functionality. Nucleic Acids Res. 2017;45(D1):D313-D9.

74. Yang J, Yan R, Roy A, Xu D, Poisson J, Zhang Y. The I-TASSER Suite: protein structure and function prediction. Nat Methods. 2015;12(1):7-8.

75. Yang J, Zhang Y. I-TASSER server: new development for protein structure and function predictions. Nucleic Acids Res. 2015;43(W1):W174-81

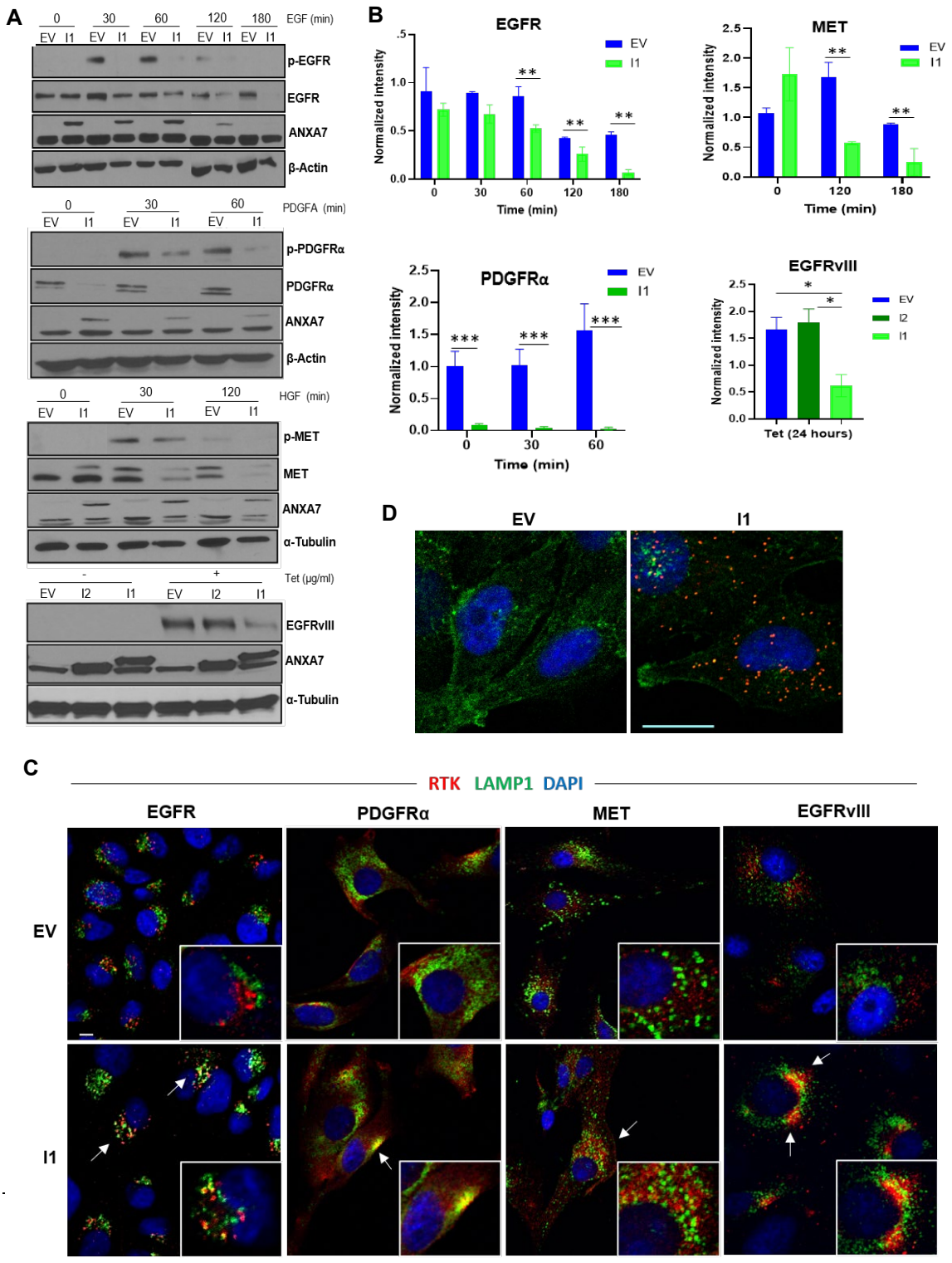
A
0
30
60
120
180
EGF (min)
EV I1
p-EGFR
EGFR
ANXA7
β-Actin
PDGFA (min)
p-PDGFRα
PDGFRα
ANXA7
β-Actin
HGF (min)
p-MET
MET
ANXA7
α-Tubulin
Tet (μg/ml)
EV I2 I1
EGFRvIII
ANXA7
α-Tubulin
B
EGFR
MET
PDGFRα
EGFRvIII
Normalized intensity
Time (min)
Tet (24 hours)
EV
I1
I2
C
RTK LAMP1 DAPI
EGFR
PDGFRα
MET
EGFRvIII
EV
I1
D
EV
I1

Figure 1 - I1 downregulates RTK signaling via lysosomal degradation. (A-B). Activated and total RTK levels (EGFR, PDGFRα, MET and EGFRvIII) at various timepoints in U251 glioma cells transduced to express empty vector (EV) or ANXA7-I1. **(C)**. Co-immunostaining of RTKs with LAMP1, a lysosomal marker, in EV and I1 cells. Nuclei were counterstained with DAPI. Arrows indicate points of colocalization. Scale bars, 20μM. **(D)**. Proximity ligation assay (PLA) showing positive interaction (red spots) between ANXA7 and LAMP1 in I1 cells. Actin filaments were stained with Phalloidin, and nuclei were counterstained with DAPI. Scale bar, 20μM.

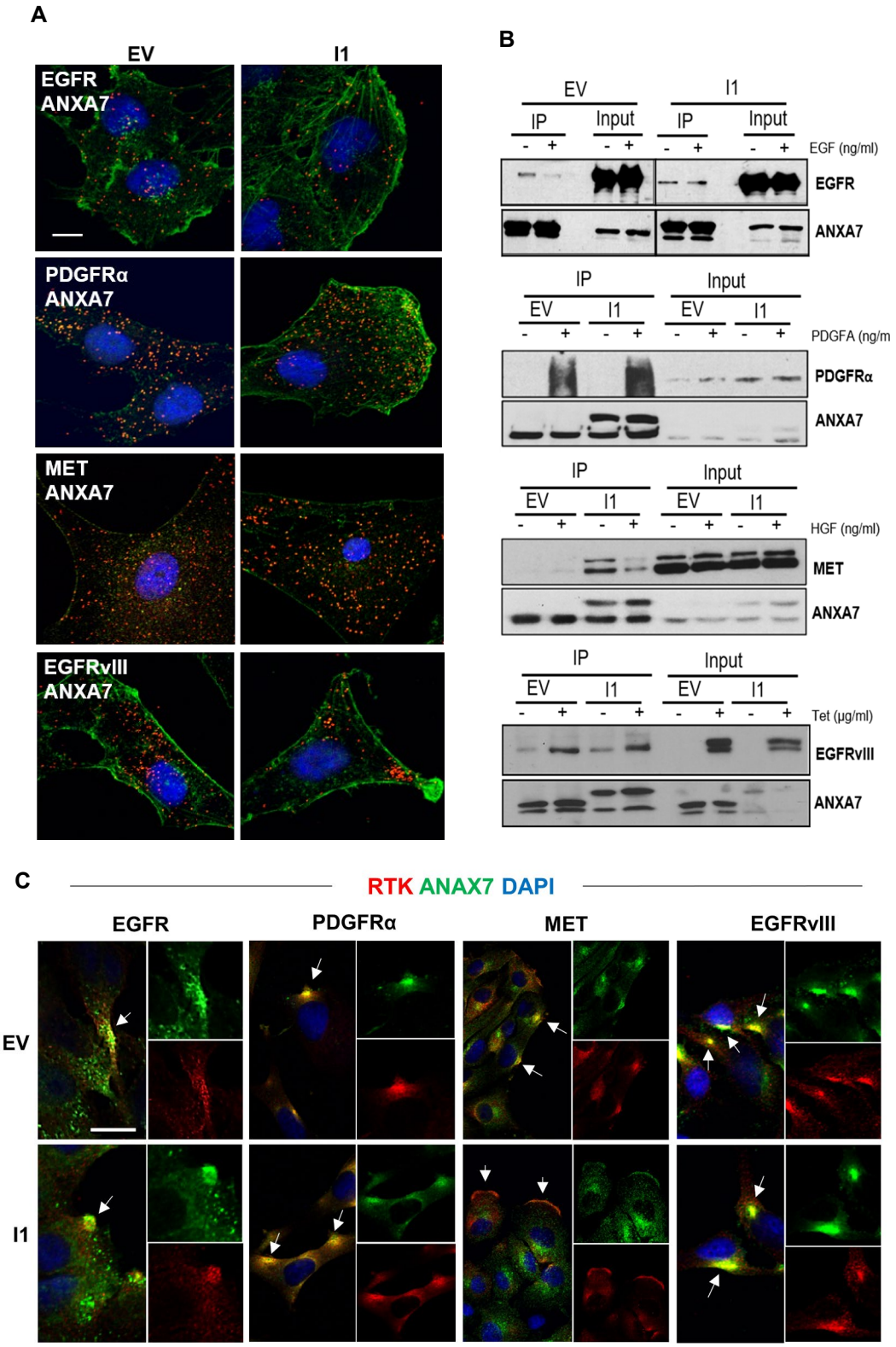
A
EV
I1
EGFR
ANXA7
PDGFRα
ANXA7
MET
ANXA7
EGFRvIII
ANXA7
B
EV
I1
IP
Input
EGF (ng/ml)
EGFR
ANXA7
PDGFA (ng/m
PDGFRα
ANXA7
HGF (ng/ml)
MET
ANXA7
Tet (μg/ml)
EGFRvIII
ANXA7
C
RTK ANAX7 DAPI
EGFR
PDGFRα
MET
EGFRvIII
EV
I1

Figure 2 – **I1 binds to and maintains sustained interactions with multiple RTKs**. **(A)**. Proximity ligation assay depicting positive interactions (red spots) between ANXA7 isoforms and RTKs in U251 glioma cells expressing empty vector (EV) or I1. Scale bar, 20 μM **(B)**. Co-immunoprecipitation assays were performed in EV and I1 cells stimulated with the appropriate ligand (20 ng/ml) and immunoprecipitated using anti-ANXA7 followed by immunoblotting for EGFR, MET, PDGFRα and EGFRvIII. **(C)**. Co-immunostaining of RTKs with ANXA7 isoforms in EV and I1 cells stimulated with the appropriate ligand (20 ng/ml) and nuclei counterstained with DAPI. Scale bars: 10μM.

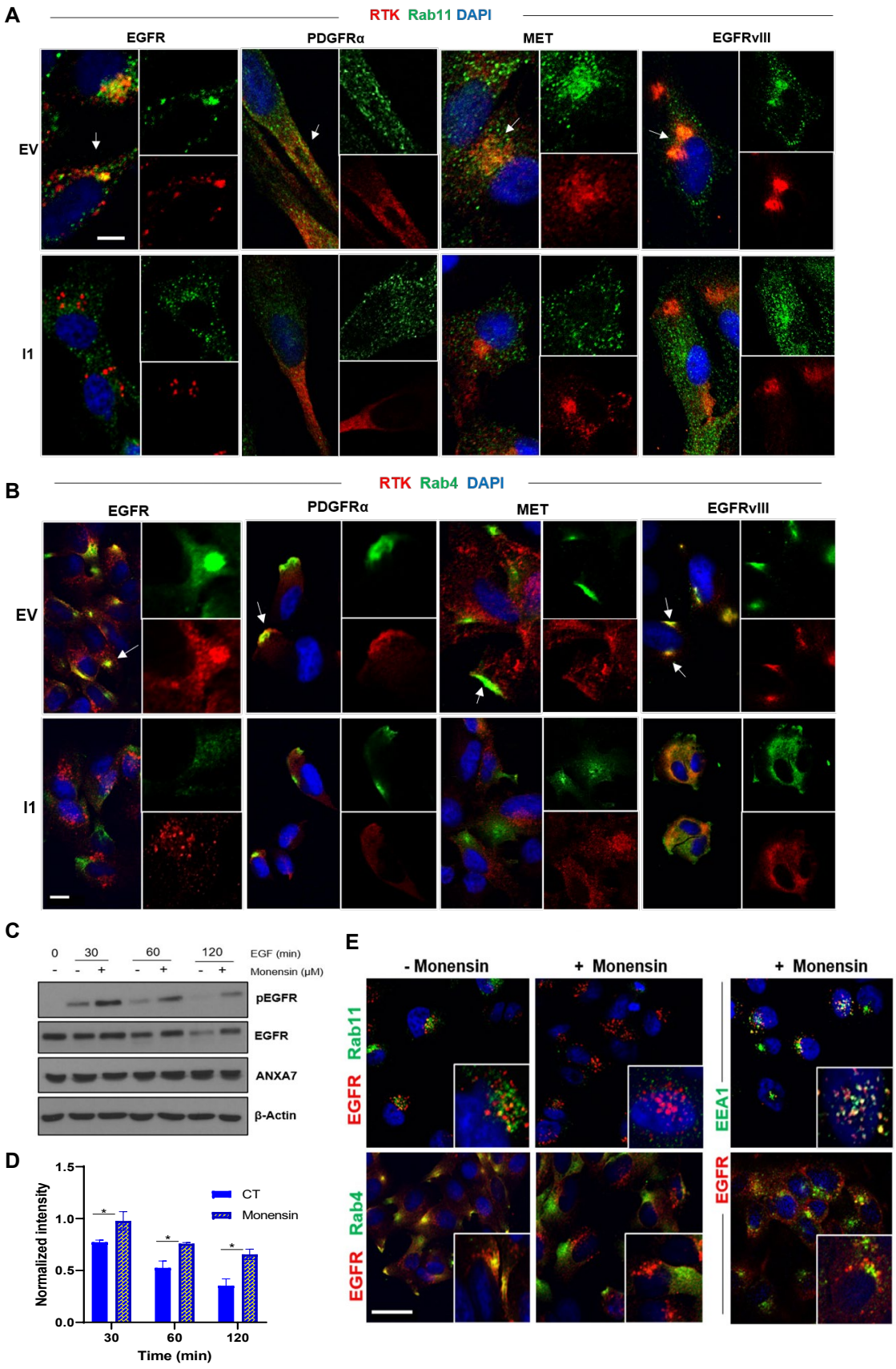
A
RTK Rab11 DAPI
EGFR
PDGFRα
MET
EGFRvIII
EV
I1
B
RTK Rab4 DAPI
EGFR
PDGFRα
MET
EGFRvIII
EV
I1
C
0
30
60
120
EGF (min)
Monensin (μM)
pEGFR
EGFR
ANXA7
β-Actin
D
Normalized intensity
1.5
1.0
0.5
0.0
CT
Monensin
30
60
120
Time (min)
E
- Monensin
+ Monensin
+ Monensin
Rab11
EGFR
EEA1
Rab4
EGFR
EGFR

Figure 3 – RTKs are recycled via fast and slow recycling endosomes in the EV cells. (A-B). Co-immunostaining of EGFR, MET, PDGFRα and EGFRvIII with slow recycling endosome marker, Rab11 (A) and fast recycling endosome marker, Rab4 (B) in EV or I1 cells. Timepoints for Rab11- EGFR, MET, EGFRvIII (60 min); PDGFRα (30min). Timepoints for Rab4- EGFR, PDGFRα, EGFRvIII (5-10 min); MET (15-20min). Arrows indicate areas of colocalization. Scale bars: 20μM**. (C-D).** Total and activated EGFR levels in EV cells post-Monensin treatment (100μM) and EGF stimulation (20 ng/ml) for various timepoints. **(E).** Co-immunostaining of EGFR with Rab11, Rab4 and EEA1 with and without Monensin treatment. Nuclei counterstained with DAPI. Scale bars: 20μM.

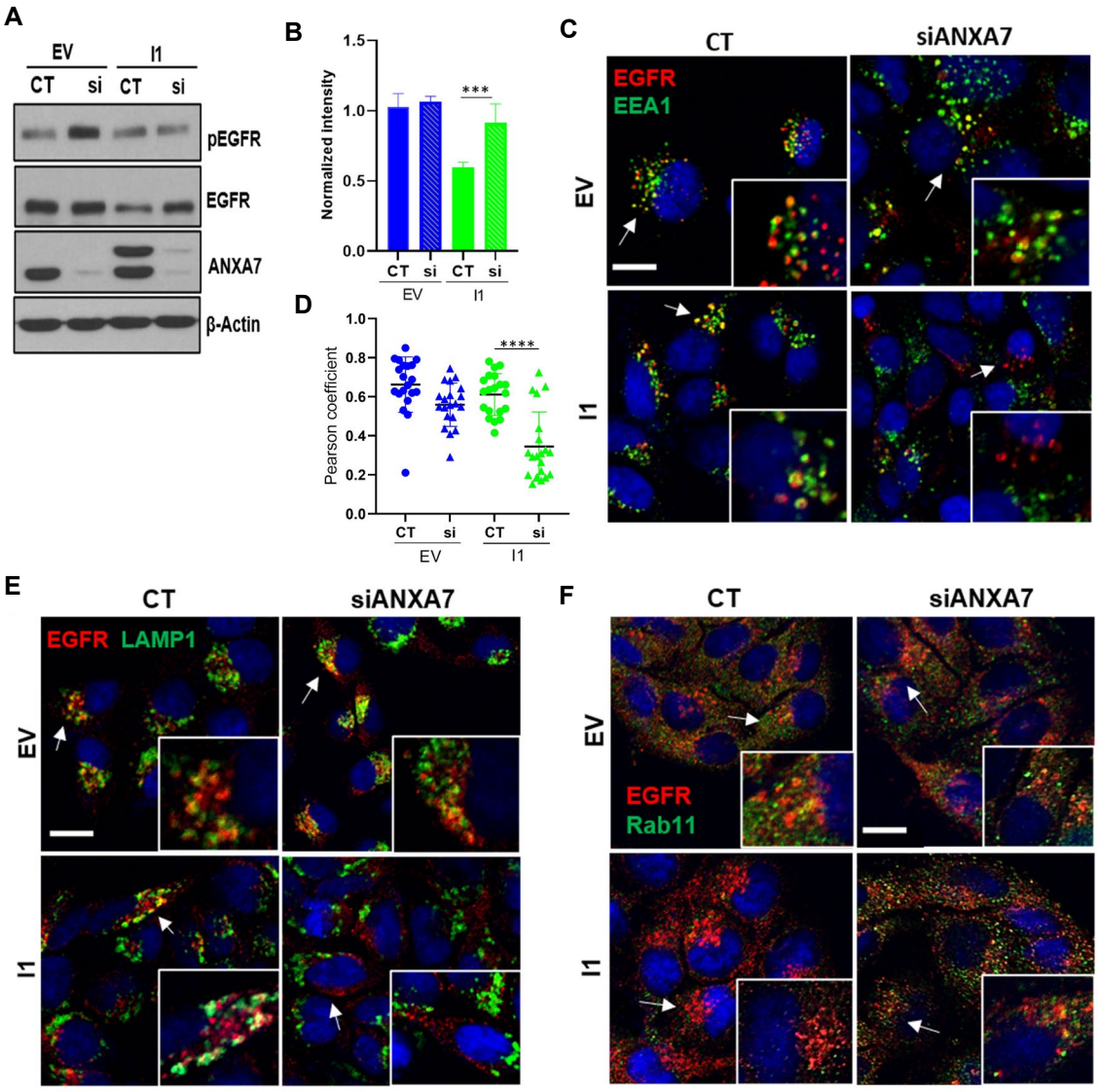

Figure 4 – Loss of I1 impairs EGFR sorting to the lysosomes and promotes recycling. (A-B). Total and activated EGFR levels in EV and I1 cells treated with control (CT) or siANXA7 (si) followed by 60 minutes of EGF stimulation. **(C).** Co-immunostaining of EGFR with EEA1 in EV and I1 cells treated with control (CT) or siANXA7 (si) followed by 15 minutes of EGF stimulation. **(D)**. Pearson's correlation coefficient for colocalization of EGFR and EEA1. n=20. **(E)** Co-immunostaining of EGFR with LAMP1 in EV and I1 cells subjected to control (CT) or siANXA7 followed by 60-minute EGF stimulation **(F).** Co-immunostaining of EGFR with Rab11 in EV and I1 cells subjected to control (CT) or siANXA7 followed by 60 minutes of EGF stimulation. Nuclei counterstained with DAPI. Scale bars: 50µM.

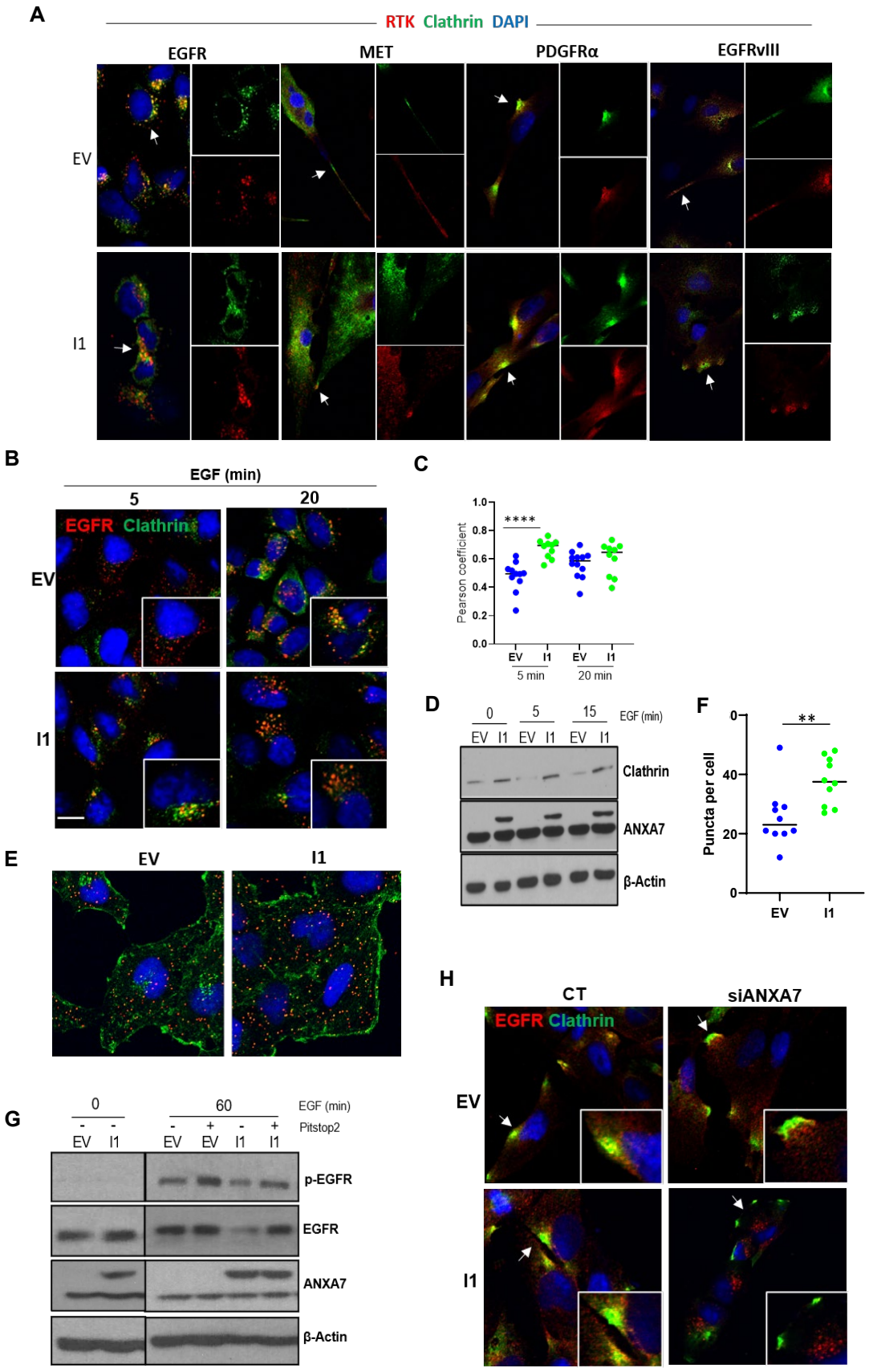
A
RTK Clathrin DAPI
EGFR
MET
PDGFRα
EGFRvIII
EV
I1
B
EGF (min)
5
20
EGFR Clathrin
EV
I1
C
Pearson coefficient
****
EV
I1
EV
I1
5 min
20 min
D
0
5
15
EGF (min)
EV I1 EV I1 EV I1
Clathrin
ANXA7
β-Actin
F
**
Puncta per cell
EV
I1
E
EV
I1
G
0
60
EGF (min)
Pitstop2
EV I1 EV EV I1 I1
p-EGFR
EGFR
ANXA7
β-Actin
H
CT
siANXA7
EGFR Clathrin
EV
I1

Figure 5 – I1-mediated degradation of EGFR is clathrin dependent. (A). Co-immunostaining of RTKs with clathrin in EV and I1 cells post-ligand stimulation **(B)**. Co-immunostaining of EGFR with clathrin in EV and I1 cells stimulated with EGF (20 ng/ml) at indicated timepoints. Scale bar: 20μM **(C)**. Pearson's correlation coefficient for colocalization of EGFR and clathrin. n=10. **(D).** Clathrin levels in EV and I1 cells post-EGF stimulation at timepoints indicated. **(E).** PLA showing the interaction between ANXA7 and clathrin in EV and I1 cells 10 min post-EGF stimulation. Scale bar 20μm. **(F).** Quantification of PLA. n=10. **(G).** Total and activated EGFR levels in EV and I1 cells treated with Pitstop2 (20μM), a clathrin inhibitor, followed by EGF stimulation. **(H).** Co-immunostaining of EGFR and Clathrin in control (CT) and siANXA7 cells following 5 minutes of EGF stimulation. Scale bars: 20μM.

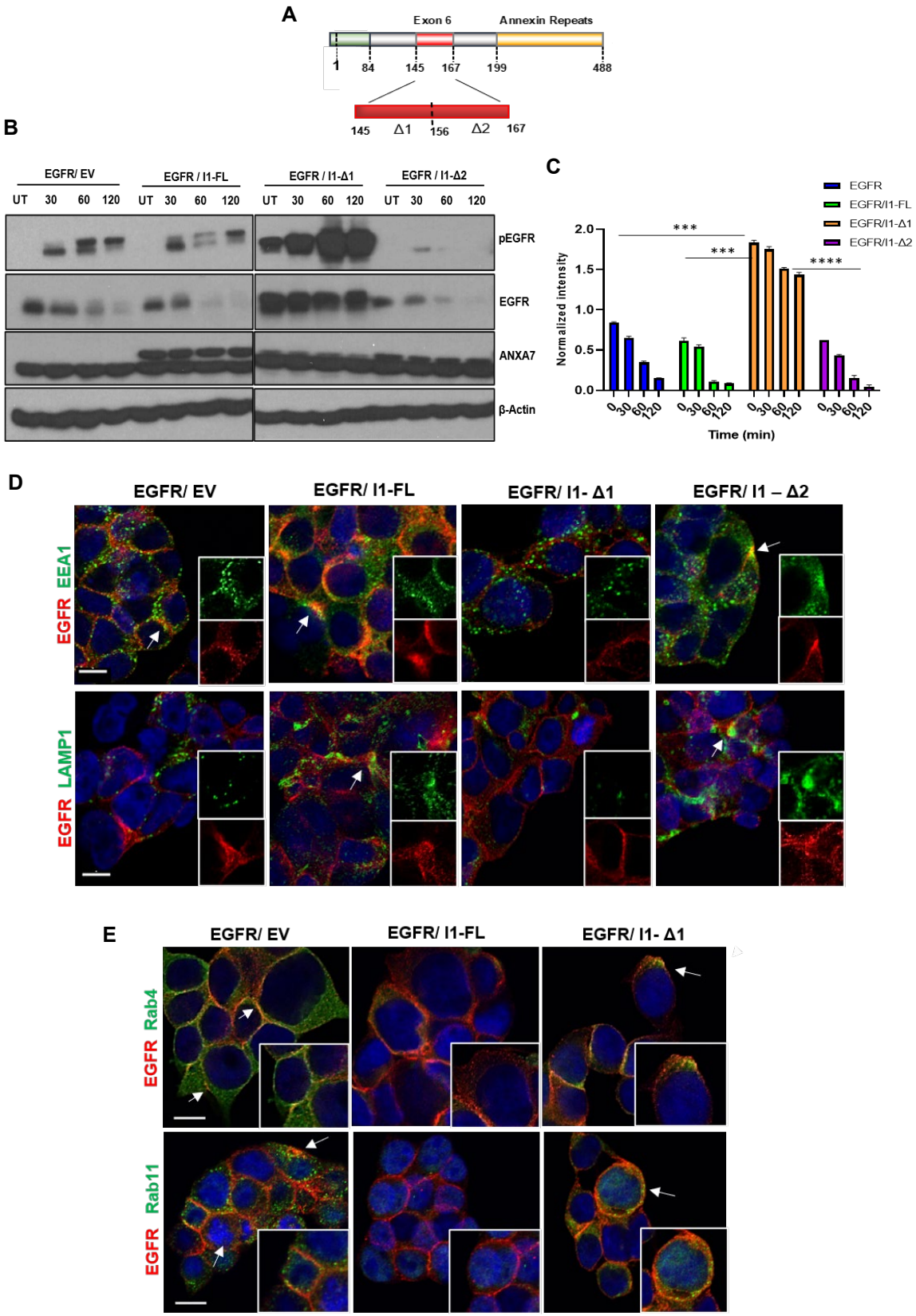
A
Exon 6
Annexin Repeats
1
84
145
167
199
488
145
Δ1
156
Δ2
167
B
EGFR/ EV
EGFR / I1-FL
EGFR / I1-Δ1
EGFR / I1-Δ2
UT 30 60 120
pEGFR
EGFR
ANXA7
β-Actin
C
EGFR
EGFR/I1-FL
EGFR/I1-Δ1
EGFR/I1-Δ2
Normalized intensity
Time (min)
D
EGFR/ EV
EGFR/ I1-FL
EGFR/ I1- Δ1
EGFR/ I1 – Δ2
EGFR EEA1
EGFR LAMP1
E
EGFR/ EV
EGFR/ I1-FL
EGFR/ I1- Δ1
EGFR Rab4
EGFR Rab11

Figure 6 – Truncated I1 fails to sort EGFR for lysosomal degradation and sorts to the recycling endosomes (A). Schematic diagram of the proposed deletions in the Exon 6 encoded region **(B-C).** Total and activated levels of EGFR in Hek293T transfected with EGFR and co-transfected with empty vector (EV), full length I1 (I1-FL) or mutant I1 models (I1-Δ1 or I1-Δ2) after EGF (20 ng/ml) stimulation in a time dependent manner. **(D).** Co-immunostaining of EGFR with EEA1 (top panel) and LAMP1 (bottom panel), in Hek293T transfected with EGFR and co-transfected with EV, I1-FL or I1 mutant models stimulated with EGF (20 ng/ml) for 5 minutes and 30 minutes, respectively. Arrows indicate areas of colocalization **(E).** Immunostaining of EGFR with Rab4 and Rab11 in Hek293T transfected with EGFR and co-transfected with EV, I1-FL or I1 mutant models stimulated with EGF (20 ng/ml) for 5 minutes and 30 minutes, respectively. Arrows indicate areas of colocalization. Scale bars: 10μM.

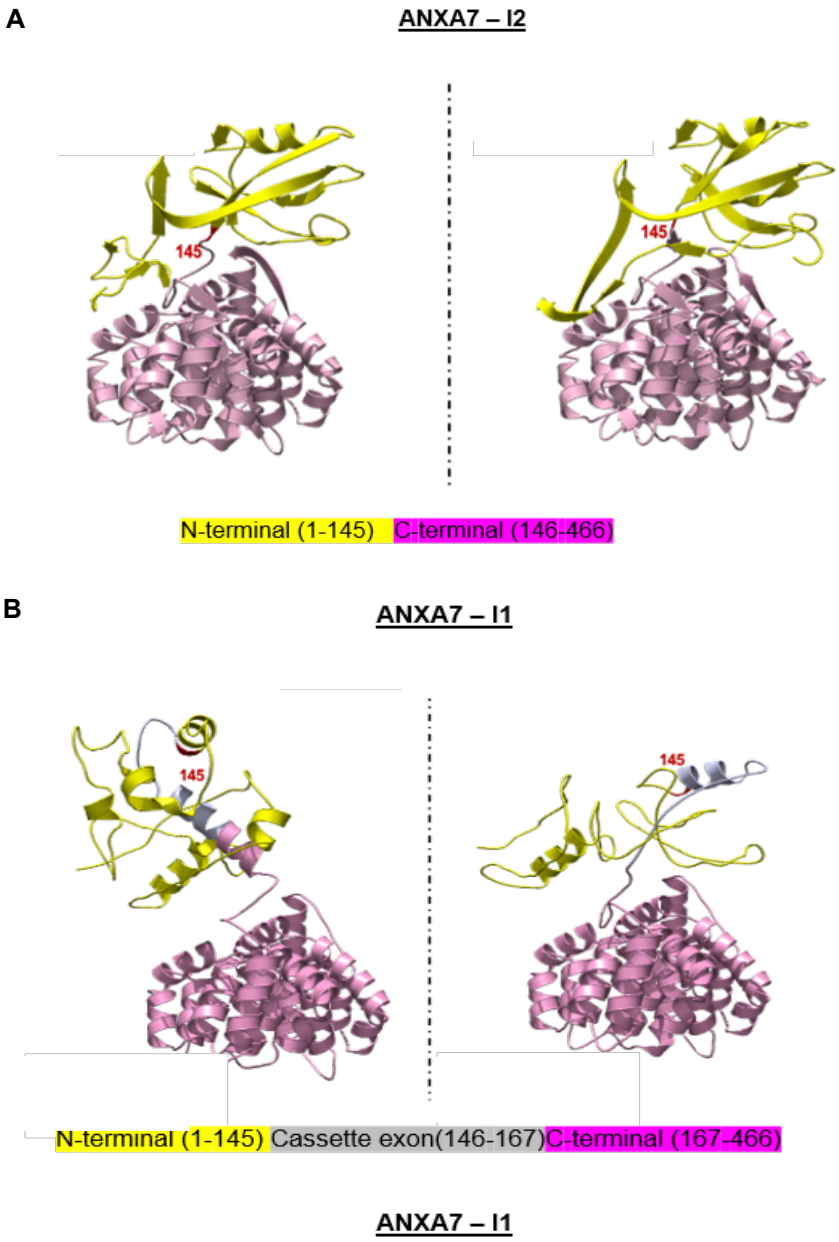

Figure 7– *ANXA7-I1* encodes a secondary structure amenable to form isoform specific protein interactions. I-TASSER modeling of ANXA7 isoforms **(A)** I2 structure **(B)**. I1 structure. N-terminal domain AA 1-145 (yellow); cassette exon region 146-167 (grey); C-terminal Annexin repeats 167-488 (pink). The last residue of the N-terminal domain, namely Glutamine 145 is indicated in red.

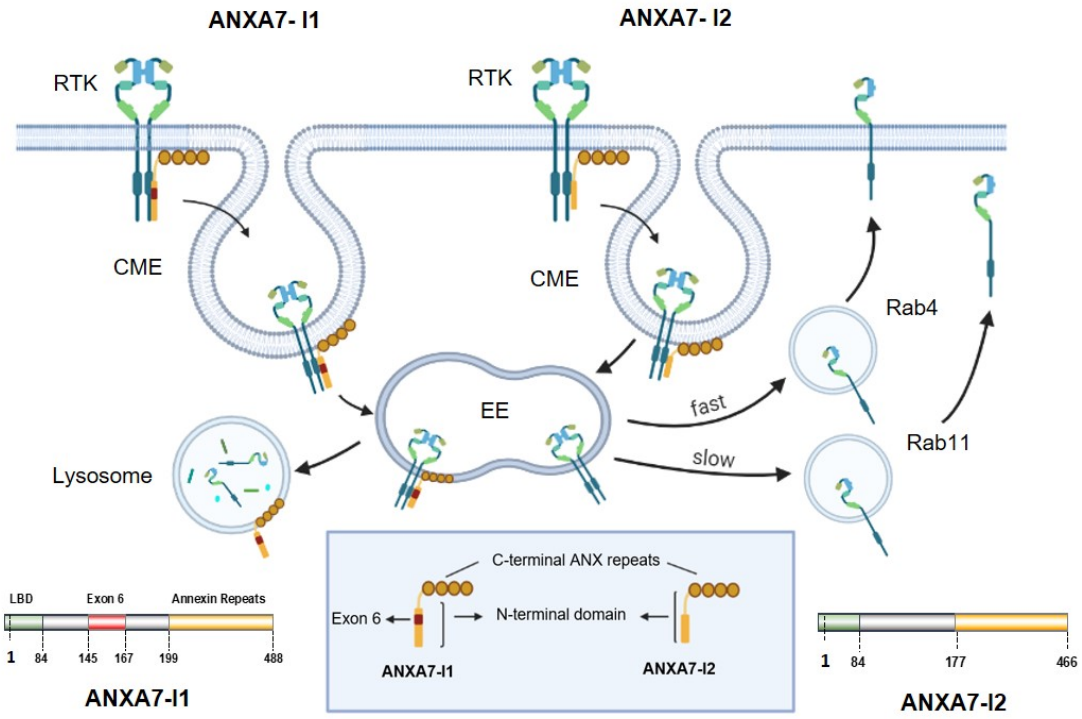

Figure 8– Proposed model of RTK regulation by ANXA7 isoforms in GBM. Representative scheme in which I1 acts as a regulator of RTK sorting by binding to individual components of the endocytic pathway. RTKs undergo I1-mediated sorting to the lysosomes for degradation in cells expressing I1. Conversely, RTKs are recycled in cells expressing I2, via the fast and slow recycling pathways promoting tumor growth and survival.

SUPPLEMENTAL FIGURES

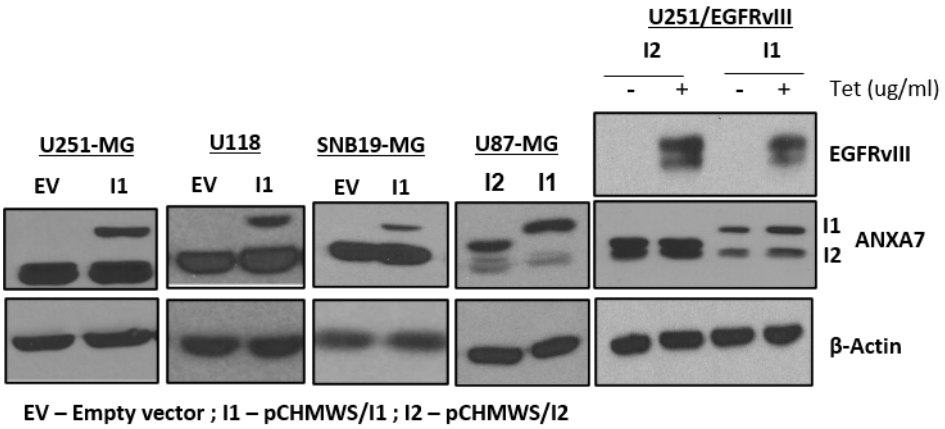

S. Fig 1: **GBM models overexpressing I1 or I2**. Established glioma cell lines transduced with empty vector (EV) or I1. U87-MG was transduced to overexpress I2 or I1. EGFRvIII was overexpressed into U251-MG cells using a Tet inducible system and co-transfected with I2 or I1.

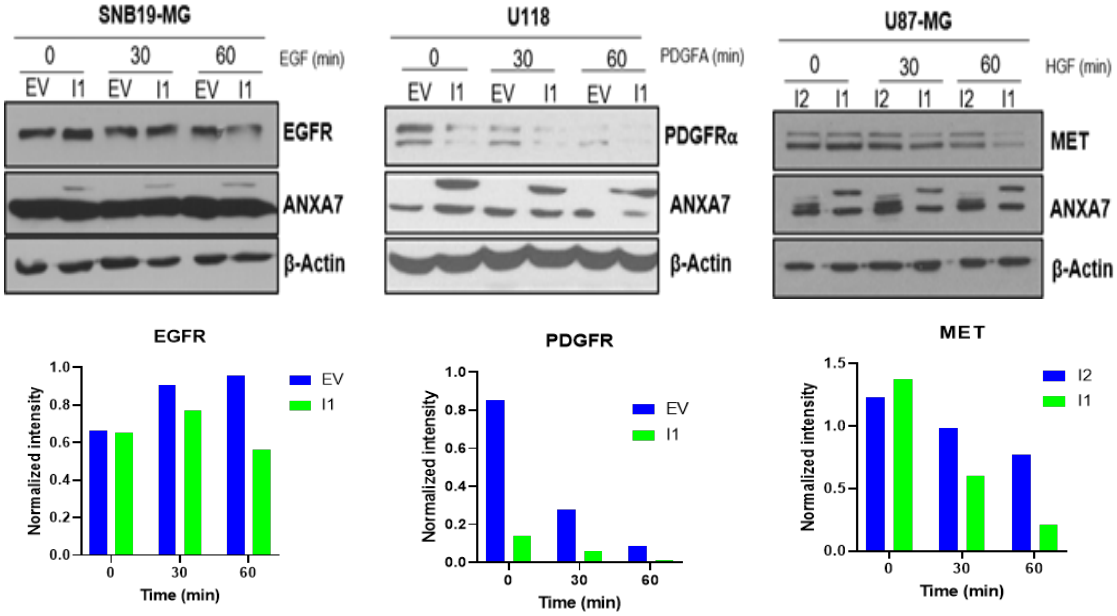

S. Fig 2: **I1 mediates downregulation of RTK signaling.** Total EGFR (left), PDGFRα (center) and MET (right) levels in SNB19, U118 and U87 cells overexpressing I1 at various timepoints post-ligand stimulation. Downregulation of EGFR is observed at 60 minutes in SNB19/I1 cells, PDGFRα is downregulated at all timepoints in U118/I1 cells and MET is downregulated at 60 minutes in U87-MG/I1 cells.

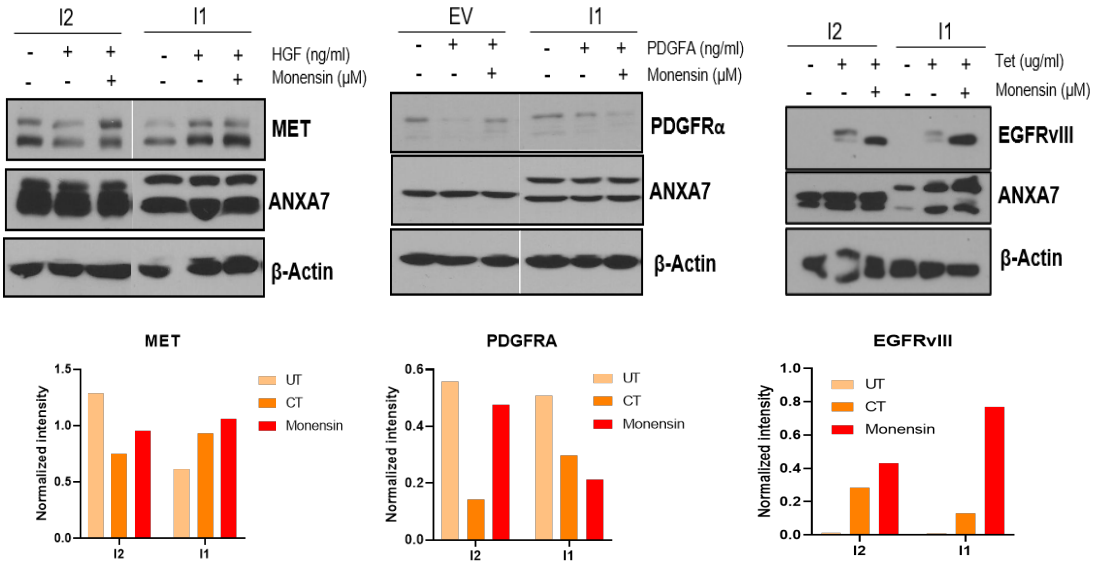

S. Fig 3: RTKs are recycled in cells expressing I2. Total RTK levels in EV and I1 cells pre-treated with or without Monensin (100μM) followed by ligand stimulation. An increase in MET (left), PDGFRα (center) and EGFRvIII (right) levels are seen in all monensin-treated I2 cells; increased levels of EGFRvIII is also evident to some extent an in I1 cells treated with monensin.

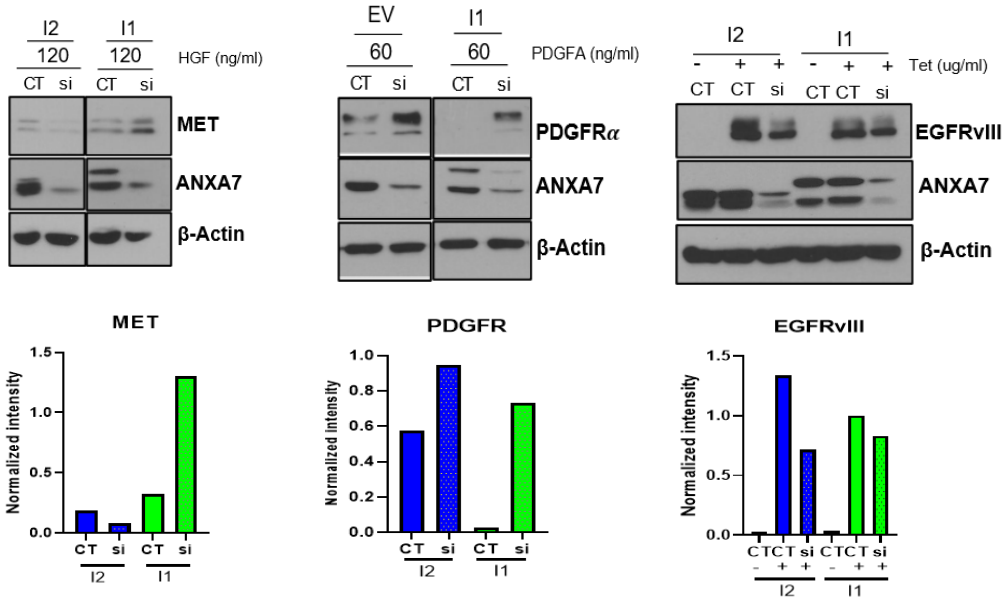

S. Fig 4: Loss of I1 elevates RTK levels. RTK levels in EV and I1 cells treated with control (CT) or siANXA7 (si) followed by ligand stimulation for appropriate timepoints. Increase in MET levels are observed in I1/siANXA7 cells at the 120min timepoint (left); at 60min in the I1/siANXA7 for PDGFRα (center); and a minimal change is observed in EGFRvIII treated with siANXA7 in I2 and I1 cells (right).

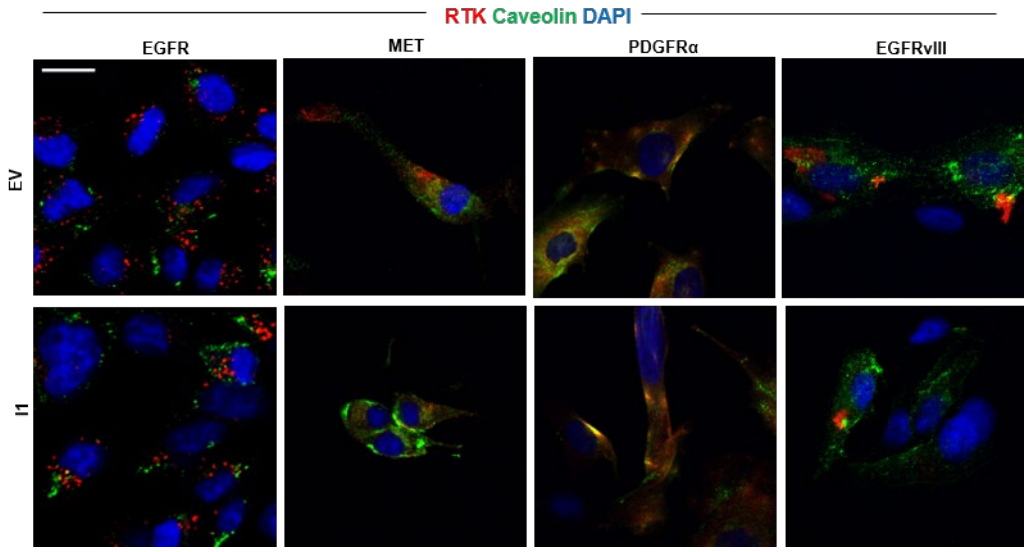

S. Fig 5: I1-mediated RTK sorting is a caveolin independent process. (A) Co-immunostaining of RTKs with caveolin post-ligand stimulation in both EV and I1 cells. Nuclei counterstained with DAPI. Scale bars 20µM.

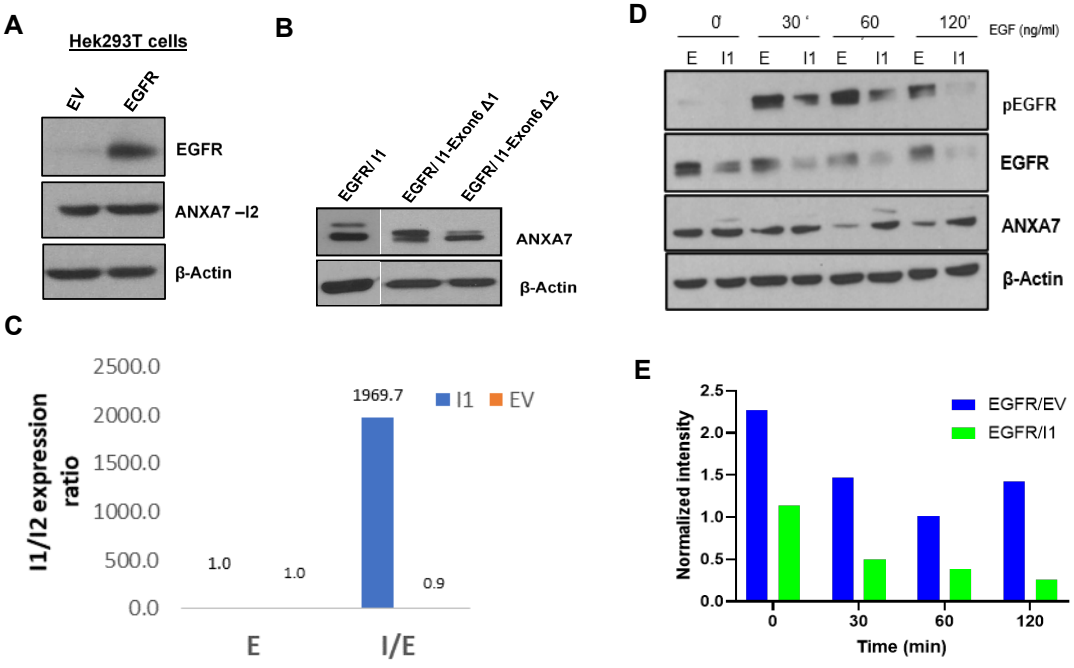

S. Fig 6: Mutant ANXA7 models (A-B) Hek293T cells were transfected with empty vector (EV) or EGFR and then co-transfected with full length I1 (I1-FL), I1-Δ1 or I1-Δ2**. (C).** I1 to I2 mRNA expression ratio in Hek293T EV (E) cells transfected with I1 (I/E). **(D-E).** Activated and total EGFR levels in Hek293T cells either expressing EGFR/EV (E) or EGFR/I1 (I1) at various timepoints post-EGF (20 ng/ml) stimulation.

CHAPTER 3

NOVEL *EGFR* ECTODOMAIN MUTATIONS ASSOCIATED WITH LIGAND-INDEPENDENT ACTIVATION AND CETUXIMAB RESISTANCE IN HEAD AND NECK CANCER

by

SINDHU NAIR, HOA Q. TRUMMEL, RAJANI RAJBHANDARI, NANDA K. THUDI, SUSAN E. NOZELL, JASON M. WARRAM, CHRISTOPHER D. WILLEY, EDDY S. YANG, WILLIAM J. PLACZEK, JAMES A. BONNER, MARKUS BREDEL

PloS ONE
doi.org/10.1371/journal.pone.0229077

Format adapted for dissertation

ABSTRACT

Epidermal growth factor receptor (EGFR) is a pro-tumorigenic receptor tyrosine kinase that facilitates growth for cancer cells that overexpress the receptor. Monoclonal anti-EGFR antibody Cetuximab (CTX) provides significant clinical benefit in patients with head and neck squamous cell carcinoma (HNSCC). Missense mutations in the ectodomain (ECD) of EGFR can be acquired under CTX treatment and mimic the effect of large deletions on spontaneous untethering and activation of the receptor. Little is known about the contribution of EGFR ECD mutations to EGFR activation and CTX resistance in HNSCC. We identified two concurrent non-synonymous missense mutations (G33S and N56K) mapping to domain I in or near the EGF binding pocket of the EGFR ECD in patient-derived HNSCC cells that were selected for CTX resistance through repeated exposure to the agent in an effort to mimic what may occur clinically. Structural modeling predicted that the G33S and N56K mutants would restrict adoption of a fully closed (tethered) and inactive EGFR conformation while not permitting association of EGFR with the EGF ligand or CTX. Binding studies confirmed that the mutant, untethered receptor displayed a reduced affinity for both EGF and CTX but demonstrated sustained activation and presence at the cell surface with diminished internalization and sorting for endosomal degradation, leading to persistent downstream AKT signaling. Our results demonstrate that HNSCC cells can select for EGFR ECD mutations under CTX exposure that converge to trap the receptor in an open, ligand-independent, constitutively activated state. These mutants impede the receptor's competence to bind CTX possibly explaining certain cases of CTX treatment-induced or de novo resistance to CTX.

INTRODUCTION

Head and neck squamous cell carcinoma (HNSCC) is a biologically, phenotypically, and clinically heterogeneous disease [1–3]. Epidermal growth factor (EGFR) is a paradigmatic receptor tyrosine kinase (RTK) that serves as a master conduit for many cell growth and differentiation pathways in this disease [4]. Moreover, inhibition of EGFR has become an important therapeutic target for these patients [5, 6]. EGFR is overexpressed in most and amplified and/or mutated in up to 15% of HNSCC [1]. Mutations involving the EGFR RTK domain usually lead to a constitutively active receptor [1]. Mutations in the ectodomain (ECD) of EGFR have been well-documented in other cancers [7–10]. Their contribution to HNSCC pathogenesis and therapy response has received little attention but could have therapeutic implications [7]. It has been demonstrated that EGFR ECD missense mutations can unexpectedly cause spontaneous receptor untethering that removes a restraint on RTK activation and that such mutants can be targeted by specific monoclonal antibodies (mAbs) [11].

The ECD of EGFR is composed of 4 discrete domains—two leucine-rich domains for ligand binding (I and III) and two cysteine-rich domains (II and IV) [12–14]. EGFR is activated by EGF-ligand binding to domains I and III that favors a conformational change of the ECD from a closed, self-inhibited ‘tethered’—locked by the molecular interaction between domain II and IV—to an open ‘untethered’ state [15]. This spatial rearrangement of the ECD exposes domains II and IV to bind to the corresponding domains of the adjacent receptor facilitating homo- or hetero-dimerization, auto-phosphorylation, and activation [12, 13, 15, 16]. Some evidence suggests that EGFR can preexist as an inactive dimer prior to ligand binding [17]. Upon ligand binding, the EGFR transmembrane

domain rotates resulting in the reorientation of the intracellular RTK domain dimer from a symmetric inactive configuration to an asymmetric active configuration ('rotational model') [17]. This model helps explain how ECD missense mutations can potentially activate the receptor in the absence of EGF ligand without necessarily assuming that the mutations induce receptor dimerization [18]. This hypothesis is strengthened by recent evidence indicating that ECD missense mutations located at the domain I-II interface away from the self-inhibitory tether, can favor a third, untethered but compact intermediate EGFR conformation occurring transiently from the tethered-to-untethered transition [11]. This conformation originates from a rotation of ECD domain I—which binds EGF—and has been postulated to expose a cryptic, cancer-characteristic epitope in a similar way as does the constitutively active EGFRvIII mutant that lacks the ECD [11, 19]. These observations suggest that ECD missense mutations can have structural and functional consequences that are equivalent to large-spanning ECD deletion changes [11].

Current therapeutic strategies targeting the ECD of EGFR seek to competitively interfere with ligand binding at domains I and III [16, 20]. Cetuximab (CTX)—a therapeutic monoclonal antibody (mAb) [5, 21]—structurally inhibits the receptor by binding to domain III of EGFR's tethered ECD, thereby sterically overlapping the ligand-binding site and stabilizing the receptor in the closed conformation [13, 16, 22, 23]. CTX provides significant clinical benefit in patients with HNSCC [5, 6]. However, treatment failure occurs and has been shown to correlate with biological elevation of EGFR expression [24], genetic or epigenetic alterations of the EGFR [25–28], or downstream targets [1, 3, 29, 30], impaired EGFR trafficking and degradation [31–33] or signaling

through alternative RTKs [34]. A single case report has described CTX resistance in a HNSCC patient as a result of an acquired CTX-binding site mutation in the EGFR ECD [35]. Herein, we characterize two novel EGFR ECD mutations that are concurrently selected for in patient-derived HNSCC cells while these cells were repeatedly exposed to CTX in an effort to mimic what may occur clinically. While the effect of small EGFR ECD missense mutations remains to be fully understood, we demonstrate that these mutations hinder EGF and CTX binding and are associated with ligand-independent activation of the receptor suggesting functional equivalence to large ECD deletion mutations. These findings have significance regarding methods of circumventing CTX resistance.

RESULTS

We selected patient-derived HNSCC cells (UM-SCC-1) for resistance by repeated, stepwise exposure to CTX in an attempt to recapitulate a clinical setting (termed UM-SCC-1R). We previously showed that the escape mechanism of these cells involved enhanced EGFR-induced downstream signaling without identifying a direct cause [21]. Recently, one study reported a G465R ECD mutation in EGFR affecting the CTX binding site on EGFR conducive to the development of resistance [35]. To date, a total of 19 mutations with respect to EGFR have been identified by The Cancer Genome Atlas (TCGA) HNSCC Project (https://portal.gdc.cancer.gov/projects/TCGA-HNSC) encompassing 17 missense mutations, one nonsense mutation, and one frameshift deletion. Amongst these, 14 mutations were specifically in the ECD. Therefore, we examined whether the resistance formation in our cells could be attributed to EGFR

sequence changes. Subsequently, Sanger sequencing identified two novel EGFR ECD mutations (G33S, N56K, **Fig 1A**). The locations of the mutated residues are highlighted in crystal structures of the ECD in complex with CTX [16] and EGF [15] in **Fig 1B and 1C**.

It is known that CTX complexes with ECD domain III of EGFR in the closed confirmation and, by partially overlapping the ligand-binding site, prevents EGF binding [13, 16, 22, 23]. Therefore, we sought to determine the possible implications of the G33S and N56K ECD mutations on how they contribute to CTX resistance. Structural modeling shows the ECD-CTX complex (**Fig 1B**) with the ECD in its closed, tethered conformation while the EGF-bound structure (**Fig 1C**) highlights how the rotation of domain II and III enables a dimeric form of the ECD in the open, untethered conformation and forms a pocket for EGF binding. In wild-type EGFR, domains I-III are arranged in a C shape and EGF is docked between domains I and III while a protruding beta-hairpin arm of each domain II holds the body of the other [36]. Structurally, G33S and N56K both mapped to ECD domain I [13]. In the closed conformation, G33S and N56K reside in a single shared pocket of the ECD with G33S situated at the end of the initial beta strand that makes contacts with domain II during formation of the closed conformation (**Fig 1B**). Following rotation, these mutants occupy distinct structural sites in the open conformation. G33S is positioned directly in the interface of domain I binding to EGF. N56K does not make direct contact with EGF in the open conformation, but rather sits at the C-terminal end of the first alpha helix in domain I that serves as the key interface between domain I and EGF (**Fig 1C**).

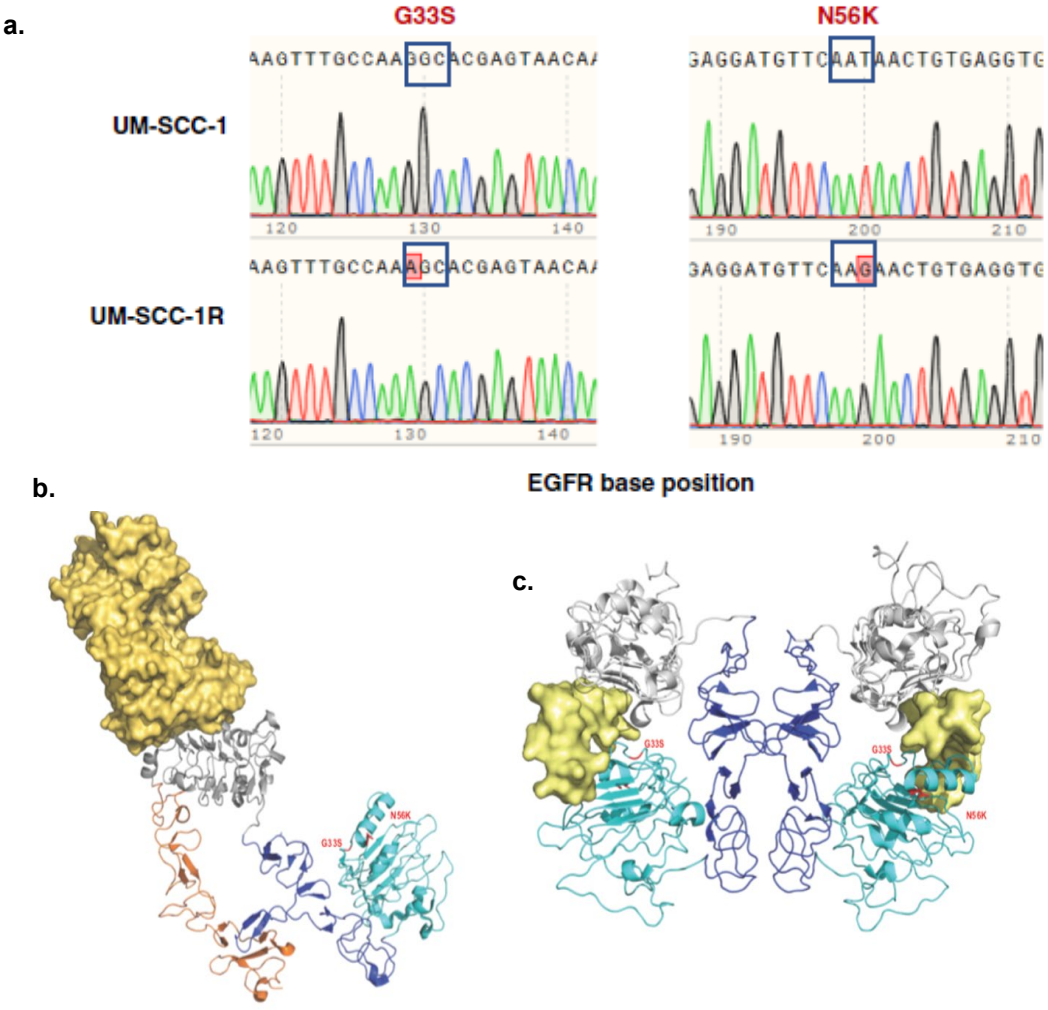

Fig 1. *EGFR* ectodomain mutants in the closed and open conformations. (**a**) EGFR G33S and N56K mutations identified in CTX-resistant UM-SCC-1R cells but not in parental UM-SCC-1 cells by Sanger sequencing. The locations of the two mutations (G33S and N56K) are highlighted in red in the closed (**b**) and open (**c**) conformations of EGFR. (**b**) The closed, tethered monomer confirmation (PDB:1yy9) is presented in complex with CTX (yellow space-filling) with ECD domain I (cyan), domain II (blue), domain III (grey), and domain IV (orange) shown in ribbons. (**c**) EGFR domains are colored as in (**b**) but are shown in the open, untethered/dimer complex confirmation bound to EGF (yellow space filling) and lack domain IV.

Given that our structural-based modeling mapped G33S and N56K into a shared EGF binding pocket, we assessed the competence of the mutant receptor to bind its own ligand. UM-SCC-1 and UM-SCC-1R cells were incubated with increasing concentrations of FITC-labelled EGF for 30 minutes, following which cells were analyzed by flow cytometry to assess ligand binding. We found that mutant UM-SCC-1R cells display diminished EGF binding affinity at low EGF concentrations (6.25–12.5 ng/mL) but that affinity increased and was almost similar to parental, non-mutant UM-SCC-1 cells at high EGF concentrations (25–50 mg/mL) (**Fig 2A**).

By contrast, UM-SCC-1 and UM-SCC-1R cells displayed notably distinct CTX binding dynamics at a broad range of concentrations of the mAb: while exposure to increasing concentrations (6.25–50 ng/mL) of CTX for 30 min led to increased binding of Cy5.5-labeled CTX in UM-SCC-1 cells, none of these concentrations reached meaningful binding in UM-SCC-1R cells (**Fig 2B**). Structural studies investigating the binding mechanisms of CTX have depicted the mAb as an antagonist by exclusively binding to domain III of the ECD of the tethered receptor, covering an epitope that partially overlaps the EGF binding site on that domain [16]. Therefore, G33S and N56K cannot directly explain the reduced CTX binding in the resistant cells. However, the CTX epitope—which we found to be not mutated (exon 12)—is fully exposed only in the transitional form of EGFR that occurs because the receptor changes from the inactive tethered conformation to an active untethered form [16]. Therefore, prolonged adoption of the extended conformation could indirectly impact the ability of CTX to bind the receptor. Stimulation of UM-SCC-1 and UM-SCC-1R cells with saturating doses (60 ng/mL) of EGF revealed sustained presence and activation of the receptor in UM-SCC-1R cells after

60 and 120 minutes (**Fig 2C**). Consistently, flow cytometry demonstrated prolonged high levels of the EGFR at the cell surface in response to saturating EGF doses in UM-SCC-1R compared to UM-SCC-1 cells, indicating impaired receptor internalization (**Fig 2D**).

Next, we examined this difference in receptor internalization with respect to intracellular trafficking of EGFR. Within minutes of activation, EGFR is typically internalized into endocytic vesicles and sorted into the endosomal machinery for recycling or degradation [37–47]. Receptor endocytosis is a spatiotemporally regulated process in which the internalized receptor is first shuttled to the early endosome followed by the late endosome and finally to the lysosome for degradation [48, 49]. We visualized and compared the internalization of EGFR in UM-SCC-1 vs. UM-SCC-1R cells by stimulating cells with saturating EGF (60 ng/mL) conjugated to Alexa Fluor 488. We observed abundant internalization and dot-like clustering of EGF-EGFR complexes in raft-like domains at 15 min in UM-SCC-1 cells but hardly in UM-SCC-1R. Lipid rafts can sequester EGFR and reduce the number of receptors on the cell membrane [50]. Consistently, co-immunofluorescence confirmed greatly reduced co-localization with early endosome antigen 1 (EEA1) in UM-SCC-1R vs. UM-SCC-1 cells, implying diminished endosomal sorting and trafficking (**Fig 2E**). These findings are consistent with previous reports that suggest CTX-resistant cells have an impaired ability to efficiently sort EGFR for degradation leading to perpetual signaling [31–33]. EGFR phosphorylation and subsequent ubiquitination and degradation is an important determinant of response to cisplatin [51], a commonly used anticancer therapeutic in H&N cancers. Given the altered endosomal sorting dynamics of EGFR in UM-SCC-1R vs. UM-SCC-1 cells, we examined their sensitivity to cisplatin but did not note an

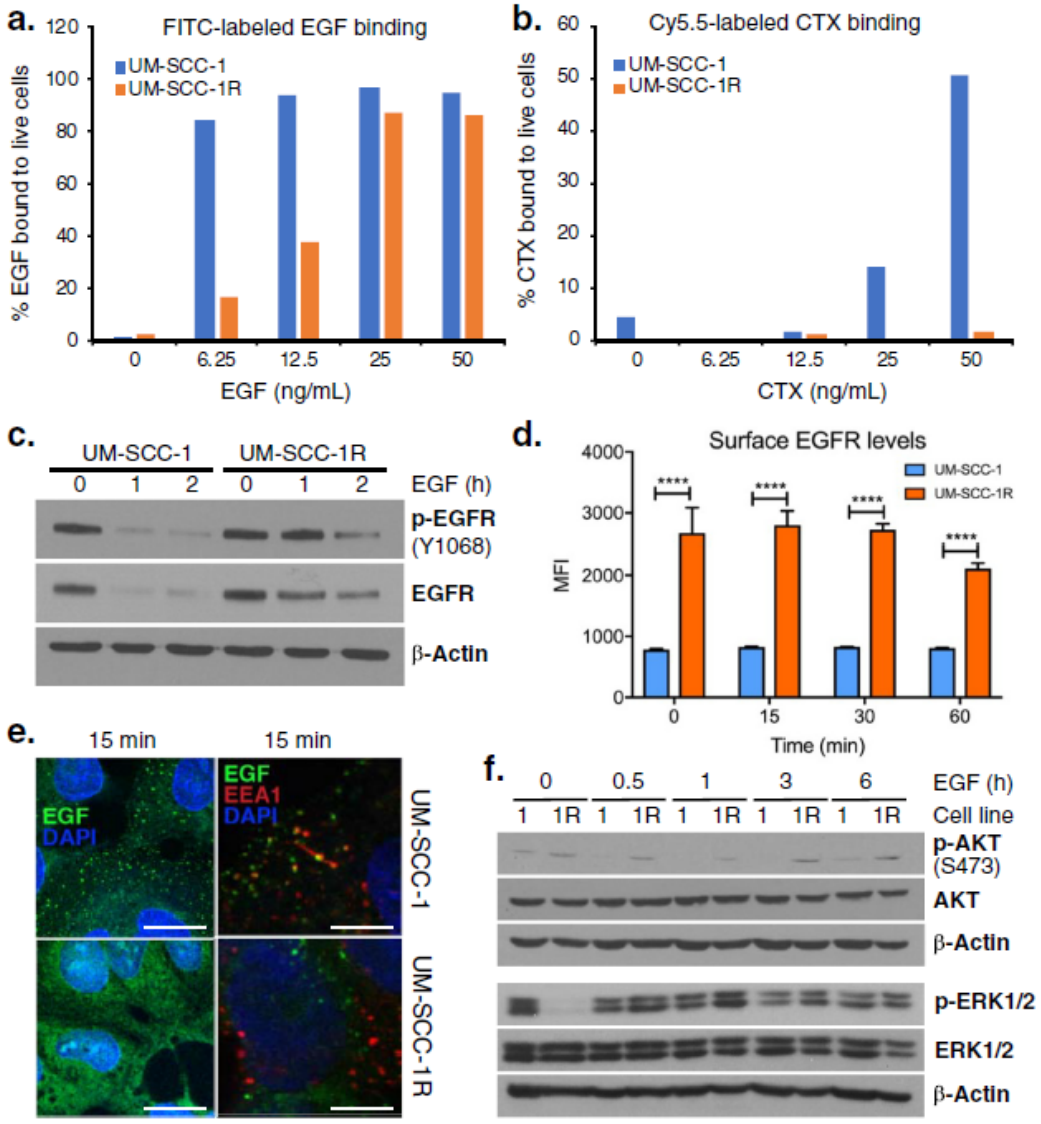

Fig 2. Effect of G33S and N56K mutants on EGF or CTX binding and EGFR activation and degradation. (**a-b**) FITC-labeled EGF and Cy5.5-labeled CTX in UM-SCC-1 vs.–SCC-1R (G33K-N56 mut) assessed by flow cytometry after 30 min of incubation with various concentrations of EGF or CTX. (**c**) Phospho- and total EGFR levels at indicated times of incubation with saturating EGF (60 ng/mL). (**d**) Surface levels of EGFR in cells stimulated with 60 ng/mL EGF in unpermeabilized/unfixed cells, by flow cytometry using a secondary goat anti-rabbit Alexa-Fluor 488 antibody. (**e**) Mapping of Alexa-Fluor 488-EGF conjugate shows internalization (green dotted lipid rafts) and co-localization with early endosome in UM-SCC-1 but not UM-SCC-1R. Scale bar represents 10 μM. (**f**) Consistently increased phospho-AKT but overall comparable (p)ERK1/2 levels in the mutant (1R = UM-SCC-1R) vs. parental (1 = UM-SCC-1) cells. Blots for (p)ERK1/2 were generated on a separate gel with its own β-actin loading control.

appreciable difference in cell growth, proliferation, or colony formation assays (data not shown).

Finally, we probed downstream EGFR signaling as these events play an important role in the growth-promoting function of EGFR [20, 37]. We previously showed that UM-SCC-1R cells display increased phospho-serine 727 and total STAT3 –a key downstream target of EGFR–expression compared to UM-SCC-1 cells [21]. AKT and ERK1/2 are major EGFR induced transforming pathway serine-threonine protein kinases. We found sustained phospho-AKT activation up to 6 hours following stimulation with saturating EGF in UM-SCC-1R but not in UM-SCC-1 but no meaningful difference in phospho-ERK1/2 levels (**Fig 2F**). A recent study investigating mechanisms of CTX resistance in HNSCC found that CTX therapy directly inhibited the activation of AKT in CAL33 HNSCC cells whereas CTX-resistant cells had constitutively activated AKT [31]. Inhibiting the PI3K/AKT pathway resulted in sensitivity towards CTX indicating that the AKT pathway has a direct role in CTX resistance [31]. Similarly, our CTX resistant cells also exhibit constitutive AKT activation suggesting that by selectively activating pro-survival pathways, CTX-resistant HNSCCs possibly ensure tumor growth and survival while also potentiating resistance in this scenario.

DISCUSSION

A better understanding of acquired CTX resistance may lead to the development of new therapies to circumvent this resistance. Therefore, we explored CTX resistance in cells that were initially sensitive to CTX but formed CTX resistance after repeated exposure to

CTX. In these studies, we identified novel missense mutations in the ECD of EGFR in patient-derived HNCC cells that render the receptor active independent of EGF ligand and resistant to CTX. Our data show that the G33S and N56K mutants impede EGFR internalization and sorting and sustain high levels of downstream signaling. Our finding of ligand-independent EGFR activation and concurrent CTX resistance as a consequence of mutations in or near the EGF binding pocket highlights the potentially profound impact and molecular mimicry small missense mutations can have on protein dynamics and function: restricting adoption of a fully closed, inactive EGFR conformation while not permitting association of EGFR with EGF; and, in parallel, restricting accessibility for domain III to interact with CTX, thereby leading to CTX resistance in our model (**Fig 3**).

Structural analysis of the ECD of EGFR has established compelling evidence that domains I, II, and III adopt a closed conformation in the absence of EGF and upon EGF binding undergo rotation of domains II and III to an extended and open conformation that exposes the EGF binding pocket [17]. This rotational model for EGF binding underscores the impact that protein dynamics have on function and further provides some insight into how the identified mutations may alter association with EGF and CTX. Importantly, the two mutations are each positioned to influence key interfaces necessary for adoption of the closed conformation with G33S and N56K located at or near the interface of domain I and EGF. We were initially surprised that the CTX resistant cells showed sustained high levels of total and activated EGFR despite the low affinity for EGF, though these results mirror previous reports of ECD missense mutations—albeit in glioblastoma—which

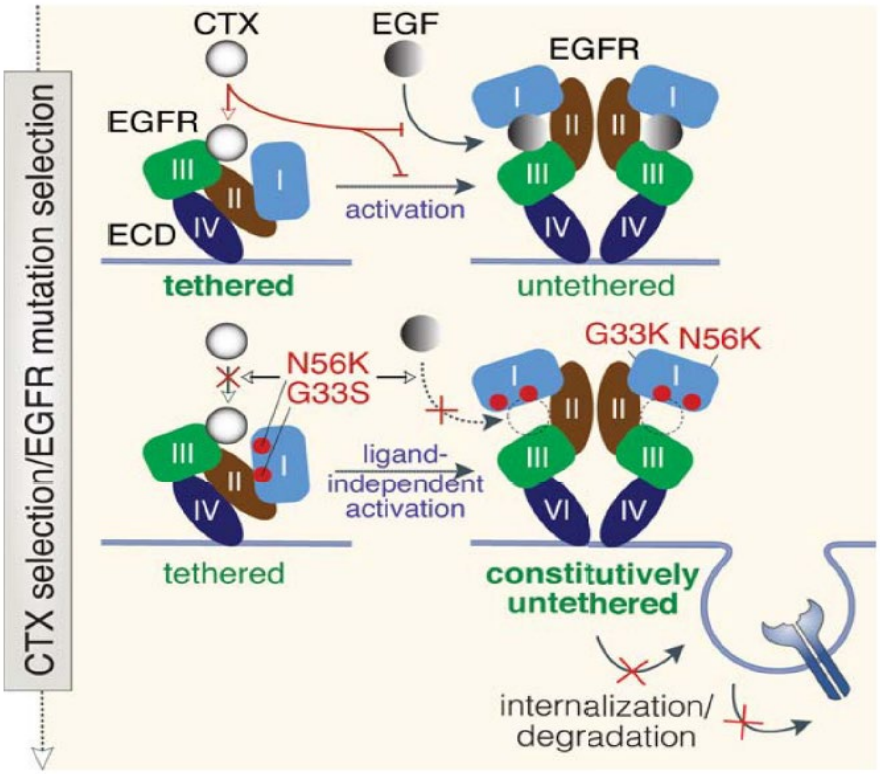

Fig 3. Model. Upon EGF binding, the ECD (contains domains I-IV) of EGFR switches from a closed, inactive ('tethered') state to an open, active ('untethered') state. Upon CTX selection (CTX interacts with domain III of tethered EGFR thereby preventing EGF binding), HNSCC cells acquire EGFR mutations (G33S, N56K) in domain I, which leads to ligand-independent activation and prevents receptor internalization/degradation. Mutant EGFR does not bind CTX since it is 'trapped' in the open confirmation, leading to CTX resistance.

showed constitutive EGFR activity in the absence of EGF suggesting that ECD mutations can have tumorigenic receptor-activating potential [7, 52, 53].

Our subsequent structural analysis regarding the location of these mutations provided some insight into the observed phenotype. Specifically, the reduction in EGF affinity is likely a direct result of G33S and N56K impacting the receptor's affinity towards EGF as these are both positioned in or near the EGF binding pocket.

Likewise, the CTX resistance of the mutants can be possibly explained by the constitutive presence of EGFR in an untethered state, which perturbs the normal closed conformation of the ECD and thus limits the availability of domain III to associate with CTX thereby decreasing affinity. Thus, the identified mutations could have the impact of both restricting the adoption of a fully closed and inactive EGFR conformation while not allowing the association of EGFR with EGF. This restriction may be expected to alter the accessibility for domain III to interact with CTX, thereby leading to the reduction in CTX association observed in our assay. While our data establish that continuous exposure to an anti-EGFR agent can select for EGFR ectodomain mutations that are associated with low affinity to that agent or EGFR, full validation of the significance of these mutants will require combinations of site-directed mutagenesis and wildtype EGFR knockout experiments in additional patient-derived head and neck cancer cell lines.

Our results add to an emerging body of evidence suggesting that EGFR ECD missense mutations can cause spontaneous EGFR untethering that promotes activation of the RTK [11]. Missense mutations located at the domain I-II interface away from the self-inhibitory tether, have been shown to increase ECD flexibility to an open conformation by removing an ECD fragment that acts as steric hindrance to prevent RTK activation [11]. Such heterogenous ECD mutants can present opportunities for molecular targeting and are for example responsive to cancer-specific mAbs [7, 11, 54–57]. Moreover, first-in-class anti-EGFR mixtures of recombinant, human-mouse chimeric mAbs have also demonstrated some initial promise to overcome CTX resistance mediated by EGFR ECD mutations [54, 57].

MATERIALS & METHODS

Head and neck squamous cell carcinoma cells

Patient-derived HNSCC cells, UM-SCC-1, were acquired from Dr. Thomas Carey at the University of Michigan. Additional details, including genotyping, origin, and unique cell identity, have been reported in [58]. Cells were grown in Dulbecco's Modified Eagle Medium (MT-10-090-CV, Gibco) supplemented with 10% fetal bovine serum (Sigma) and 5% Pen-strep (Corning) and treated with 5 μg/ml of CTX (Eli Lilly & Co) for six months to create CTX-resistant cells denoted as UM-SCC-1R as previously described [21]. Acquisition of resistance was observed by the absence of cell death in HNSCC cells and confirmation of a viable population of resistant cells by periodic cell counts using Coulter cell counter. Cells have been sporadically tested for pathogens by Charles River Research Animal Diagnostic Services, and all the results were negative.

Genomic DNA and mRNA extraction and analysis

Genomic DNA was isolated from cells using GenElute Mammalian Genomic DNA Miniprep Kit (Sigma G1N70-1KT). Standard Sanger Sequencing with BigDye v3.1 (Applied Biosystems) chemistry was performed, and the samples were run on an ABI 3730xl Genetic Analyzer. Total RNA was extracted from cells using Trizol. To assess mRNA expression levels, 1 μg of total RNA was reverse transcribed and analyzed by quantitative polymerase chain reaction (PCR). Reactions for each sample were performed in triplicate using a PCR protocol (95˚C activation for 10 min followed by 40 cycles of 95˚C for 15 sec and 60˚C for 1 min) in an ABI StepOnePlus Detection System (Applied

Biosystems). Quantitative RT-PCR (qRT-PCR) was performed via TaqMan Assay (Applied Biosystems).

Structural modeling

Mammalian EGFR is composed of four extracellular domains, named I, II, III, and IV, that alter their conformation in response to ligand binding. To model our point mutations onto EGFR in the CTX- and EGF-bound conformations, we downloaded Protein Databank (PDB) coordinates for the x-ray crystal structures of CTX- and EGF-bound forms of EGFR, 1yy9 and 1ivo, respectively. The CTX-EGFR complex (1yy9) includes coordinates for all four extracellular domains while the EGF-EGFR complex (1ivo) shows the dimer structure of EGFR with domains I, II, and III. We separated the respective domains into independent elements using PyMOL molecular visualization software (https://pymol.org) and identified the location of our point mutation in each model. The impact of specific mutations was assessed through visual analysis of space filling models of the native sidechains in the original structures and comparing this with their respective side-chain mutations. Domains that contain a point mutation were depicted as cartoons, with the location of the point mutation highlighted in a different color while domains or proteins that did not contain mutations were shown in space filling models.

Immunoblotting

Cells were grown to 70% confluency and then serum starved overnight. Whole cell lysate was collected in RIPA buffer supplemented with protease inhibitor cocktail (100nM PMSF, 100mM sodium orthovanadate, 2.5 mg/ml aprotinin, 2.5 mg/ml leupeptin, 5nM Sodium Fluoride). Protein was resolved through SDS-PAGE under denaturing conditions, transferred to polyvinylidene difluoride (PVDF) membrane, and blocked in 5% non-fat milk in TBS-T. Subsequent incubation with the indicated antibody was done overnight at 4˚C. Incubation with HRP-conjugated secondary in TBS containing 5% nonfat milk was performed for 1 hour and protein was detected using ECL chemiluminescence methods (Pierce ThermoScientific, Grand Island, NY).

Reagents and antibodies

Reagents and antibodies were obtained from the following sources: EGF from Fisher Scientific, Alexa Fluor 594 conjugated secondary (A11032, Thermo Scientific), β-Actin (3700, Cell Signaling), total EGFR (4267, Cell Signaling), phospho-EGFR (3777, Cell Signaling), Akt (9272, Cell Signaling), phospho-Akt (4058, Cell Signaling), phospho-ERK (9101, Cell Signaling), total ERK (9102, Cell Signaling), anti-mouse and anti-rabbit secondary IgG-conjugated horse radish peroxidase (7074; 7076, Cell Signaling).

Flow cytometry

Cells were treated with varying concentrations of FITC-labeled EGF (Thermofisher) and Cy 5.5-labeled CTX respectively for 30 minutes at 37˚C. Cells were collected and analyzed by BD LSR II flow cytometer for the percentage bound fraction of labeled EGF ligand or labeled CTX.

Internalization and co-localization studies

To assess EGF internalization, cells were pre-cooled to 4˚C for 30 minutes and then treated with 25 ng/ml of EGF conjugated to Alexa Fluor 488 (E13345, ThermoFisher). After incubation at 4˚C for 90 minutes, cells were transferred to 37˚C for appropriate time points, washed in ice-cold PBS, and fixed in 4% paraformaldehyde. For co-immunostaining studies, cells were treated as described above, followed by permeabilization in 0.1% Tween in PBS (PBS-T) for 10 minutes at room temperature followed by blocking in 5% bovine serum albumin in PBS at room temperature. Overnight incubation at 4˚C in primary antibody against EEA1 (3288, Cell Signaling) at 1:100 dilution was carried out after which cells were washed three times in PBS-T (0.1% Tween in PBS) and incubated in anti-rabbit secondary antibody (Alexa Flour 594) at 1:200 dilution for 1 hour at room temperature. Cells were washed three times in PBS-T and mounted in Prolong anti-fade diamond mountant with DAPI (P36962, ThermoFisher) and imaged using a Nikon A1R confocal microscope.

Statistics

Studies have been designed to incorporate multiple treatment conditions, often applying a full factorial design, for experiments that are continuous in nature. For data summary purposes, means and standard deviations were calculated within each experimental condition, and plots were examined to diagnose extreme outliers. Formal analysis, where only one experimental factor was varied, used one-way ANOVA to evaluate global differences across groups; two-way ANOVA was applied when multiple experimental factors were varied. Because of the number of statistical hypothesis tests being evaluated, multiple comparisons adjustments were not performed; rather nominal p-values <0.05 along with consistent interpretations of mechanisms over the series of experiments were used to avoid false positive conclusions. For pairwise comparisons, triplicates in each experimental condition afford 80% power at two-sided Type I error to detect differences in continuous outcomes of approximately 3 standard deviations using a t-test. All other studies used continuous readouts of binding characteristics and cell specific marker expression to evaluate the impact of EGFR ECD mutations.

Acknowledgments

We thank Dr. Michael R. Crowley, Heflin Center for Genomic Sciences at UAB (supported by O'Neal Comprehensive Cancer Center core grant CA013148), for sequencing services and the UAB High Resolution Imaging Facility (HRIF) for access to imaging equipment.

REFERENCES

1. Cancer Genome Atlas N. Comprehensive genomic characterization of head and neck squamous cell carcinomas. Nature. 2015; 517(7536):576–82. Epub 2015/01/30. https://doi.org/10.1038/nature14129 PMID: 25631445; PubMed Central PMCID: PMC4311405.

2. Leemans CR, Snijders PJF, Brakenhoff RH. The molecular landscape of head and neck cancer. Nat Rev Cancer. 2018; 18(5):269–82. Epub 2018/03/03. https://doi.org/10.1038/nrc.2018.11 PMID:29497144.

3. Stransky N, Egloff AM, Tward AD, Kostic AD, Cibulskis K, Sivachenko A, et al. The mutational landscape of head and neck squamous cell carcinoma. Science. 2011;333(6046):1157–60. Epub 2011/07/30. https://doi.org/10.1126/science.1208130 PMID: 21798893; PubMed Central PMCID: PMC3415217.

4. Downward J, Yarden Y, Mayes E, Scrace G, Totty N, Stockwell P, et al. Close similarity of epidermal growth factor receptor and v-erb-B oncogene protein sequences. Nature. 1984; 307(5951):521–7.Epub 1984/02/09. https://doi.org/10.1038/307521a0 PMID: 6320011.

5. Bonner JA, Harari PM, Giralt J, Azarnia N, Shin DM, Cohen RB, et al. Radiotherapy plus cetuximab for squamous-cell carcinoma of the head and neck. N Engl J Med. 2006; 354(6):567–78. Epub 2006/02/10. https://doi.org/10.1056/NEJMoa053422 PMID: 16467544.

6. Bonner JA, Harari PM, Giralt J, Cohen RB, Jones CU, Sur RK, et al. Radiotherapy plus cetuximab for locoregionally advanced head and neck cancer:

5-year survival data from a phase 3 randomised trial, and relation between cetuximab-induced rash and survival. Lancet Oncol. 2010; 11(1):21–8. Epub 2009/11/10. https://doi.org/10.1016/S1470-2045(09)70311-0 PMID: 19897418.

7. Binder ZA, Thorne AH, Bakas S, Wileyto EP, Bilello M, Akbari H, et al. Epidermal Growth Factor Receptor Extracellular Domain Mutations in Glioblastoma Present Opportunities for Clinical Imaging and Therapeutic Development. Cancer Cell. 2018; 34(1):163–77 e7. Epub 2018/07/11. https://doi.org/10.1016/j.ccell.2018.06.006 PMID: 29990498; PubMed Central PMCID: PMC6424337.

8. Yu S, Zhang Y, Pan Y, Cheng C, Sun Y, Chen H. The non-small cell lung cancer EGFR extracellular domain mutation, M277E, is oncogenic and drug-sensitive. Onco Targets Ther. 2017; 10:4507–15.https://doi.org/10.2147/OTT.S131999 PMID: 28979142; PubMed Central PMCID: PMC5602469.

9. Keller J, Nimnual AS, Varghese MS, VanHeyst KA, Hayman MJ, Chan EL. A Novel EGFR Extracellular Domain Mutant, EGFRDelta768, Possesses Distinct Biological and Biochemical Properties in Neuroblastoma. Mol Cancer Res. 2016; 14(8):740–52. https://doi.org/10.1158/1541-7786.MCR-15-0477 PMID: 27216155; PubMed Central PMCID: PMC4987210.

10. Arena S, Bellosillo B, Siravegna G, Martinez A, Canadas I, Lazzari L, et al. Emergence of Multiple EGFR Extracellular Mutations during Cetuximab Treatment in Colorectal Cancer. Clin Cancer Res. 2015; 21(9):2157–66. https://doi.org/10.1158/1078-0432.CCR-14-2821 PMID: 25623215.

11. Orellana L, Thorne AH, Lema R, Gustavsson J, Parisian AD, Hospital A, et al. Oncogenic mutations at the EGFR ectodomain structurally converge to remove a steric hindrance on a kinase-coupled cryptic epitope. Proc Natl Acad Sci U S A. 2019; 116(20):10009–18. Epub 2019/04/28. https://doi.org/10.1073/pnas.1821442116 PMID: 31028138; PubMed Central PMCID: PMC6525488.

12. Wee P, Wang Z. Epidermal Growth Factor Receptor Cell Proliferation Signaling Pathways. Cancers (Basel). 2017; 9(5). https://doi.org/10.3390/cancers9050052 PMID: 28513565; PubMed Central PMCID: PMC5447962.

13. Ferguson KM. Structure-based view of epidermal growth factor receptor regulation. Annu Rev Biophys.2008; 37:353–73. https://doi.org/10.1146/annurev.biophys.37.032807.125829 PMID: 18573086; PubMed Central PMCID: PMC2745238.

14. Needham SR, Zanetti-Domingues LC, Hirsch M, Rolfe DJ, Tynan CJ, Roberts SK, et al. Structure-function relationships and supramolecular organization of the EGFR (epidermal growth factor receptor) on the cell surface. Biochem Soc Trans. 2014; 42(1):114–9. https://doi.org/10.1042/BST20130236 PMID:24450637.

15. Klein P, Mattoon D, Lemmon MA, Schlessinger J. A structure-based model for ligand binding and dimerization of EGF receptors. Proc Natl Acad Sci U S A. 2004; 101(4):929–34. Epub 2004/01/21. https://doi.org/10.1073/pnas.0307285101 PMID: 14732694; PubMed Central PMCID: PMC327119.

16. Li S, Schmitz KR, Jeffrey PD, Wiltzius JJ, Kussie P, Ferguson KM. Structural basis for inhibition of the epidermal growth factor receptor by cetuximab. Cancer

Cell.2005;7(4):301–11.Epub2005/04/20.https://doi.org/
10.1016/j.ccr.2005.03.003 PMID: 15837620.

17. Purba ER, Saita EI, Maruyama IN. Activation of the EGF Receptor by Ligand Binding and Oncogenic Mutations: The "Rotation Model". Cells. 2017; 6(2). https://doi.org/10.3390/cells6020013 PMID:28574446; PubMed Central PMCID: PMC5492017.

18. Bessman NJ, Bagchi A, Ferguson KM, Lemmon MA. Complex relationship between ligand binding and dimerization in the epidermal growth factor receptor. Cell Rep. 2014; 9(4):1306–17. Epub 2014/12/03. https://doi.org/10.1016/j.celrep.2014.10.010 PMID: 25453753; PubMed Central PMCID: PMC4254573.

19. Wong AJ, Ruppert JM, Bigner SH, Grzeschik CH, Humphrey PA, Bigner DS, et al. Structural alterations of the epidermal growth factor receptor gene in human gliomas. Proc Natl Acad Sci U S A. 1992; 89 (7):2965–9. Epub 1992/04/01. https://doi.org/10.1073/pnas.89.7.2965 PMID: 1557402; PubMed Central PMCID: PMC48784.

20. Seshacharyulu P, Ponnusamy MP, Haridas D, Jain M, Ganti AK, Batra SK. Targeting the EGFR signaling pathway in cancer therapy. Expert Opin Ther Targets. 2012; 16(1):15–31. Epub 2012/01/14. https://doi.org/10.1517/14728222.2011.648617 PMID: 22239438; PubMed Central PMCID: PMC3291787.

21. Willey CD, Anderson JC, Trummell HQ, Naji F, de Wijn R, Yang ES, et al. Differential escape mechanisms in cetuximab-resistant head and neck cancer cells. Biochem Biophys Res Commun. 2019; 517 (1):36–42. Epub 2019/07/18. https://doi.org/10.1016/j.bbrc.2019.06.159 PMID: 31311651.

22. Harari PM. Epidermal growth factor receptor inhibition strategies in oncology. Endocr Relat Cancer. 2004; 11(4):689–708. https://doi.org/10.1677/erc.1.00600 PMID: 15613446.

23. Herbst RS, Shin DM. Monoclonal antibodies to target epidermal growth factor receptor-positive tumors: a new paradigm for cancer therapy. Cancer. 2002; 94(5):1593–611. https://doi.org/10.1002/cncr.10372 PMID: 11920518.

24. Licitra L, Storkel S, Kerr KM, Van Cutsem E, Pirker R, Hirsch FR, et al. Predictive value of epidermal growth factor receptor expression for first-line chemotherapy plus cetuximab in patients with head and neck and colorectal cancer: analysis of data from the EXTREME and CRYSTAL studies. Eur J Cancer. 2013; 49(6):1161–8. Epub 2012/12/26. https://doi.org/10.1016/j.ejca.2012.11.018 PMID: 23265711.

25. Braig F, Kriegs M, Voigtlaender M, Habel B, Grob T, Biskup K, et al. Cetuximab Resistance in Head and Neck Cancer Is Mediated by EGFR-K521 Polymorphism. Cancer Res. 2017; 77(5):1188–99. Epub 2016/12/30. https://doi.org/10.1158/0008-5472.CAN-16-0754 PMID: 28031227.

26. Liao HW, Hsu JM, Xia W, Wang HL, Wang YN, Chang WC, et al. PRMT1-mediated methylation of the EGF receptor regulates signaling and cetuximab

response. The Journal of clinical investigation. 2015; 125(12):4529–43. Epub 2015/11/17. https://doi.org/10.1172/JCI82826 PMID: 26571401; PubMed Central PMCID: PMC4665782.

27. Wheeler DL, Dunn EF, Harari PM. Understanding resistance to EGFR inhibitors-impact on future treatment strategies. Nat Rev Clin Oncol. 2010; 7(9):493–507. Epub 2010/06/17. https://doi.org/10.1038/nrclinonc.2010.97 PMID: 20551942; PubMed Central PMCID: PMC2929287.

28. Wheeler SE, Suzuki S, Thomas SM, Sen M, Leeman-Neill RJ, Chiosea SI, et al. Epidermal growth factor receptor variant III mediates head and neck cancer cell invasion via STAT3 activation. Oncogene. 2010; 29(37):5135–45. Epub 2010/07/14. https://doi.org/10.1038/onc.2009.279 PMID: 20622897; PubMed Central PMCID: PMC2940981.

29. Rampias T, Giagini A, Siolos S, Matsuzaki H, Sasaki C, Scorilas A, et al. RAS/PI3K crosstalk and cetuximab resistance in head and neck squamous cell carcinoma. Clin Cancer Res. 2014; 20(11):2933–46. Epub 2014/04/04. https://doi.org/10.1158/1078-0432.CCR-13-2721 PMID: 24696319.

30. Brand TM, Iida M, Wheeler DL. Molecular mechanisms of resistance to the EGFR monoclonal antibody cetuximab. Cancer Biol Ther. 2011; 11(9):777–92. Epub 2011/02/05. https://doi.org/10.4161/cbt.11.9. 15050 PMID: 21293176; PubMed Central PMCID: PMC3100630.

31. Rebucci M, Peixoto P, Dewitte A, Wattez N, De Nuncques MA, Rezvoy N, et al. Mechanisms underlying resistance to cetuximab in the HNSCC cell line: role of

AKT inhibition in bypassing this resistance. Int J Oncol. 2011; 38(1):189–200. PMID: 21109940.

32. Wheeler DL, Huang S, Kruser TJ, Nechrebecki MM, Armstrong EA, Benavente S, et al. Mechanisms of acquired resistance to cetuximab: role of HER (ErbB) family members. Oncogene. 2008; 27(28):3944–56. https://doi.org/10.1038/onc.2008.19 PMID: 18297114; PubMed Central PMCID: PMC2903615.

33. Okada Y, Kimura T, Nakagawa T, Okamoto K, Fukuya A, Goji T, et al. EGFR Downregulation after Anti-EGFR Therapy Predicts the Antitumor Effect in Colorectal Cancer. Mol Cancer Res. 2017; 15 (10):1445–54. https://doi.org/10.1158/1541-7786.MCR-16-0383 PMID: 28698359.

34. Brand TM, Iida M, Stein AP, Corrigan KL, Braverman CM, Luthar N, et al. AXL mediates resistance to cetuximab therapy. Cancer Res. 2014; 74(18):5152–64. Epub 2014/08/20. https://doi.org/10.1158/0008-5472.CAN-14-0294 PMID: 25136066; PubMed Central PMCID: PMC4167493.

35. Khattri A, Sheikh N, Acharya R, Tan Y-HC, Kochanny S, Lingen MW, et al. Mechanism of acquired resistance to cetuximab in head and neck cancer. Journal of Clinical Oncology. 2018; 36(15_suppl):e18061–e. https://doi.org/10.1200/JCO.2018.36.15_suppl.e18061

36. Ogiso H, Ishitani R, Nureki O, Fukai S, Yamanaka M, Kim JH, et al. Crystal structure of the complex of human epidermal growth factor and receptor

extracellular domains. Cell. 2002; 110(6):775–87. Epub 2002/09/26. https://doi.org/10.1016/s0092-8674(02)00963-7 PMID: 12297050.

37. Bakker J, Spits M, Neefjes J, Berlin I. The EGFR odyssey—from activation to destruction in space and time. J Cell Sci. 2017; 130(24):4087–96. Epub 2017/11/29. https://doi.org/10.1242/jcs.209197 PMID:29180516.

38. Umebayashi K, Stenmark H, Yoshimori T. Ubc4/5 and c-Cbl continue to ubiquitinate EGF receptor after internalization to facilitate polyubiquitination and degradation. Mol Biol Cell. 2008; 19(8):3454–62. Epub 2008/05/30. https://doi.org/10.1091/mbc.E07-10-0988 PMID: 18508924; PubMed Central PMCID: PMC2488299.

39. Haglund K, Schmidt MH, Wong ES, Guy GR, Dikic I. Sprouty2 acts at the Cbl/CIN85 interface to inhibit epidermal growth factor receptor downregulation. EMBO Rep. 2005; 6(7):635–41. Epub 2005/06/18. https://doi.org/10.1038/sj.embor.7400453 PMID: 15962011; PubMed Central PMCID: PMC1369112.

40. Piper RC, Dikic I, Lukacs GL. Ubiquitin-dependent sorting in endocytosis. Cold Spring Harb Perspect Biol. 2014; 6(1). Epub 2014/01/05. https://doi.org/10.1101/cshperspect.a016808 PMID: 24384571.PubMed Central PMCID: PMC3941215.

41. Stang E, Blystad FD, Kazazic M, Bertelsen V, Brodahl T, Raiborg C, et al. Cbl-dependent ubiquitination is required for progression of EGF receptors into clathrin-coated pits. Mol Biol Cell. 2004; 15(8):3591–604. Epub 2004/06/15.

https://doi.org/10.1091/mbc.E04-01-0041 PMID: 15194809; PubMed Central PMCID: PMC491821.

42. Ravid T, Heidinger JM, Gee P, Khan EM, Goldkorn T. c-Cbl-mediated ubiquitinylation is required for epidermal growth factor receptor exit from the early endosomes. J Biol Chem. 2004; 279(35):37153–62. Epub 2004/06/24. https://doi.org/10.1074/jbc.M403210200 PMID: 15210722.

43. Mohapatra B, Ahmad G, Nadeau S, Zutshi N, An W, Scheffe S, et al. Protein tyrosine kinase regulation by ubiquitination: critical roles of Cbl-family ubiquitin ligases. Biochim Biophys Acta. 2013; 1833(1):122– 39. https://doi.org/10.1016/j.bbamcr.2012.10.010 PMID: 23085373; PubMed Central PMCID: PMC3628764.

44. Sigismund S, Algisi V, Nappo G, Conte A, Pascolutti R, Cuomo A, et al. Threshold-controlled ubiquitination of the EGFR directs receptor fate. EMBO J. 2013; 32(15):2140–57. Epub 2013/06/27. https://doi.org/10.1038/emboj.2013.149 PMID: 23799367; PubMed Central PMCID: PMC3730230.

45. Polo S, Di Fiore PP, Sigismund S. Keeping EGFR signaling in check: ubiquitin is the guardian. Cell Cycle. 2014; 13(5):681–2. Epub 2014/02/15. https://doi.org/10.4161/cc.27855 PMID: 24526125; PubMed Central PMCID: PMC3979896.

46. Capuani F, Conte A, Argenzio E, Marchetti L, Priami C, Polo S, et al. Quantitative analysis reveals how EGFR activation and downregulation are coupled in normal but not in cancer cells. Nat Commun. 2015; 6:7999. Epub

2015/08/13. https://doi.org/10.1038/ncomms8999 PMID: 26264748; PubMed Central PMCID: PMC4538861.

47. Sorkin A, von Zastrow M. Endocytosis and signalling: intertwining molecular networks. Nat Rev Mol Cell Biol. 2009; 10(9):609–22. Epub 2009/08/22. https://doi.org/10.1038/nrm2748 PMID: 19696798; PubMed Central PMCID: PMC2895425.

48. Mellman I, Yarden Y. Endocytosis and cancer. Cold Spring Harb Perspect Biol. 2013; 5(12):a016949. https://doi.org/10.1101/cshperspect.a016949 PMID: 24296170; PubMed Central PMCID: PMC3839607.

49. Schmid SL. Reciprocal regulation of signaling and endocytosis: Implications for the evolving cancer cell. J Cell Biol. 2017; 216(9):2623–32. https://doi.org/10.1083/jcb.201705017 PMID: 28674108; PubMed Central PMCID: PMC5584184.

50. Roepstorff K, Thomsen P, Sandvig K, van Deurs B. Sequestration of epidermal growth factor receptors in non-caveolar lipid rafts inhibits ligand binding. J Biol Chem. 2002; 277(21):18954–60. Epub 2002/03/ 12. https://doi.org/10.1074/jbc.M201422200 PMID: 11886870.

51. Ahsan A, Hiniker SM, Ramanand SG, Nyati S, Hegde A, Helman A, et al. Role of epidermal growth factor receptor degradation in cisplatin-induced cytotoxicity in head and neck cancer. Cancer Res. 2010; 70(7):2862–9. Epub 2010/03/11. https://doi.org/10.1158/0008-5472.CAN-09-4294 PMID: 20215522; PubMed Central PMCID: PMC2848889.

52. Lee JC, Vivanco I, Beroukhim R, Huang JH, Feng WL, DeBiasi RM, et al. Epidermal growth factor receptor activation in glioblastoma through novel missense mutations in the extracellular domain. PLoS Med. 2006; 3(12):e485. https://doi.org/10.1371/journal.pmed.0030485 PMID: 17177598; PubMed Central PMCID: PMC1702556.

53. Pines G, Kostler WJ, Yarden Y. Oncogenic mutant forms of EGFR: lessons in signal transduction and targets for cancer therapy. FEBS Lett. 2010; 584(12) :2699–706. https://doi.org/10.1016/j.febslet.2010. 04.019 PMID: 20388509; PubMed Central PMCID: PMC2892754.

54. Sanchez-Martin FJ, Bellosillo B, Gelabert-Baldrich M, Dalmases A, Canadas I, Vidal J, et al. The First in-class Anti-EGFR Antibody Mixture Sym004 Overcomes Cetuximab Resistance Mediated by EGFR Extracellular Domain Mutations in Colorectal Cancer. Clin Cancer Res. 2016; 22(13):3260–7. Epub2016/02/19. https://doi.org/10.1158/1078-0432.CCR-15-2400 PMID: 26888827.

55. Kojima T, Yamazaki K, Kato K, Muro K, Hara H, Chin K, et al. Phase I dose-escalation trial of Sym004, an anti-EGFR antibody mixture, in Japanese patients with advanced solid tumors. Cancer Sci. 2018; 109(10):3253–62. Epub 2018/08 /14. https://doi.org/10.1111/cas.13767 PMID: 30099818; PubMed Central PMCID: PMC6172077.

56. Montagut C, Argiles G, Ciardiello F, Poulsen TT, Dienstmann R, Kragh M, et al. Efficacy of Sym004 in Patients With Metastatic Colorectal Cancer With Acquired

Resistance to Anti-EGFR Therapy and Molecularly Selected by Circulating Tumor DNA Analyses: A Phase 2 Randomized Clinical Trial. JAMA Oncol. 2018;4(4):e175245.Epub2018/02/10. https://doi.org/10.1001/jamaoncol.2017.5245 PMID: 29423521; PubMed Central PMCID: PMC5885274.

57. Dienstmann R, Patnaik A, Garcia-Carbonero R, Cervantes A, Benavent M, Rosello S, et al. Safety and Activity of the First-in-Class Sym004 Anti-EGFR Antibody Mixture in Patients with Refractory Colorectal Cancer. Cancer Discov. 2015; 5(6):598–609. Epub 2015/05/13. https://doi.org/10.1158/2159-8290.CD-14-1432 PMID: 25962717.

58. Brenner JC, Graham MP, Kumar B, Saunders LM, Kupfer R, Lyons RH, et al. Genotyping of 73 UMSCC head and neck squamous cell carcinoma cell lines. Head Neck. 2010; 32(4):417–26. Epub 2009/ 09/18. https://doi.org/10.1002/hed.21198 PMID: 1970794; Pubmed Central PMCID: PMC32921

CHAPTER 4

DISCUSSION & FUTURE DIRECTIONS

GBM is a challenging disease to treat due to its highly aggressive behavior and a constantly evolving transcriptional and proteomic profile in response to various stimuli such as the tumor microenvironment or therapeutic vulnerabilities. Aberrations in RTK signaling is the cornerstone of GBM tumorigenicity with extensive inter- and intratumoral heterogeneity in RTK expression. Therapeutic targeting of RTKs often fail due to oncogenic switching in RTK expression highlighting the need to better understand conserved endogenous mechanisms that regulate RTKs and how they can be therapeutically targeted. In this dissertation, we establish how ANXA7-I1 acts as a master regulator of multiple tumorigenic RTKs in GBM by modulating their trafficking and signaling dynamics.

AS of primary gene transcripts into isoforms expands the transcriptome and by extension the proteome by enabling functional diversity in a given cell or tissue type. Functionally, alternative isoforms may or may not share interaction partners and as a result may act like distinct proteins themselves. Global analysis of alternative transcripts of human genes has shown that alternative splicing products can either be isoforms (functionally similar) or alloforms (functionally divergent) (122). This is attributed to the inclusion or exclusion of cassette exons, where interaction domains or motifs are localized, consequently altering protein interaction networks (122, 123). There is strong

evidence now that AS is vital and tightly regulated during neurodevelopment. Previous work from our group has shown how isoform switching from I2 to I1 occurs during neuronal development indicating that the AS of *ANXA7* in the brain is both temporal and lineage specific (124). Functionally, we observed divergent impacts of I1 and I2 on EGFR signaling dynamics with I1 inhibiting EGFR signaling, while I2 augmented EGFR signaling indicating that the *ANXA7* isoforms behave like functional alloforms. Therefore, the expression of a specific isoform at a particular stage of neurodevelopment most likely depends on the necessity for EGFR signaling – EGFR signaling is dispensable in postmitotic mature neurons entailing I1 expression; in neural and glial precursors, EGFR signaling is essential for proliferation and maintenance and therefore these cells are enriched for I2. Consequently, in GBM, aberrant splicing in favor of I2 ensures that EGFR signals unabated indicative of a dedifferentiated phenotype. It is therefore reasonable to conclude that tumor cells inherit these splicing traits from precursor cells considered putative cells of origin for GBM (124).

The research presented in Chapter 1 of this dissertation delineates the mechanism by which ANXA7 isoforms differentially regulate the fate of multiple RTKs like EGFR, MET, PDGFRα and EGFRvIII in GBM. We show how reintroducing I1 into multiple GBM cell lines establishes it as the dominant isoform with a resultant inhibition of RTK signaling via lysosomal degradation and a reversal of the phenotype previously observed with I2 alone. Additionally, phosphorylated levels of these RTKs are also significantly decreased in I1 cells indicating that I1 impacts the activation of the receptor post-ligand stimulation. On the contrary, RTKs are preferentially recycled in the I2 cells post-activation through the fast and slow recycling pathways ensuring sustained signaling. The

phenomenon of functional alloforms has been previously observed in multiple studies, albeit in receptor genes themselves, and not in genes regulating receptor trafficking. Richardson et al. found that *RET* gene, a receptor tyrosine kinase, expressed in neuroendocrine tissues was spliced at the 3' end to produce isoforms RET9 which was efficiently degraded and RET51 which was recycled leading to sustained signaling (125). Tanowitz et al. found that Mu opioid receptor, MOR1, failed to recycle back to the surface in the absence of cassette exon 4 as compared to full length MOR1 suggesting that a recycling sequence was encoded by the alternate exon 4 (126). Collectively, our observations along with these studies establish how AS dictates post-endocytic sorting of receptors.

With advances in whole genome transcription profiling, the functional relevance of alternative isoforms has been better defined. A previous assumption that all transcripts generated from a gene are translated into functional proteins has been now disproved with the discovery of non-functional isoforms (127, 128). We found that I2 is largely non-functional in GBM cells as depleting ANXA7 via siRNA knockdown did not seem to impact overall RTK levels post-activation or receptor trafficking - RTKs were sorted to the EE as well as to the Rab4 and Rab11 recycling pathways indicating that these processes were independent of I2. Transcript variants deemed non-functional could be due to low abundance, quick degradation following translation or failure to be translated into functional proteins. Additionally, it has been proposed that the role of these splicing variants may not be at a protein level, instead at a pre-mRNA level where it may modulate the self-expression (122, 127). Although our results pinpoint to the non-functionality of I2 with respect to RTK trafficking in GBM, it is reasonable to assume

that it may participate in interactions or roles that are yet to be characterized. In the I1 cells, ANXA7 knockdown severely impaired the trafficking of RTKs to the EE and subsequently to the lysosomes resulting in an elevation of total RTK levels. Interestingly, the loss of ANXA7 in I1 expressing cells caused RTKs to be diverted to the recycling pathway, comparable to I2 cells. This substantiates our hypothesis that recycling is independent of ANXA7.

The ANXA7 mediated internalization of RTKs was observed to be clathrin-dependent. However, only I1, and not I2, is essential for RTKs to be internalized into clathrin pits post-activation. Upon knocking down ANXA7, EGFR failed to internalize into clathrin pits in I1 cells as compared to I2 cells, where colocalization was observed. Additionally, I1 formed faster and stronger interactions with clathrin immediately post-ligand stimulation as compared to I2 cells. I1 also interacted with multiple downstream endocytic partners such as the EE and lysosomes at appropriate timepoints indicating that I1 possibly forms interaction networks or scaffolds that facilitate the trafficking of RTKs through distinct steps of the endocytic pathway. Multiple studies have shown that cassette exons contain protein segments or domains that act as binding sites modulating various protein-protein interactions (PPI) (122, 129, 130). We propose that the cassette exon 6 encoded region in I1 contains motifs or domains that regulate the sorting and trafficking of RTKs through different steps of the endocytic pathway by facilitating PPI between RTK and endocytic proteins. Domain mapping of ANXA7 revealed that the region encoded by exon 6 formed a secondary structure opening up a region of potential PPI in I1. Due to exon skipping, this secondary structure is absent in I2, with a consequent loss of putative interaction sites and PPI.

The existence of this domain is also substantiated by our ANXA7-I1 mutagenesis models in which deletion of amino acids 145-156 of the exon 6 region of I1 lead to a failure in sorting and degradation of EGFR indicating that the motif necessary for I1-mediated inhibition of RTKs is localized to this region. Additionally, loss of this domain caused I1 to revert to an I2 phenotype by promoting recycling of EGFR suggesting a loss of inhibitory function. Collectively, our results show that inclusion or exclusion of a cassette exon impacts the domain structure consequently modifying isoform-specific PPI. From a disease perspective, dysregulated AS in cancers is beneficial for recapitulating cancer-associated phenotypes via domain exclusion (131, 132). Our research shows how GBM cells reprogram AS by upregulating PTBP1 which in turn splices in favor of I2. Thus, tumor cells subvert the tumor suppressive effect of I1, which is critical for terminating RTK signaling.

Considering the extent of aberrant AS in cancers, targeting AS is now a logical approach in cancer therapeutics. Currently, several small molecules that modulate splicing by targeting different parts of the splicing machinery have been successfully tested invitro in breast cancer, lung adenocarcinoma, colon cancer and certain leukemias. H3B-8800, a derivative of pladienolide-B, is currently being used in a phase 1 clinical trial targeting patients with relapsed/refractory myeloid neoplasms (133, 134). More recently, splicing modulators like antisense oligonucleotides (ASO), short oligonucleotides about 15-25 bases long, have been used to bind and modulate protein expression through various mechanisms. ASO's are complementary to a specific RNA transcript and can mediate either – exon inclusion by preventing the spliceosome from accessing the transcript or exon skipping by conjugating the ASO to a splicing enhancer

to splice out disease-causative frameshift or nonsense mutations (133-137). Due to their high specificity, ASOs are a versatile tool that can be used to modify RNA expression and have been tested successfully in patients with Duchenne muscular dystrophy, spinal muscular atrophy, and amyotrophic lateral sclerosis (135, 138-140). In cancers, ASOs have only been tested in vitro and in mice models for prostate cancer, hepatocellular carcinoma and colorectal cancer models and are yet to progress to clinical trials (141, 142). Theoretically, in GBM cells, an ASO conjugated to a splicing inhibitor can prevent the splicing out of cassette exon 6 in *ANXA7*, retaining I1 expression and consequently its tumor suppressive effect on RTK signaling.

Our research demonstrates how isoform-specific interactions of ANXA7 differentially regulate RTK dynamics in GBM. However, some critical aspects that need to be addressed include elucidating the domains within proteins that are interaction partners for I1. These include conserved sequences in the intracellular domain of RTKs as well as within the endocytic proteins that participate in the I1-mediated sorting and degradation of RTKs. Identification of these domains will help us better understand the molecular underpinnings of ANXA7 isoforms' regulation of RTKs in GBM,

Despite decades of research, GBM remains a deadly and incurable disease highlighting the need for new approaches to inhibit GBM growth and progression. The research presented in this dissertation is an in-depth analysis of how GBM cells manipulate AS and rewire protein interactions to subvert tumor suppression and how targeting aberrant splicing is a favorable point of intervention that can be exploited therapeutically.

REFERENCES

1. Aldape K, Brindle KM, Chesler L, Chopra R, Gajjar A, Gilbert MR, et al. Challenges to curing primary brain tumours. Nat Rev Clin Oncol. 2019;16(8):509-20.
2. Focusing on brain tumours and brain metastasis. Nat Rev Cancer. 2020;20(1):1.
3. [Available from: https://www.cancer.net/cancer-types/brain-tumor/introduction.
4. Perkins A, Liu G. Primary Brain Tumors in Adults: Diagnosis and Treatment. Am Fam Physician. 2016;93(3):211-7.
5. Louis DN, Perry A, Reifenberger G, von Deimling A, Figarella-Branger D, Cavenee WK, et al. The 2016 World Health Organization Classification of Tumors of the Central Nervous System: a summary. Acta Neuropathol. 2016;131(6):803-20.
6. Omuro A, DeAngelis LM. Glioblastoma and other malignant gliomas: a clinical review. Jama. 2013;310(17):1842-50.
7. Tan AC, Ashley DM, Lopez GY, Malinzak M, Friedman HS, Khasraw M. Management of glioblastoma: State of the art and future directions. CA Cancer J Clin. 2020;70(4):299-312.
8. Kristensen BW, Priesterbach-Ackley LP, Petersen JK, Wesseling P. Molecular pathology of tumors of the central nervous system. Ann Oncol. 2019;30(8):1265-78.

9. Wood MD, Halfpenny AM, Moore SR. Applications of molecular neuro-oncology - a review of diffuse glioma integrated diagnosis and emerging molecular entities. Diagn Pathol. 2019;14(1):29.

10. Hanif F, Muzaffar K, Perveen K, Malhi SM, Simjee Sh U. Glioblastoma Multiforme: A Review of its Epidemiology and Pathogenesis through Clinical Presentation and Treatment. Asian Pacific journal of cancer prevention : APJCP. 2017;18(1):3-9.

11. Ohgaki H, Kleihues P. The definition of primary and secondary glioblastoma. Clin Cancer Res. 2013;19(4):764-72.

12. Taylor OG, Brzozowski JS, Skelding KA. Glioblastoma Multiforme: An Overview of Emerging Therapeutic Targets. Front Oncol. 2019;9:963.

13. Tamimi AF, Juweid M. Epidemiology and Outcome of Glioblastoma. In: De Vleeschouwer S, editor. Glioblastoma. Brisbane (AU)2017.

14. M IJ-K, Snijders TJ, de Graeff A, Teunissen S, de Vos FYF. Prevalence of symptoms in glioma patients throughout the disease trajectory: a systematic review. J Neurooncol. 2018;140(3):485-96.

15. Comelli I, Lippi G, Campana V, Servadei F, Cervellin G. Clinical presentation and epidemiology of brain tumors firstly diagnosed in adults in the Emergency Department: a 10-year, single center retrospective study. Ann Transl Med. 2017;5(13):269.

16. D'Alessio A, Proietti G, Sica G, Scicchitano BM. Pathological and Molecular Features of Glioblastoma and Its Peritumoral Tissue. Cancers (Basel). 2019;11(4).

17. Urbanska K, Sokolowska J, Szmidt M, Sysa P. Glioblastoma multiforme - an overview. Contemp Oncol (Pozn). 2014;18(5):307-12.

18. Vollmann-Zwerenz A, Leidgens V, Feliciello G, Klein CA, Hau P. Tumor Cell Invasion in Glioblastoma. Int J Mol Sci. 2020;21(6).

19. Hara A, Kanayama T, Noguchi K, Niwa A, Miyai M, Kawaguchi M, et al. Treatment Strategies Based on Histological Targets against Invasive and Resistant Glioblastoma. J Oncol. 2019;2019:2964783.

20. Lah TT, Novak M, Breznik B. Brain malignancies: Glioblastoma and brain metastases. Semin Cancer Biol. 2020;60:262-73.

21. Catarina Fernandes AC, Lígia Osório, Rita Costa Lago, Paulo Linhares, Bruno Carvalho, Cláudia Caeiro. Current Standards of Care in Glioblastoma Therapy2017.

22. Adamson C, Kanu OO, Mehta AI, Di C, Lin N, Mattox AK, et al. Glioblastoma multiforme: a review of where we have been and where we are going. Expert opinion on investigational drugs. 2009;18(8):1061-83.

23. Ohka F, Natsume A, Wakabayashi T. Current trends in targeted therapies for glioblastoma multiforme. Neurology research international. 2012;2012:878425.

24. Ostrom QT, Cote DJ, Ascha M, Kruchko C, Barnholtz-Sloan JS. Adult Glioma Incidence and Survival by Race or Ethnicity in the United States From 2000 to 2014. JAMA Oncol. 2018;4(9):1254-62.

25. Minniti G, Niyazi M, Alongi F, Navarria P, Belka C. Current status and recent advances in reirradiation of glioblastoma. Radiat Oncol. 2021;16(1):36.

26. van Linde ME, Brahm CG, de Witt Hamer PC, Reijneveld JC, Bruynzeel AME, Vandertop WP, et al. Treatment outcome of patients with recurrent glioblastoma multiforme: a retrospective multicenter analysis. J Neurooncol. 2017;135(1):183-92.

27. Perrin SL, Samuel MS, Koszyca B, Brown MP, Ebert LM, Oksdath M, et al. Glioblastoma heterogeneity and the tumour microenvironment: implications for preclinical research and development of new treatments. Biochem Soc Trans. 2019;47(2):625-38.

28. Tirosh I, Suva ML. Tackling the Many Facets of Glioblastoma Heterogeneity. Cell Stem Cell. 2020;26(3):303-4.

29. Noch EK, Ramakrishna R, Magge R. Challenges in the Treatment of Glioblastoma: Multisystem Mechanisms of Therapeutic Resistance. World Neurosurg. 2018;116:505-17.

30. Puchalski RB, Shah N, Miller J, Dalley R, Nomura SR, Yoon JG, et al. An anatomic transcriptional atlas of human glioblastoma. Science. 2018;360(6389):660-3.

31. Johnson BE, Mazor T, Hong C, Barnes M, Aihara K, McLean CY, et al. Mutational analysis reveals the origin and therapy-driven evolution of recurrent glioma. Science. 2014;343(6167):189-93.

32. Lauko A, Lo A, Ahluwalia MS, Lathia JD. Cancer cell heterogeneity & plasticity in glioblastoma and brain tumors. Semin Cancer Biol. 2021.

33. Cancer Genome Atlas Research N. Comprehensive genomic characterization defines human glioblastoma genes and core pathways. Nature. 2008;455(7216):1061-8.

34. Verhaak RG, Hoadley KA, Purdom E, Wang V, Qi Y, Wilkerson MD, et al. Integrated genomic analysis identifies clinically relevant subtypes of glioblastoma characterized by abnormalities in PDGFRA, IDH1, EGFR, and NF1. Cancer Cell. 2010;17(1):98-110.

35. Wang Q, Hu B, Hu X, Kim H, Squatrito M, Scarpace L, et al. Tumor Evolution of Glioma-Intrinsic Gene Expression Subtypes Associates with Immunological Changes in the Microenvironment. Cancer Cell. 2017;32(1):42-56 e6.

36. Brennan CW, Verhaak RG, McKenna A, Campos B, Noushmehr H, Salama SR, et al. The somatic genomic landscape of glioblastoma. Cell. 2013;155(2):462-77.

37. Patel AP, Tirosh I, Trombetta JJ, Shalek AK, Gillespie SM, Wakimoto H, et al. Single-cell RNA-seq highlights intratumoral heterogeneity in primary glioblastoma. Science. 2014;344(6190):1396-401.

38. Du Z, Lovly CM. Mechanisms of receptor tyrosine kinase activation in cancer. Mol Cancer. 2018;17(1):58.

39. Lemmon MA, Schlessinger J. Cell signaling by receptor tyrosine kinases. Cell. 2010;141(7):1117-34.

40. Yamaoka T, Kusumoto S, Ando K, Ohba M, Ohmori T. Receptor Tyrosine Kinase-Targeted Cancer Therapy. Int J Mol Sci. 2018;19(11).

41. Bergeron JJ, Di Guglielmo GM, Dahan S, Dominguez M, Posner BI. Spatial and Temporal Regulation of Receptor Tyrosine Kinase Activation and Intracellular Signal Transduction. Annu Rev Biochem. 2016;85:573-97.

42. Casaletto JB, McClatchey AI. Spatial regulation of receptor tyrosine kinases in development and cancer. Nat Rev Cancer. 2012;12(6):387-400.

43. Kumari S, Mg S, Mayor S. Endocytosis unplugged: multiple ways to enter the cell. Cell Res. 2010;20(3):256-75.

44. Aguilar RC, Wendland B. Endocytosis of membrane receptors: two pathways are better than one. Proc Natl Acad Sci U S A. 2005;102(8):2679-80.

45. Bache KG, Slagsvold T, Stenmark H. Defective downregulation of receptor tyrosine kinases in cancer. EMBO J. 2004;23(14):2707-12.

46. Goh LK, Sorkin A. Endocytosis of receptor tyrosine kinases. Cold Spring Harb Perspect Biol. 2013;5(5):a017459.

47. Yuan W, Song C. The Emerging Role of Rab5 in Membrane Receptor Trafficking and Signaling Pathways. Biochem Res Int. 2020;2020:4186308.

48. Wandinger-Ness A, Zerial M. Rab proteins and the compartmentalization of the endosomal system. Cold Spring Harb Perspect Biol. 2014;6(11):a022616.

49. Homma Y, Hiragi S, Fukuda M. Rab family of small GTPases: an updated view on their regulation and functions. FEBS J. 2021;288(1):36-55.

50. Stommel JM, Kimmelman AC, Ying H, Nabioullin R, Ponugoti AH, Wiedemeyer R, et al. Coactivation of receptor tyrosine kinases affects the response of tumor cells to targeted therapies. Science. 2007;318(5848):287-90.

51. Parker NR, Khong P, Parkinson JF, Howell VM, Wheeler HR. Molecular heterogeneity in glioblastoma: potential clinical implications. Front Oncol. 2015;5:55.

52. Gong Y DY, Cui J, Sun Q, Zhen Z, Gao Y, Su J, Ren H. Receptor Tyrosine Kinase Interaction with the Tumor Microenvironment in Malignant Progression of Human Glioblastoma. Glioma - Contemporary Diagnostic and Therapeutic Approaches2019.

53. Snuderl M, Fazlollahi L, Le LP, Nitta M, Zhelyazkova BH, Davidson CJ, et al. Mosaic amplification of multiple receptor tyrosine kinase genes in glioblastoma. Cancer Cell. 2011;20(6):810-7.

54. Little SE, Popov S, Jury A, Bax DA, Doey L, Al-Sarraj S, et al. Receptor tyrosine kinase genes amplified in glioblastoma exhibit a mutual exclusivity in variable proportions reflective of individual tumor heterogeneity. Cancer Res. 2012;72(7):1614-20.

55. Szerlip NJ, Pedraza A, Chakravarty D, Azim M, McGuire J, Fang Y, et al. Intratumoral heterogeneity of receptor tyrosine kinases EGFR and PDGFRA amplification in glioblastoma defines subpopulations with distinct growth factor response. Proc Natl Acad Sci U S A. 2012;109(8):3041-6.

56. Wei W, Shin YS, Xue M, Matsutani T, Masui K, Yang H, et al. Single-Cell Phosphoproteomics Resolves Adaptive Signaling Dynamics and Informs Targeted Combination Therapy in Glioblastoma. Cancer Cell. 2016;29(4):563-73.

57. Baralle FE, Giudice J. Alternative splicing as a regulator of development and tissue identity. Nat Rev Mol Cell Biol. 2017;18(7):437-51.

58. Blencowe BJ. Alternative splicing: new insights from global analyses. Cell. 2006;126(1):37-47.

59. Bessa C, Matos P, Jordan P, Goncalves V. Alternative Splicing: Expanding the Landscape of Cancer Biomarkers and Therapeutics. Int J Mol Sci. 2020;21(23).

60. Wilkinson ME, Charenton C, Nagai K. RNA Splicing by the Spliceosome. Annu Rev Biochem. 2020;89:359-88.

61. Roy B, Haupt LM, Griffiths LR. Review: Alternative Splicing (AS) of Genes As An Approach for Generating Protein Complexity. Curr Genomics. 2013;14(3):182-94.

62. Wang Y, Liu J, Huang BO, Xu YM, Li J, Huang LF, et al. Mechanism of alternative splicing and its regulation. Biomed Rep. 2015;3(2):152-8.

63. Rodriguez JM, Pozo F, di Domenico T, Vazquez J, Tress ML. An analysis of tissue-specific alternative splicing at the protein level. PLoS Comput Biol. 2020;16(10):e1008287.

64. Taliaferro JM, Alvarez N, Green RE, Blanchette M, Rio DC. Evolution of a tissue-specific splicing network. Genes Dev. 2011;25(6):608-20.

65. Tapial J, Ha KCH, Sterne-Weiler T, Gohr A, Braunschweig U, Hermoso-Pulido A, et al. An atlas of alternative splicing profiles and functional associations reveals new regulatory programs and genes that simultaneously express multiple major isoforms. Genome Res. 2017;27(10):1759-68.

66. Weyn-Vanhentenryck SM, Feng H, Ustianenko D, Duffie R, Yan Q, Jacko M, et al. Precise temporal regulation of alternative splicing during neural development. Nat Commun. 2018;9(1):2189.

67. Raj B, Blencowe BJ. Alternative Splicing in the Mammalian Nervous System: Recent Insights into Mechanisms and Functional Roles. Neuron. 2015;87(1):14-27.

68. Xie ZC, Wu HY, Dang YW, Chen G. Role of alternative splicing signatures in the prognosis of glioblastoma. Cancer Med. 2019;8(18):7623-36.

69. Fuentes-Fayos AC, Vazquez-Borrego MC, Jimenez-Vacas JM, Bejarano L, Pedraza-Arevalo S, F LL, et al. Splicing machinery dysregulation drives glioblastoma development/aggressiveness: oncogenic role of SRSF3. Brain. 2020;143(11):3273-93.

70. Zeng Y, Zhang P, Wang X, Wang K, Zhou M, Long H, et al. Identification of Prognostic Signatures of Alternative Splicing in Glioma. J Mol Neurosci. 2020;70(10):1484-92.

71. Wang L, Shamardani K, Babikir H, Catalan F, Nejo T, Chang S, et al. The evolution of alternative splicing in glioblastoma under therapy. Genome Biol. 2021;22(1):48.

72. Bielli P, Pagliarini V, Pieraccioli M, Caggiano C, Sette C. Splicing Dysregulation as Oncogenic Driver and Passenger Factor in Brain Tumors. Cells. 2019;9(1).

73. Moss SE, Morgan RO. The annexins. Genome Biol. 2004;5(4):219.

74. Rescher U, Gerke V. Annexins--unique membrane binding proteins with diverse functions. J Cell Sci. 2004;117(Pt 13):2631-9.

75. Gerke V, Moss SE. Annexins: from structure to function. Physiol Rev. 2002;82(2):331-71.

76. Gerke V, Creutz CE, Moss SE. Annexins: linking Ca2+ signalling to membrane dynamics. Nat Rev Mol Cell Biol. 2005;6(6):449-61.

77. Schloer S, Pajonczyk D, Rescher U. Annexins in Translational Research: Hidden Treasures to Be Found. Int J Mol Sci. 2018;19(6).

78. Zhuang C, Wang P, Sun T, Zheng L, Ming L. Expression levels and prognostic values of annexins in liver cancer. Oncol Lett. 2019;18(6):6657-69.

79. Ganesan T, Sinniah A, Ibrahim ZA, Chik Z, Alshawsh MA. Annexin A1: A Bane or a Boon in Cancer? A Systematic Review. Molecules. 2020;25(16).

80. Lecona E, Barrasa JI, Olmo N, Llorente B, Turnay J, Lizarbe MA. Upregulation of annexin A1 expression by butyrate in human colon adenocarcinoma cells: role of p53, NF-Y, and p38 mitogen-activated protein kinase. Mol Cell Biol. 2008;28(15):4665-74.

81. Patton KT, Chen HM, Joseph L, Yang XJ. Decreased annexin I expression in prostatic adenocarcinoma and in high-grade prostatic intraepithelial neoplasia. Histopathology. 2005;47(6):597-601.

82. Biaoxue R, Xiguang C, Shuanying Y. Annexin A1 in malignant tumors: current opinions and controversies. Int J Biol Markers. 2014;29(1):e8-20.

83. Christensen MV, Hogdall CK, Jochumsen KM, Hogdall EVS. Annexin A2 and cancer: A systematic review. Int J Oncol. 2018;52(1):5-18.

84. Mahdi AF, Malacrida B, Nolan J, McCumiskey ME, Merrigan AB, Lal A, et al. Expression of Annexin A2 Promotes Cancer Progression in Estrogen Receptor Negative Breast Cancers. Cells. 2020;9(7).

85. Qiu LW, Liu YF, Cao XQ, Wang Y, Cui XH, Ye X, et al. Annexin A2 promotion of hepatocellular carcinoma tumorigenesis via the immune microenvironment. World J Gastroenterol. 2020;26(18):2126-37.

86. Zhai H, Acharya S, Gravanis I, Mehmood S, Seidman RJ, Shroyer KR, et al. Annexin A2 promotes glioma cell invasion and tumor progression. J Neurosci. 2011;31(40):14346-60.

87. Lamb DS, Sondhauss S, Dunne JC, Woods L, Delahunt B, Ferguson P, et al. Proteins Annexin A2 and PSA in Prostate Cancer Biopsies Do Not Predict Biochemical Failure. Anticancer Res. 2017;37(12):6943-6.

88. Du R, Liu B, Zhou L, Wang D, He X, Xu X, et al. Downregulation of annexin A3 inhibits tumor metastasis and decreases drug resistance in breast cancer. Cell Death Dis. 2018;9(2):126.

89. Liu YF, Liu QQ, Zhang YH, Qiu JH. Annexin A3 Knockdown Suppresses Lung Adenocarcinoma. Anal Cell Pathol (Amst). 2016;2016:4131403.

90. Jung EJ, Moon HG, Park ST, Cho BI, Lee SM, Jeong CY, et al. Decreased annexin A3 expression correlates with tumor progression in papillary thyroid cancer. Proteomics Clin Appl. 2010;4(5):528-37.

91. Tong M, Fung TM, Luk ST, Ng KY, Lee TK, Lin CH, et al. ANXA3/JNK Signaling Promotes Self-Renewal and Tumor Growth, and Its Blockade Provides a Therapeutic Target for Hepatocellular Carcinoma. Stem Cell Reports. 2015;5(1):45-59.

92. Gou R, Zhu L, Zheng M, Guo Q, Hu Y, Li X, et al. Annexin A8 can serve as potential prognostic biomarker and therapeutic target for ovarian cancer: based on the comprehensive analysis of Annexins. J Transl Med. 2019;17(1):275.

93. Zhang ZG, Chen JN, Wang YD, Gao JT, Jin Y. The Role of Annexin A4 in Triple-Negative Breast Cancer Progression and Its Clinical Application. Ann Clin Lab Sci. 2016;46(5):515-21.

94. Yao H, Sun C, Hu Z, Wang W. The role of annexin A4 in cancer. Front Biosci (Landmark Ed). 2016;21:949-57.

95. Wei B, Guo C, Liu S, Sun MZ. Annexin A4 and cancer. Clin Chim Acta. 2015;447:72-8.

96. Wang X, Dai Y, Zhao Y, Li M, Zhang J, Ci Y, et al. AnnexinA5 Might Suppress the Phenotype of Human Gastric Cancer Cells via ERK Pathway. Front Oncol. 2021;11:665105.

97. Peng B, Guo C, Guan H, Liu S, Sun MZ. Annexin A5 as a potential marker in tumors. Clin Chim Acta. 2014;427:42-8.

98. Rajcevic U, Petersen K, Knol JC, Loos M, Bougnaud S, Klychnikov O, et al. iTRAQ-based proteomics profiling reveals increased metabolic activity and cellular cross-talk in angiogenic compared with invasive glioblastoma phenotype. Mol Cell Proteomics. 2009;8(11):2595-612.

99. Noreen S, Gardner QA, Fatima I, Sadaf S, Akhtar MW. Upregulated Expression of Calcium-Dependent Annexin A6: A Potential Biomarker of Ovarian Carcinoma. Proteomics Clin Appl. 2020;14(2):e1900078.

100. Korolkova OY, Widatalla SE, Williams SD, Whalen DS, Beasley HK, Ochieng J, et al. Diverse Roles of Annexin A6 in Triple-Negative Breast Cancer Diagnosis, Prognosis and EGFR-Targeted Therapies. Cells. 2020;9(8).

101. Hoque M, Elmaghrabi YA, Kose M, Beevi SS, Jose J, Meneses-Salas E, et al. Annexin A6 improves anti-migratory and anti-invasive properties of tyrosine kinase inhibitors in EGFR overexpressing human squamous epithelial cells. FEBS J. 2020;287(14):2961-78.

102. Meier EM, Rein-Fischboeck L, Pohl R, Wanninger J, Hoy AJ, Grewal T, et al. Annexin A6 protein is downregulated in human hepatocellular carcinoma. Mol Cell Biochem. 2016;418(1-2):81-90.

103. Leighton X, Bera A, Eidelman O, Bubendorf L, Zellweger T, Banerjee J, et al. Tissue microarray analysis delineate potential prognostic role of Annexin A7 in prostate cancer progression. PLoS One. 2018;13(10):e0205837.

104. Guo C, Liu S, Greenaway F, Sun MZ. Potential role of annexin A7 in cancers. Clin Chim Acta. 2013;423:83-9.

105. Liu H, Guo D, Sha Y, Zhang C, Jiang Y, Hong L, et al. ANXA7 promotes the cell cycle, proliferation and cell adhesion-mediated drug resistance of multiple myeloma cells by up-regulating CDC5L. Aging (Albany NY). 2020;12(11):11100-15.

106. Hata H, Tatemichi M, Nakadate T. Involvement of annexin A8 in the properties of pancreatic cancer. Mol Carcinog. 2014;53(3):181-91.

107. Ma F, Li X, Fang H, Jin Y, Sun Q, Li X. Prognostic Value of ANXA8 in Gastric Carcinoma. J Cancer. 2020;11(12):3551-8.

108. Lee MJ, Yu GR, Yoo HJ, Kim JH, Yoon BI, Choi YK, et al. ANXA8 down-regulation by EGF-FOXO4 signaling is involved in cell scattering and tumor metastasis of cholangiocarcinoma. Gastroenterology. 2009;137(3):1138-50, 50 e1-9.

109. Miyoshi N, Yamamoto H, Mimori K, Yamashita S, Miyazaki S, Nakagawa S, et al. ANXA9 gene expression in colorectal cancer: A novel marker for prognosis. Oncol Lett. 2014;8(5):2313-7.

110. Salom C, Alvarez-Teijeiro S, Fernandez MP, Morgan RO, Allonca E, Vallina A, et al. Frequent Alteration of Annexin A9 and A10 in HPV-Negative Head and Neck Squamous Cell Carcinomas: Correlation with the Histopathological Differentiation Grade. J Clin Med. 2019;8(2).

111. Munksgaard PP, Mansilla F, Brems Eskildsen AS, Fristrup N, Birkenkamp-Demtroder K, Ulhoi BP, et al. Low ANXA10 expression is associated with disease aggressiveness in bladder cancer. Br J Cancer. 2011;105(9):1379-87.

112. Wei T, Zhu X. Knockdown of ANXA10 inhibits proliferation and promotes apoptosis of papillary thyroid carcinoma cells by down-regulating TSG101 thereby inactivating the MAPK/ERK signaling pathway. J Bioenerg Biomembr. 2021.

113. Ishikawa A, Kuraoka K, Zaitsu J, Saito A, Kuwai T, Suzuki T, et al. Loss of Annexin A10 Expression Is Associated with Poor Prognosis in Early Gastric Cancer. Acta Histochem Cytochem. 2020;53(5):113-9.

114. Qi J, Wang Z, Zhao Z, Liu L. EIF3J-AS1 promotes glioma cell growth via up-regulating ANXA11 through sponging miR-1343-3p. Cancer Cell Int. 2020;20:428.

115. Liu Z, Wang Y, Wang L, Yao B, Sun L, Liu R, et al. Long non-coding RNA AGAP2-AS1, functioning as a competitive endogenous RNA, upregulates ANXA11 expression by sponging miR-16-5p and promotes proliferation and metastasis in hepatocellular carcinoma. J Exp Clin Cancer Res. 2019;38(1):194.

116. Hua K, Li Y, Zhao Q, Fan L, Tan B, Gu J. Downregulation of Annexin A11 (ANXA11) Inhibits Cell Proliferation, Invasion, and Migration via the AKT/GSK-3beta Pathway in Gastric Cancer. Med Sci Monit. 2018;24:149-60.

117. Jiang G, Wang P, Wang W, Li W, Dai L, Chen K. Annexin A13 promotes tumor cell invasion in vitro and is associated with metastasis in human colorectal cancer. Oncotarget. 2017;8(13):21663-73.

118. Padden J, Ahrens M, Kalsch J, Bertram S, Megger DA, Bracht T, et al. Immunohistochemical Markers Distinguishing Cholangiocellular Carcinoma (CCC) from Pancreatic Ductal Adenocarcinoma (PDAC) Discovered by Proteomic Analysis of Microdissected Cells. Mol Cell Proteomics. 2016;15(3):1072-82.

119. Clemen CS, Herr C, Hovelmeyer N, Noegel AA. The lack of annexin A7 affects functions of primary astrocytes. Exp Cell Res. 2003;291(2):406-14.

120. Ferrarese R, Harsh GRt, Yadav AK, Bug E, Maticzka D, Reichardt W, et al. Lineage-specific splicing of a brain-enriched alternative exon promotes glioblastoma progression. J Clin Invest. 2014;124(7):2861-76.

121. Yadav AK, Renfrow JJ, Scholtens DM, Xie H, Duran GE, Bredel C, et al. Monosomy of chromosome 10 associated with dysregulation of epidermal growth factor signaling in glioblastomas. Jama. 2009;302(3):276-89.

122. Yang X, Coulombe-Huntington J, Kang S, Sheynkman GM, Hao T, Richardson A, et al. Widespread Expansion of Protein Interaction Capabilities by Alternative Splicing. Cell. 2016;164(4):805-17.

123. Ghadie MA, Lambourne L, Vidal M, Xia Y. Domain-based prediction of the human isoform interactome provides insights into the functional impact of alternative splicing. PLoS Comput Biol. 2017;13(8):e1005717.

124. Ferrarese R, Harsh GRt, Yadav AK, Bug E, Maticzka D, Reichardt W, et al. Lineage-specific splicing of a brain-enriched alternative exon promotes glioblastoma progression. J Clin Invest. 2014;124(7):2861-76.

125. Richardson DS, Rodrigues DM, Hyndman BD, Crupi MJ, Nicolescu AC, Mulligan LM. Alternative splicing results in RET isoforms with distinct trafficking properties. Mol Biol Cell. 2012;23(19):3838-50.

126. Tanowitz M, Hislop JN, von Zastrow M. Alternative splicing determines the post-endocytic sorting fate of G-protein-coupled receptors. J Biol Chem. 2008;283(51):35614-21.

127. Tress ML, Abascal F, Valencia A. Most Alternative Isoforms Are Not Functionally Important. Trends Biochem Sci. 2017;42(6):408-10.

128. Bush SJ, Chen L, Tovar-Corona JM, Urrutia AO. Alternative splicing and the evolution of phenotypic novelty. Philos Trans R Soc Lond B Biol Sci. 2017;372(1713).

129. Buljan M, Chalancon G, Eustermann S, Wagner GP, Fuxreiter M, Bateman A, et al. Tissue-specific splicing of disordered segments that embed binding motifs rewires protein interaction networks. Mol Cell. 2012;46(6):871-83.

130. D'Antonio M, Masseroli M. Extraction, integration and analysis of alternative splicing and protein structure distributed information. BMC Bioinformatics. 2009;10 Suppl 12:S15.

131. Climente-Gonzalez H, Porta-Pardo E, Godzik A, Eyras E. The Functional Impact of Alternative Splicing in Cancer. Cell Rep. 2017;20(9):2215-26.

132. Louadi Z, Yuan K, Gress A, Tsoy O, Kalinina OV, Baumbach J, et al. DIGGER: exploring the functional role of alternative splicing in protein interactions. Nucleic Acids Res. 2021;49(D1):D309-D18.

133. Martinez-Montiel N, Rosas-Murrieta NH, Anaya Ruiz M, Monjaraz-Guzman E, Martinez-Contreras R. Alternative Splicing as a Target for Cancer Treatment. Int J Mol Sci. 2018;19(2).

134. Zhang Y, Qian J, Gu C, Yang Y. Alternative splicing and cancer: a systematic review. Signal Transduct Target Ther. 2021;6(1):78.

135. Dhuri K, Bechtold C, Quijano E, Pham H, Gupta A, Vikram A, et al. Antisense Oligonucleotides: An Emerging Area in Drug Discovery and Development. J Clin Med. 2020;9(6).

136. Havens MA, Duelli DM, Hastings ML. Targeting RNA splicing for disease therapy. Wiley Interdiscip Rev RNA. 2013;4(3):247-66.

137. Lee SC, Abdel-Wahab O. Therapeutic targeting of splicing in cancer. Nat Med. 2016;22(9):976-86.

138. Frank DE, Schnell FJ, Akana C, El-Husayni SH, Desjardins CA, Morgan J, et al. Increased dystrophin production with golodirsen in patients with Duchenne muscular dystrophy. Neurology. 2020;94(21):e2270-e82.

139. Ly CV, Miller TM. Emerging antisense oligonucleotide and viral therapies for amyotrophic lateral sclerosis. Curr Opin Neurol. 2018;31(5):648-54.

140. Scaglioni D, Catapano F, Ellis M, Torelli S, Chambers D, Feng L, et al. The administration of antisense oligonucleotide golodirsen reduces pathological regeneration in patients with Duchenne muscular dystrophy. Acta Neuropathol Commun. 2021;9(1):7.

141. De Velasco MA, Kura Y, Sakai K, Hatanaka Y, Davies BR, Campbell H, et al. Targeting castration-resistant prostate cancer with androgen receptor antisense oligonucleotide therapy. JCI Insight. 2019;4(17).

142. Harada T, Matsumoto S, Hirota S, Kimura H, Fujii S, Kasahara Y, et al. Chemically Modified Antisense Oligonucleotide Against ARL4C Inhibits Primary and Metastatic Liver Tumor Growth. Mol Cancer Ther. 2019;18(3):602-12.